

HARMONIC ANALYSIS OF AC/DC CONVERTERS USING
THE HARMONIC ADMITTANCE METHOD

CENTRE FOR NEWFOUNDLAND STUDIES

**TOTAL OF 10 PAGES ONLY
MAY BE XEROXED**

(Without Author's Permission)

NARAYANAN RAJAGOPAL





National Library
of Canada

Acquisitions and
Bibliographic Services Branch

395 Wellington Street
Ottawa, Ontario
K1A 0N4

Bibliothèque nationale
du Canada

Direction des acquisitions et
des services bibliographiques

395, rue Wellington
Ottawa (Ontario)
K1A 0N4

Your file Votre référence

Our file Notre référence

NOTICE

The quality of this microform is heavily dependent upon the quality of the original thesis submitted for microfilming. Every effort has been made to ensure the highest quality of reproduction possible.

If pages are missing, contact the university which granted the degree.

Some pages may have indistinct print especially if the original pages were typed with a poor typewriter ribbon or if the university sent us an inferior photocopy.

Reproduction in full or in part of this microform is governed by the Canadian Copyright Act, R.S.C. 1970, c. C-30, and subsequent amendments.

AVIS

La qualité de cette microforme dépend grandement de la qualité de la thèse soumise au microfilmage. Nous avons tout fait pour assurer une qualité supérieure de reproduction.

S'il manque des pages, veuillez communiquer avec l'université qui a conféré le grade.

La qualité d'impression de certaines pages peut laisser à désirer, surtout si les pages originales ont été dactylographiées à l'aide d'un ruban usé ou si l'université nous a fait parvenir une photocopie de qualité inférieure.

La reproduction, même partielle, de cette microforme est soumise à la Loi canadienne sur le droit d'auteur, SRC 1970, c. C-30, et ses amendements subséquents.

**HARMONIC ANALYSIS OF AC/DC CONVERTERS
USING THE
HARMONIC ADMITTANCE METHOD**

By

© Narayanan Rajagopal

A thesis submitted to the School of Graduate Studies
in partial fulfillment of the requirements for the degree of
Master of Engineering

Faculty of Engineering and Applied Science
Memorial University of Newfoundland
March, 1993

St. John's

Newfoundland

Canada



National Library
of Canada

Acquisitions and
Bibliographic Services Branch

395 Wellington Street
Ottawa, Ontario
K1A 0N4

Bibliothèque nationale
du Canada

Direction des acquisitions et
des services bibliographiques

395, rue Wellington
Ottawa (Ontario)
K1A 0N4

Your file Votre référence

Our file Notre référence

The author has granted an irrevocable non-exclusive licence allowing the National Library of Canada to reproduce, loan, distribute or sell copies of his/her thesis by any means and in any form or format, making this thesis available to interested persons.

The author retains ownership of the copyright in his/her thesis. Neither the thesis nor substantial extracts from it may be printed or otherwise reproduced without his/her permission.

L'auteur a accordé une licence irrévocable et non exclusive permettant à la Bibliothèque nationale du Canada de reproduire, prêter, distribuer ou vendre des copies de sa thèse de quelque manière et sous quelque forme que ce soit pour mettre des exemplaires de cette thèse à la disposition des personnes intéressées.

L'auteur conserve la propriété du droit d'auteur qui protège sa thèse. Ni la thèse ni des extraits substantiels de celle-ci ne doivent être imprimés ou autrement reproduits sans son autorisation.

ISBN 0-315-82626-2

Abstract

Phase control technique used in ac/dc converters results in the generation of harmonics which can disrupt the operation of critical and sensitive loads. In general, the level of harmonics in the system depends on the interaction between the ac network and the harmonics generated by the converter.

This thesis develops a technique for the harmonic analysis of phase-controlled ac/dc converters connected to the ac network. The analysis method is based on the harmonic admittance model, which uses the multi-port network concept to define a relationship between the input ac voltages and currents, and the output dc voltage and current. The matrix representation of the relationships is expressed in terms of A , B , C , D parameters, which contain the harmonic components of the switching functions of the converter and the admittance of the commutating inductance.

A single phase model of the harmonic admittance technique is first implemented. The model is used to determine the harmonics at various nodes in the system. It is shown that in addition to providing quantitative information about the harmonic levels, the model accurately predicts the operating conditions and harmonic instabilities in the system.

The method is extended to model a three-phase system. For simplicity, the operation of the converter with commutating overlap angle less than 60° (i.e. mode-I operation) is considered. However, based on the procedure described in the thesis, the model for other modes of operation can be developed. The model is used to study the harmonic interaction in a simple HVDC system. Specifically, the distortion at the point of common coupling, the effects of ac source harmonics and unbalance in ac network impedance on the system voltages are investigated.

The harmonic admittance models developed in the thesis are verified by EMTF simulation. The model accurately predicts the harmonics and system behaviour. It is shown that the harmonic admittance method provides an alternate tool to study the harmonic interactions in power systems with converters.

ACKNOWLEDGEMENTS

I am grateful to Dr. J.E. Quicoe for his invaluable technical guidance, incessant encouragement and monetary support throughout the program.

I wish to thank the Faculty of Engineering, Memorial University for the financial support through graduate assistantships.

Finally I thank the staff at CCAE, faculty and friends for all the useful discussions.

Contents

ABSTRACT	ii
ACKNOWLEDGEMENTS	iv
List of Figures	ix
List of Tables	xiii
1 Introduction	1
1.1 Review of Methods for Harmonic Evaluation	3
1.1.1 Time Domain Analysis	3
1.1.2 Frequency Domain Analysis	3
1.1.3 Harmonic Admittance Analysis	6
1.2 Simulation of Power Systems	7
1.3 Thesis Objectives and Outline	9
2 Harmonic Analysis of AC/DC Converters- The Classical Approach	11
2.1 Harmonic Analysis of the Single Phase AC/DC Converter System .	11
2.1.1 The Single Phase AC/DC Converter System	11
2.1.2 Analysis of the Converter System	12
2.1.3 Procedure for Computing Voltage Harmonics	16
2.1.4 Results	17
2.2 Harmonic Analysis of the Three-phase AC/DC Converter System .	23

2.2.1	The Three-Phase Converter System	23
2.2.2	Analysis of the Converter System	24
2.2.3	Procedure for Computing Voltage Harmonics	27
2.2.4	Results	28
2.3	Summary	30
3	Harmonic Admittance Model for the Single Phase Converter	35
3.1	The Single Phase Converter Connected to the AC System	35
3.2	Harmonic Admittance Matrix for the Single Phase Converter	36
3.3	Elements of the Harmonic Admittance Matrix	37
3.3.1	Harmonic Representation of the Switching Functions	39
3.3.2	Harmonic Representation of the AC Current	39
3.3.3	Harmonic Representation of the DC Voltage	44
3.3.4	A, B, C and D parameters of the Single Phase Converter	44
3.4	Solution of System Equations	46
3.4.1	Constraint Equation	46
3.4.2	Procedure for the Solution of System Equations	47
3.5	System Example	47
3.5.1	Simulation using the Harmonic Admittance Algorithm	48
3.6	EMTP Simulation of the Single Phase Converter	56
3.6.1	System Waveforms	57
3.7	Summary	58
4	Harmonic Admittance Model for the Three-Phase Converter	67
4.1	The Three-Phase Converter System	67
4.2	Harmonic Admittance Matrix for the Three-Phase Converter	68
4.3	Elements of the Harmonic Admittance Matrix	69
4.3.1	Harmonic Representation of the Current Switching Functions	72

4.3.2	Harmonic Representation of the Voltage Switching Functions	74
4.3.3	Harmonic Representation of the Current in Phase-a	75
4.3.4	Harmonic Representation of the Currents in Phase-b and Phase-c	82
4.3.5	Harmonic Representation of the DC Voltage	83
4.3.6	<i>A, B, C</i> and <i>D</i> Parameters of the Three-Phase Converter .	84
4.4	Solution of System Equations	87
4.4.1	Constraint Equations	88
4.4.2	Procedure for the Solution of Equations	88
4.5	System Example	89
4.5.1	Simulation Using the Harmonic Admittance Algorithm . . .	89
4.6	Simulation Using EMTP	90
4.7	System Waveforms	94
4.8	Summary	95
5	Harmonic Analysis of an HVDC system	102
5.1	The Three Phase Converter Connected to an AC Network	102
5.1.1	System Equations	103
5.1.2	System Example	104
5.1.3	Simulation Results	106
5.1.4	System Waveforms	106
5.2	The Three-Phase Converter System with Source Harmonics	108
5.2.1	Simulation using the Harmonic Admittance Algorithm . . .	113
5.2.2	System Waveforms	113
5.3	The Three Phase Converter System with Unbalanced System Impedances	120
5.3.1	Simulation using the Harmonic Admittance Algorithm . . .	120
5.3.2	Simulation Results	122

5.4 Summary	126
6 Conclusions	127
6.1 Scope for Further Development	128
Appendix A: Gate Pulse Generator	136
Appendix B: Synchronization of Triggering Pulses in an HVDC System	141

List of Figures

2.1	The Single Phase Converter System	12
2.2	Simplified Single Phase Converter Model	13
2.3	Ideal Waveforms	14
2.4	DC Current for Rectifier Operation	18
2.5	DC Current for Inverter Operation	18
2.6	Voltage Distortion Factor	19
2.7	Output Voltage-Rectifier Operation	20
2.8	Output Voltage-Inverter Operation	20
2.9	Line Current-Rectifier Operation	21
2.10	Line Current-Inverter Operation	21
2.11	Voltage at P_{cc} -Rectifier Operation	22
2.12	Voltage at P_{cc} -Inverter Operation	22
2.13	A Simplified Diagram of the Three Phase Converter System	23
2.14	Ideal DC-side Voltage and AC-side Current Waveforms	25
2.15	DC Current in the Three Phase Converter-Converter Operation	29
2.16	DC Current in the Three Phase Converter-Inverter Operation	29
2.17	Voltage Distortion Factor in Three Phase Converter	30
2.18	Output Voltage of the Three Phase Converter-Rectifier Operation	31
2.19	Output Voltage of the Three Phase Converter-Inverter Operation	31
2.20	Voltage at P_{cc} of the Three Phase Converter-Rectifier Operation	32
2.21	Voltage at P_{cc} of the Three Phase Converter-Inverter Operation	32

2.22	Line Current in the Three Phase Converter-Rectifier Operation . . .	33
2.23	Line Current in the Three Phase Converter-Inverter Operation . . .	33
3.1	Single Phase Converter System	36
3.2	Switching Functions	38
3.3	Single Phase Converter Example	49
3.4	AC System Impedance	49
3.5	DC Component of the Converter Output Current	51
3.6	DC Component of the Converter Output Voltage	51
3.7	Harmonics in the AC Current	52
3.8	Harmonics in the Voltage at the Point of Common Coupling	52
3.9	Harmonics in the Output Current	53
3.10	Harmonics in the Output Voltage	53
3.11	Frequency Spectrum of the AC Current for $\alpha = 45^\circ$	54
3.12	Frequency Spectrum of the AC Voltage at the Point of Common Coupling (P_{cc}) for $\alpha = 45^\circ$	54
3.13	Frequency Spectrum of the Converter Output Voltage for $\alpha = 45^\circ$	55
3.14	EMTP Model of the Single Phase Converter System	56
3.15	Voltage at the point of common coupling (P_{cc}), $\alpha = 57^\circ$	59
3.16	Voltage at the point of common coupling (P_{cc}), $\alpha = 45^\circ$	60
3.17	Voltage at the Converter AC Terminals, $\alpha = 57^\circ$	61
3.18	Voltage at the Converter AC Terminals, $\alpha = 45^\circ$	62
3.19	AC Current Waveform, $\alpha = 57^\circ$	63
3.20	AC Current Waveform, $\alpha = 45^\circ$	64
3.21	Voltage at the DC Terminals of the Converter, $\alpha = 57^\circ$	65
3.22	Voltage at the DC Terminals of the Converter, $\alpha = 45^\circ$	66
4.1	Three-Phase Converter Circuit	68

4.2	Switching Functions	70
4.3	Phase Currents and Output Voltage	71
4.4	Three-Phase Line Commutated Converter	78
4.5	Example HVDC System	89
4.6	DC Component of the Converter Output Current	91
4.7	DC Component of the Converter Output Voltage	91
4.8	Frequency Spectrum of the AC Current	92
4.9	Frequency Spectrum of the Output Voltage	92
4.10	Harmonics in the AC Current	93
4.11	Harmonics in the Output Voltage	93
4.12	Node Details of EMTP Model	94
4.13	Voltage at the Converter AC Terminals v_A^{ac} , $\alpha = 18^\circ$	96
4.14	Voltage at the Converter AC Terminals v_A^{ac} , $\alpha = 8^\circ$	97
4.15	AC Current Waveform i_a^{ac} , $\alpha = 18^\circ$	98
4.16	AC Current Waveform i_a^{ac} , $\alpha = 8^\circ$	99
4.17	Voltage at the DC Terminals of the Converter v_d^{dc} , $\alpha = 18^\circ$	100
4.18	Voltage at the DC Terminals of the Converter v_d^{dc} , $\alpha = 8^\circ$	101
5.1	Three Phase Converter Connected to the AC Network	103
5.2	An HVDC System Example	105
5.3	Harmonic Impedance of the Filter Network	106
5.4	Frequency Spectrum of the AC Current	107
5.5	Frequency Spectrum of the Output Voltage	107
5.6	Voltage at the Point of Common Coupling, v_a^{ac} , $\alpha = 18^\circ$	109
5.7	Voltage at the Converter AC Terminals, v_A^{ac} , $\alpha = 18^\circ$	110
5.8	AC Current Waveform, i_a^{ac} , $\alpha = 18^\circ$	111
5.9	Voltage at the DC Terminals of the Converter, v_d^{dc} , $\alpha = 18^\circ$	112
5.10	Source Voltage Spectrum	114

5.11	P_{cc} Voltage Spectrum	114
5.12	AC Current Spectrum	115
5.13	Output Voltage Spectrum	115
5.14	Voltage at the Point of Common Coupling, v_a^{ac} , $\alpha = 18^\circ$	116
5.15	Voltage at the Converter AC Terminals, v_A^{ac} , $\alpha = 18^\circ$	117
5.16	AC Current Waveform, i_a^{ac} , $\alpha = 18^\circ$	118
5.17	Voltage at the DC Terminals of the Converter, v_d^{dc} , $\alpha = 18^\circ$	119
5.18	Voltage at the DC Terminals of the Converter v_d^{dc} , $\alpha = 18^\circ$	123
5.19	Uncharacteristic Harmonics in the P_{cc} Voltage	124
5.20	Uncharacteristic Harmonics in the Converter Output Voltage	125
A.1	Gate Pulse Generation Concept	137
A.2	Gate Pulse Generation Steps	138
A.3	Double Pulsing	139
B.1	TACS model for input voltage tracking	142

List of Tables

4.1	Voltage Switching Functions	75
5.1	Parameters of the Filters	104
5.2	Modified Voltage Switching Functions	121
5.3	Modified Current Switching Functions	121

Chapter 1

Introduction

The study of harmonic interaction in ac power systems has taken on great importance because of the widespread use of electronic switching devices for power conversion and other nonlinear devices. Electronic switching in ac/dc converters generate current harmonics, which in turn interact with the ac system impedance to cause voltage distortions in the power system.

Depending on the amplitude of the harmonics entering the ac network and the dc line, some of the following undesirable effects may occur.

- Instability of the converter control.
- Errors in electronic instrumentation and control.
- Overheating of system equipment.
- Interference with telecommunication systems, especially noise on telephone lines. This effect may be propagated over great distances.

Power utilities are responsible for ensuring the quality and reliability of the power delivered to the consumers. Hence at a system planning level, there is a great need for evaluating the expected harmonics beforehand so that devices for the elimination of the undesired harmonics can be designed and implemented. The effectiveness of a system model to study the harmonic levels in the ac power system with converters depends on the following factors:

1. The extent to which the system model is simplified. Oversimplification leads to inaccurate prediction of the system harmonics.
2. The capability of the model to give a qualitative as well as quantitative information about the system.
3. The capability of the model to predict all harmonics, including uncharacteristic harmonics and harmonic instabilities.
4. The capability of the model to account for ac source harmonics as well as the harmonics generated by the converter.

Several researchers have addressed the problem of modeling accuracy for harmonic studies. Ultimately the accurate prediction of harmonics depends on the model of the source of harmonics, i.e. the converter. However, the model of the converter depends on the configuration, the ac voltages at the terminals of the converter, the dc load and the control principle for firing pulse generation.

For a given converter, the control principle determines the harmonics generated. Control principles that are commonly used can be classified as follows.

1. Phase control: The firing pulses are generated with the commutating voltage as the reference. The pulses are delayed with respect to the reference voltage.
2. Constant phase-angle control: Firing instants equally spaced with reference to their corresponding commutating voltages.
3. Equidistant firing control: Consecutive firings at equal intervals of the supply frequency.
4. Modulated phase-angle control: The firing pulses are phase-modulated.
5. Integral cycle control: Selects an integer number of complete cycles or half cycles of the supply frequency.

Of these methods, phase-angle control is the most widely used. Consequently in this thesis the phase angle control is selected for the study of harmonics generated by ac/dc converters.

1.1 Review of Methods for Harmonic Evaluation

Several harmonic analysis methods have been proposed in the literature to study the harmonic interaction between the power system and the power converter. These methods can be grouped into three categories: time domain analysis; frequency domain analysis; harmonic admittance analysis.

1.1.1 Time Domain Analysis

The time domain method is based on establishing a set of differential equations which describe the system. The solution of the equations is obtained using numerical integrating techniques. Reeve [1] and Kitchin [2] have discussed the use of time domain analysis method to model the overall system. In the proposed methods, numerical techniques are used to obtain a point-by-point representation of the system voltages and currents. On reaching steady-state, the harmonic spectra of the system voltages and currents are obtained using Fourier analysis. The results are to a great extent dependent on the time step used in the numerical solution. The method is capable of predicting the transient behaviour and harmonic instability in the system. However it is computationally demanding especially when applied to large systems.

1.1.2 Frequency Domain Analysis

The conventional approach widely used to evaluate harmonics in power converters is the frequency domain analysis. Kitchin [2] explains the theoretical basis of the method in detail. This approach is based on the assumption that the phase con-

trolled converter draws current from purely sinusoidal sources with purely inductive source impedances. Fourier analysis of the current waveforms resulting from the operation of the converter predicts characteristic harmonic components of the order $n = pk \pm 1$, where p is the number of pulses of the converter and $k=1,2,\dots$. The converter is modeled as an ideal harmonic current source and the effect of each harmonic component on the system is considered separately. The overall effect of harmonics on the system is obtained in the frequency domain using the principle of superposition. The method, also referred to as the current injection method, can be modified to include the effects of the phase control angle and the commutating inductance. It can also be extended to systems connected to multiple converters. The method is too idealized for practical systems. Converters, in practice, do not generate constant harmonic currents irrespective of the conditions that exist in the ac power system. In addition, the method cannot predict harmonics under resonant conditions.

Many researchers have made efforts to use more advanced frequency domain methods to study the effects of individual system parameters on harmonics under steady-state conditions. The effect of uncharacteristic harmonics and errors in the firing pulses are investigated in [3]. Unbalance condition in the transformer impedance and its effect on the operation and harmonics is discussed by Rao [4]. If the ac system voltage is unbalanced additional uncharacteristic harmonics are generated in the ac current. This problem is investigated by Reeve, *et. al.*, [5]. Although these methods are helpful in demonstrating the effect of particular parameters on harmonics they do not consider the interaction between the dc harmonics and the ac harmonics since the dc side current is assumed to be harmonic-free.

Mathur [6] presents a technique for evaluating the dc side current and voltage harmonics for unbalanced ac sources due to the reactance of the converter transformer. However the ac side is treated separately from the dc side and the

harmonic interactions between the two sides are not considered in the algorithm. Reeve, *et. al.*, [7] propose a technique which attempts to eliminate or overcome most of the above-mentioned disadvantages. The technique determines the new operating conditions of the system by iteratively updating the system voltages. This technique is very effective in studying the system behaviour along with the harmonic interaction, but it neglects the dc side impedances.

A method for harmonic studies based on nonlinear frequency domain analysis has been proposed by Christoforidis, *et. al.* [8]. The method gives a comprehensive model of the ac power system, converter substation and the dc side load. Although the work makes an important contribution in the selection of the type of ac system model for harmonic studies, it does not give the details of the various operating regions of the converter.

A state-variable approach has been proposed in the literature to automatically formulate three-phase ac network equations for harmonic studies [2]. These equations are then linked with the nonlinear converter equations to obtain a solution for the overall system. The results thus obtained account for the interaction of harmonics on the ac side. The method exhibits poor convergence characteristics and in some applications, has been found to diverge [7].

A comprehensive state-variable technique which eliminates most of the above mentioned disadvantages has been proposed by Yacamini [9]. The technique accounts for dc-side impedances, as well as the ac side imperfections such as harmonic voltage distortions on the supply voltages, unbalance conditions in the input voltages and system impedances. The method assumes a set of busbar voltages as the initial conditions and based on the method of firing used for the converter, the converter currents are calculated. The results are then used with the current injection method to calculate the dc side voltage and current harmonics and the ac side quantities. The method suffers from the limitations of the classical method,

i.e. inability to account for harmonic coupling on the dc and ac sides and to predict the stable regions of operation in terms of the firing angle and the overlap angle.

1.1.3 Harmonic Admittance Analysis

To overcome the drawbacks of the methods mentioned above, Jalali *et. al.* [10] proposed the harmonic admittance technique. This method uses the concept of transmission parameters (or A, B, C, D parameters) to obtain a relationship between the ac side and dc side quantities. Specifically the relationship between the input and output voltages and currents is obtained in terms of parameters which model the converter and the ac system. The converter parameters are defined in terms of the Fourier series representation of the switching functions which determine the converter current and voltage waveforms in every interval. The ac system impedance is modeled as an infinite-dimensional diagonal matrix at various harmonic frequencies.

The main features of the technique can be summarized as follows:

1. The approach models each component in the system (eg. the converter and the ac system) as a harmonic admittance matrix represented by the terminal voltages and currents in the Fourier form. The matrices are then coupled to represent the overall system. Apart from predicting the harmonic levels at any point for any required operating conditions, the method gives qualitative idea of the converter operation. It also allows the modeling procedure to be modularized so that different systems can be studied without extensive modifications of the system equations.
2. The harmonic admittance matrix of the converter couples all harmonics by means of a relationship between harmonic quantities on the ac side and the dc side expressed through the switching functions. The model also allows ac source harmonics to be incorporated and accurately models the interaction

between the power system and the converter.

3. The solution to the system equations provides a locally stable point which satisfies the operating conditions of the converter. Unbalanced systems can be studied because the phase voltage matrices and the phase impedance matrices are separately represented. The approach therefore is capable of predicting unstable operation or regions where periodic operation is not possible.

So far the harmonic admittance model has been confined to single phase systems [10]. With necessary modifications the technique can be applied to three-phase converter circuits and extended to any type of converter system connected to the ac network. This thesis focusses on the harmonic admittance technique and extends the concept to the implementation of a three-phase model of the ac/dc converter system and to the study of simple HVDC systems.

1.2 Simulation of Power Systems

Many techniques and models have been developed by researchers over the years to simulate the behaviour of a power system [11]-[15]. Since 1962 the electromagnetic transient program (EMTP) has become the accepted tool for the simulation, analysis, operation and design of power systems [16]- [18]. The EMTP is used to verify the correctness of the algorithm developed for the harmonic admittance technique presented in the thesis.

The EMTP is a complex and versatile computer program which helps utilities analyze electromagnetic transients affecting the operation and design of power systems.

The basic concepts and coding for modeling and simulation of power systems are presented in the EMTP rulebook [19]. The algorithm used in the EMTP is based on the solution of algebraic and differential equations associated with the

interconnection of electrical power system components and control systems. The equations are written in nodal-admittance form and are solved by ordered triangular factorisation. The program automatically determines the initial conditions using the linear elements. Under steady-state conditions normally the nonlinear elements are ignored. The output from the program lists the branch voltages and currents, node voltages and currents, values of control variables etc., as functions of time. One of the advantages of the program is the flexibility in modeling.

The addition of the module, Transient Analysis of Control Systems (TACS) to the EMTP makes the program more powerful and allows the dynamic interaction of the power system transients and control systems to be studied. It also provides means for modeling and simulating HVDC systems, static VAR compensators and other power system elements involving static switches, periodic pulses etc. TACS is used to simulate the triggering systems and the thyristors in the converter systems studied in the thesis. The methods for modeling various control system components are described in [20].

The components of the power system in EMTP are referred to as Network. The Network and TACS are considered to be two separate programs. They have different modeling techniques and input algorithms, and are solved separately and alternately. The Network solution is obtained from the time instant $t - \Delta t$ to t . But this solution uses the TACS variable conditions at time instant $t - \Delta t$. A similar process is repeated for every time instant. The time step, Δt is very important in the implementation of the triggering pulse generator. A longer time step would introduce delays in the application of the firing pulse. A smaller time step will result in minimum delay between the TACS and the Network. However, too small a time step will result in increased number of computations and memory.

1.3 Thesis Objectives and Outline

The harmonic admittance technique, first proposed by Jalali and Lasseter [10] for the single phase converter system, is the focus of the thesis. The broad aim of the research program is to develop a tool for accurately evaluating the harmonics and predicting the stable operating regions in a power system which incorporates ac/dc converters and static VAR compensators. As a first step towards realizing this goal, this thesis carries out harmonic studies in single phase and three-phase ac/dc converter systems using the harmonic admittance technique. The objectives of the thesis can be summarized as follows.

1. Develop a harmonic admittance model to predict the harmonics and stable operating conditions in an ac network connected to the three-phase converter.
2. Develop harmonic admittance model to predict the harmonics in an ac network with source harmonics and unbalanced ac side impedances.
3. Develop EMTF models and simulation of the system studied above in order to verify the harmonic admittance method.

The work presented in the thesis is organized as follows:

In chapter 2, the classical method for determining the harmonics in single phase and three-phase ac/dc converters is presented. Results based on the Fourier analysis of the converter waveforms are presented.

Chapter 3 introduces the harmonic admittance concept for the single phase ac/dc converter. The harmonic admittance model of a simple power system incorporating the single phase ac/dc converter is developed. The model is used to predict the harmonics and the operation of the single phase system. The results of the harmonic admittance model are verified using the EMTF.

In chapter 4, the implementation of the harmonic admittance method for a three-phase system is presented. A model of the three-phase ac/dc converter is

developed and used to predict the harmonic currents and voltages in a simple three-phase network. The correctness of the model and the algorithm is verified using EMTP to simulate the three-phase system.

The application of the harmonic admittance technique to the harmonic evaluation in a system with harmonics in the input source and a system with unbalanced ac side impedance is presented in chapter 5. An EMTP simulation of the same is also given.

Chapter 6 summarizes the results and contribution of the research and presents recommendations for further work.

Chapter 2

Harmonic Analysis of AC/DC Converters- The Classical Approach

As indicated in the previous chapter, the classical or conventional approach to calculate harmonic voltages is to first determine the Fourier series components of the ac current, and then multiply each harmonic current by the corresponding harmonic source impedance. This chapter provides a review of the conventional method and identifies the drawbacks associated with the method. The procedure and basic equations of the method are presented for the single-phase and three-phase ac/dc converter.

2.1 Harmonic Analysis of the Single Phase AC/DC Converter System

This section presents the classical method to compute the harmonics in the single-phase, phase-controlled ac/dc converters.

2.1.1 The Single Phase AC/DC Converter System

In order to demonstrate the analysis procedure for determining the harmonic interaction of the single phase converter with the ac system, the configuration of Fig. 2.1 is considered. The commutating inductance L_c may represent the inductance of the

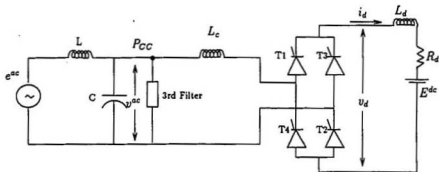


Figure 2.1: The Single Phase Converter System

transformer which connects the converter to the ac system, or in the absence of a transformer, L_c represents the line inductance. The filter network consists of a third-order tuned filter and low-pass filter L-C. The filter network may be more complex than shown. For simplicity all resistances on the ac side are neglected. The dc load consists of a dc reactor, L_d and resistance R_d in series with a dc source E^{dc} . In Fig. 2.1, P_{cc} represents the point of common coupling, the supply point to other loads, where the voltage distortions are of interest.

The system can be reduced to a simple model which allows the voltage distortion at P_{cc} to be determined. Figure 2.2 shows a simplified model of the converter system. The ac source with the filter is modeled as a voltage source v_{ac} in series with an equivalent inductance L_{ac} .

2.1.2 Analysis of the Converter System

In order to reduce the harmonic analysis problem to manageable proportions, the following assumptions are made.

- The converter switches are ideal.
- The converter switching is ideal and symmetrical.

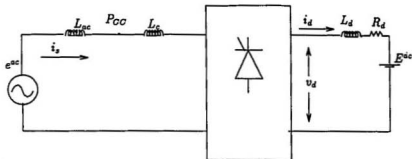


Figure 2.2: Simplified Single Phase Converter Model

- The inductance on the dc side is infinite, giving perfectly a smooth dc current.
- The converter operates in the continuous current mode.
- The resistances in the ac network are neglected.
- The ac source harmonics are neglected.

Figure 2.3 shows the ideal waveforms of the dc voltage, v_d and the ac current i_s .

1. DC-side Voltage Harmonics

The harmonic components of the dc voltage are obtained using Fourier series analysis [21]. The dc voltage, v_d can be expressed as

$$v_d = V_d + \sum_{n=1}^{\infty} A_n \cos n\omega t + B_n \sin n\omega t \quad (2.1)$$

where A_n and B_n are the Fourier coefficients and V_d is the dc component of the output voltage. From Fig. 2.3 the Fourier components are obtained as

$$A_n = \frac{2E_s}{\pi} \int_0^{\alpha} -\sin \omega t \cos n\omega t d(\omega t) + \frac{2E_s}{\pi} \int_{\alpha+\mu}^{\pi} \sin \omega t \cos n\omega t d(\omega t) \quad (2.2)$$

$$B_n = \frac{2E_s}{\pi} \int_0^{\alpha} -\sin \omega t \sin n\omega t d(\omega t) + \frac{2E_s}{\pi} \int_{\alpha+\mu}^{\pi} \sin \omega t \sin n\omega t d(\omega t) \quad (2.3)$$

and V_d is given by [22]

$$V_d = \frac{2E_s}{\pi} \left[\cos \alpha - \frac{X_s I_d}{E_s} \right] \quad (2.4)$$

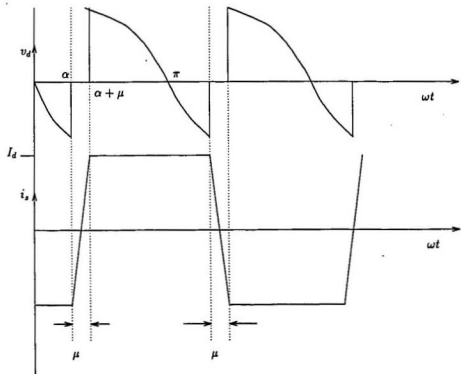


Figure 2.3: Ideal Waveforms

where

E_s is the peak value of the ac source voltage

α is the delay angle

μ is the commutating angle

X_s is the total source reactance at the fundamental frequency (i.e. $X_s = \omega(L_{ac} + L_c)$)

I_d is the dc current

The commutating angle μ is obtained from [22]

$$\cos(\alpha + \mu) = \cos\alpha - \frac{2X_s I_d}{E_s} \quad (2.5)$$

and the dc current I_d is given by

$$I_d = \frac{V_d - E^{dc}}{R_d} \quad (2.6)$$

2. AC-side Current Harmonics

The ideal line current waveform (approximated to trapezoidal waveshape) shown in Fig. 2.3 is an odd function and can be represented by the Fourier series

$$i_{sn} = \sum_{n=1,3,5}^{\infty} b_n \sin n\omega t \quad (2.7)$$

where

$$b_n = \frac{2}{\pi} \int_0^{\mu/2} \frac{I_d}{2} \sin n\omega t d(\omega t) + \frac{2}{\pi} \int_{\mu/2}^{\pi-\mu/2} I_d \sin n\omega t d(\omega t) + \frac{2}{\pi} \int_{\pi-\mu/2}^{\pi} \frac{I_d}{2} (\pi - \omega t) \sin n\omega t d(\omega t) \quad (2.8)$$

Equation (2.8) reduces to

$$b_n = \frac{2I_d \sin n(\mu/2)(1 - \cos n\pi)}{(\mu/2)\pi n^2} \quad (2.9)$$

or

$$b_n = \frac{4I_d \sin n(\mu/2)}{\frac{\mu}{2}\pi n^2}, n = 1, 3, 5... \quad (2.10)$$

Equation (2.10) shows that the ac side harmonics consist of the characteristic frequency components defined by

$$h = 2k \pm 1 \quad k = 1, 2, 3, \dots \quad (2.11)$$

3. AC-side Voltage Harmonics

The voltage harmonics at the point of common coupling are obtained by multiplying each harmonic component by the corresponding source impedance. At the point of common coupling the voltage harmonic is given by

$$V_n^{ac} = E_{sn}^{ac} - I_{sn} X_{acn} \quad (2.12)$$

The fundamental voltage at P_{cc} is obtained by subtracting (vectorially) the fundamental voltage drop across X_{ac1} from the undistorted source voltage.

$$V_1^{ac} = E_1^{ac} - I_{s1} X_{ac1} \quad (2.13)$$

and the percentage voltage distortion factor is defined by

$$DF = \frac{100}{V_1^{ac}} \sqrt{\sum_{n \neq 1}^{\infty} (V_n^{ac})^2} \quad (2.14)$$

2.1.3 Procedure for Computing Voltage Harmonics

Computation of the ac-side voltage harmonics requires the determination of the dc-side quantities V_d and I_d . For given values of the delay angle α , E^{dc} and R_d , equations (2.4) and (2.6) are solved for V_d and I_d . The commutation angle is then determined from equation (2.5). Equations (2.12) and (2.14) show that the computation of the ac-side harmonic voltages requires the knowledge of each harmonic current injected in the supply by the ac/dc converter. The harmonic currents are calculated from equation (2.10).

2.1.4 Results

Using the procedure outlined above, the voltage harmonics, voltage distortion factor and the effect of the ac-side inductance on the harmonics are investigated. For simplicity a reactance factor K defined by

$$K = \frac{X_c}{X_c + X_{sc}} \quad (2.15)$$

is introduced to study the effect of the ac-side inductance on the harmonics. The dc-side current is normalized with respect to the value of current corresponding to an overlap angle of 58° . The first twenty harmonics were used in the computation. The plots were obtained for the following values of the system parameters:

$$E^{dc} = 318 \text{ V}$$

$$R_d = 0.05 \ \Omega$$

$$L_d = 26.5 \text{ mH}$$

$$L_c = 0.265 \text{ mH}$$

$$E_s = 707 \text{ V}$$

1. DC-side Current as a Function of Overlap Angle

Figures 2.4 and 2.5 show the variation of the dc-side current I_d with the overlap angle for rectifier operation and inverter operation respectively for various firing angles, α . The classical method predicts a stable operation for a wide range of values of the commutation angle μ .

2. Voltage Distortion Factor

The effect of the ac-side reactance on the voltage distortion factor at the point, P_{cc} is shown in Fig. 2.6. The plots were obtained at various firing angles α as shown in the figure. It is observed that as the source reactance decreases in relation to the

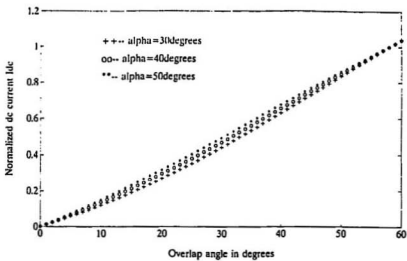


Figure 2.4: DC Current for Rectifier Operation

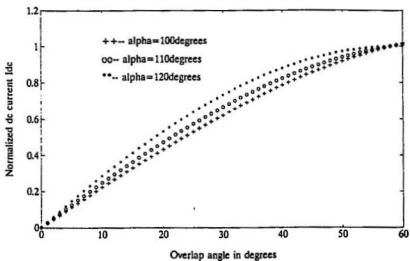


Figure 2.5: DC Current for Inverter Operation

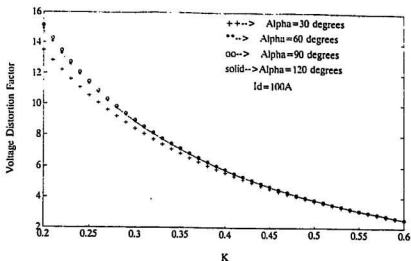


Figure 2.6: Voltage Distortion Factor

commutating reactance, the distortion factor decreases.

3. System Waveforms

Figures 2.7 and 2.8 show the reconstructed output voltage waveforms for $\alpha = 30^\circ$ and $\alpha = 101^\circ$. The waveforms are normalized with respect to E_s , and the value of μ was chosen to be 10 degrees. The accuracy of the waveforms can be improved by increasing the number of harmonic terms used in the calculation. The waveforms are as expected. Figures 2.9 and 2.10 show the corresponding ac currents normalized with respect to the steady-state dc current.

The reconstructed normalized voltage at the point of common coupling is shown in Figures 2.11 and 2.12 for rectifier and inverter operation. The figures clearly show that commutation produces notches which distort the waveform at P_{ce} .

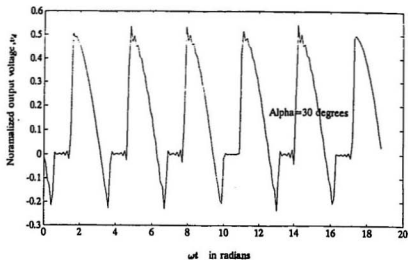


Figure 2.7: Output Voltage-Rectifier Operation

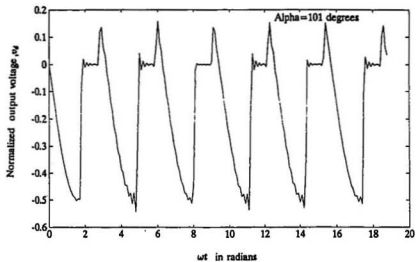


Figure 2.8: Output Voltage-Inverter Operation

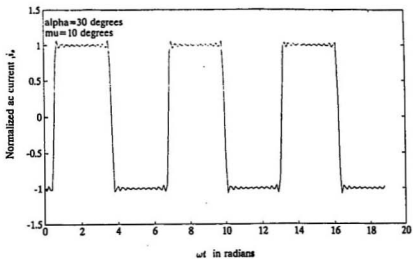


Figure 2.9: Line Current-Rectifier Operation

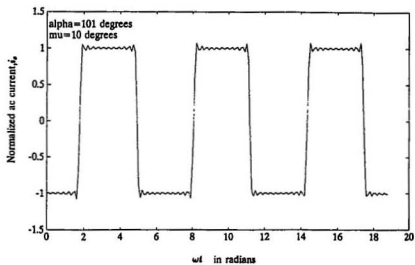
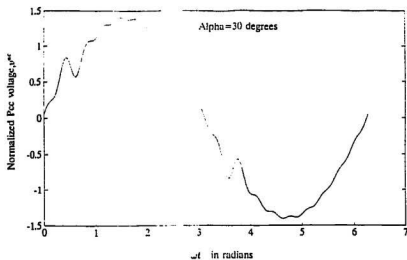
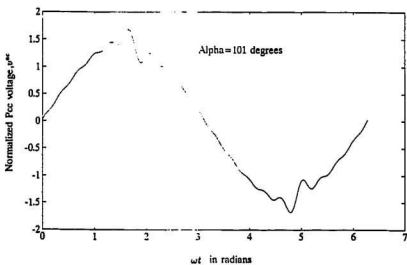


Figure 2.10: Line Current-Inverter Operation

Figure 2.11: Voltage at P_{cc} -Rectifier OperationFigure 2.12: Voltage at P_{cc} -Inverter Operation

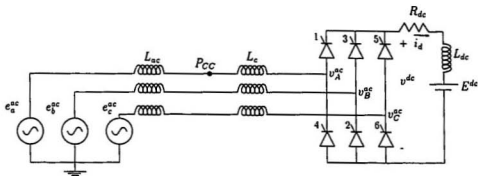


Figure 2.13: A Simplified Diagram of the Three Phase Converter System

2.2 Harmonic Analysis of the Three-phase AC/DC Converter System

The conventional method for determining harmonics in three-phase line commutated phase controlled converters is presented in this section. The characteristic harmonics of the converter on the ac side are presented in terms of the delay and commutation angles. Voltage harmonics and distortion factor at the point of common coupling are determined using a simple harmonic equivalent circuit model. Finally the limitations of the model are discussed.

2.2.1 The Three-Phase Converter System

The simplified three-phase converter system used for the study is shown in Fig. 2.13. The inductances L_{ac} and L_c respectively represent the source and transformer inductances and are assumed to be balanced. The source and transformer resistances are neglected. It is assumed that the dc inductor L_{dc} is sufficiently large to make the dc current constant and ripple-free. The thyristors are controlled using the conventional phase control firing scheme. The imperfections in the firing controller are neglected.

2.2.2 Analysis of the Converter System

Figure 2.14 shows the ideal waveforms of the dc voltage, v_d and the ac side current in phases a, b and c. Because of the source and transformer inductances the transfer of current from one phase to another is not instantaneous but requires a small commutation interval, μ . This introduces additional phase lag in the fundamental component of the phase current.

1. DC-side Voltage Harmonics

The harmonic components of the dc voltage are obtained using Fourier series analysis. The dc voltage, v_d can be expressed as

$$v_d = V_d + \sum_{n=1}^{\infty} C_n \cos(n\omega t + \phi_n) \quad (2.16)$$

where V_d is given by [23].

$$V_d = \frac{3E_m}{\pi} \cos\alpha - \frac{3X_s}{\pi} I_d \quad (2.17)$$

E_m is the peak value of the line-to-neutral source voltage. The rms values of the harmonic components of the output voltage are obtained using the formula [23]

$$\frac{C_n^2}{V_{do}^2} = \left(\frac{\cos[(n-1)\mu/2]}{n-1} \right)^2 + \left(\frac{\cos[(n+1)\mu/2]}{n+1} \right)^2 - 2 \left(\frac{\cos[(n-1)\mu/2]}{n-1} \right) \left(\frac{\cos[(n+1)\mu/2]}{n+1} \right) \cos(2\alpha + \mu) \quad (2.18)$$

where, α is the delay angle

μ is the commutating angle

n is the harmonic order

and V_{do} is the no load direct voltage given by

$$V_{do} = 3\sqrt{3}E_m/\pi \quad (2.19)$$

The angle ϕ_n in equation (2.18) is obtained using the formula [23]

$$\phi_n = \frac{(n+1)\alpha + (n+1)\delta}{n+1} - \frac{(n-1)\alpha + (n-1)\delta}{n-1} \quad (2.20)$$

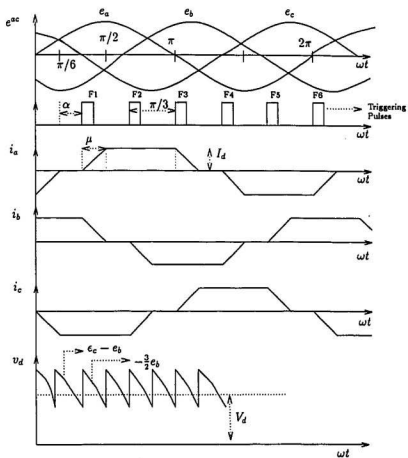


Figure 2.14: Ideal DC-side Voltage and AC-side Current Waveforms

where,

$$\delta = \alpha + \mu$$

The commutating angle μ is given by [22]

$$\cos(\alpha + \mu) = \cos\alpha - \frac{2X_s I_d}{\sqrt{3}E_m} \quad (2.21)$$

where, $X_s = X_{ac} + X_c$

and the dc current I_d is given by

$$I_d = \frac{V_d - E^{dc}}{R_d} \quad (2.22)$$

2. AC-side Current Harmonics

The current in phase-a can be represented by the Fourier series [24]

$$i_{an} = \sum_{n=1,5,7..}^{\infty} D_n \cos(n\omega t + \theta_n) \quad (2.23)$$

where,

$$D_1 = \frac{\sqrt{3}E_m}{\pi X_s \sqrt{2}} \sqrt{a_1^2 + b_1^2} \quad (2.24)$$

$$a_1 = \frac{\sqrt{3}}{4}\mu + \frac{3}{8} [\cos(2\alpha) - \cos(2\delta)] - \frac{\sqrt{3}}{8} [\sin(2\delta) - \sin(2\alpha)] \quad (2.25)$$

$$b_1 = \frac{3}{4}\mu + \frac{3}{8} [\sin(2\alpha) - \sin(2\delta)] - \frac{\sqrt{3}}{8} [\cos(2\delta) - \cos(2\alpha)] \quad (2.26)$$

$$\theta_1 = \tan^{-1}\left(\frac{b_1}{a_1}\right) \quad (2.27)$$

and for $n \neq 1$,

$$D_n = \frac{3E_m}{\pi X_s \sqrt{2}} \sqrt{a_n^2 + b_n^2 - 2a_n b_n \cos(2\alpha + \mu)} \quad (2.28)$$

$$a_n = \frac{\sin((n+1)\mu/2)}{n+1} \quad (2.29)$$

$$b_n = \frac{\sin((n-1)\mu/2)}{n-1} \quad (2.30)$$

$$\theta_n = \frac{-(n+1)\alpha + (n+1)\delta}{n+1} - \frac{-(n-1)\alpha + (n-1)\delta}{n-1} \quad (2.31)$$

The ac side current harmonics consist of the characteristic frequency components defined by $6k \pm 1$ for $k=1,2,3,\dots$

3. AC-side Voltage Harmonics

The voltage harmonics at the point of common coupling P_{cc} are obtained by multiplying each harmonic current by the corresponding source impedance. At P_{cc} the phase-a voltage harmonic is given by

$$V_{an}^{ac} = I_{an} \cdot X_{acn} = n I_{an} X_{ac1} \quad (2.32)$$

Substituting equation (2.28) into (2.32) gives

$$V_{an}^{ac} = \frac{3(1-K)C_1 E_m}{\pi\sqrt{2}} \quad (2.33)$$

where $K = X_c/X_s$. Similar to the single-phase case, the fundamental voltage at P_{cc} is given by

$$V_{a1}^{ac} = E_{a1} - I_{a1} X_{ac1} \quad (2.34)$$

Substituting equation (2.24) into (2.34) gives

$$V_{a1}^{ac} = E_{a1} - V_{s1} \quad (2.35)$$

where,

$$V_{s1} = \frac{\sqrt{3}(1-K)C_1 E_m}{\pi\sqrt{2}} \angle \theta_n = \text{Re}\{V_{s1}\} + j\text{Im}\{V_{s1}\} \quad (2.36)$$

The voltage distortion factor at P_{cc} is defined by

$$DF = \frac{100}{V_{a1}^{ac}} \sqrt{\sum_{n \neq 1}^{\infty} (V_n^{ac})^2} \quad (2.37)$$

2.2.3 Procedure for Computing Voltage Harmonics

For a given value of the delay angle α , E^{dc} and R_d , equations (2.17) and (2.22) are solved for V_d and I_d and the commutation angle μ is then determined from equation (2.21). Equations (2.32) to (2.37) show that the computation of the ac side harmonic voltages requires the knowledge of each harmonic current injected into the supply by the ac/dc converter. The harmonic currents are calculated from equations (2.23) through (2.31).

2.2.4 Results

The voltage harmonics, voltage distortion factor and the effect of the ac side inductance on the harmonics are investigated using the method outlined above. The system parameters used are as follows

$$E_s = 195kV$$

$$L_c = 24.08mH$$

$$E^{dc} = 242kV$$

1. DC-side Current as a Function of Overlap Angle

Figures 2.15 and 2.16 show the variation of the dc-side current I_d with the overlap angle μ for rectifier operation and inverter operation respectively. The plots are normalized with respect to the dc current at an overlap angle of 10° . The classical method predicts a stable operation for a wide range of values of angle μ . The plots show that the effect of α on the dc current becomes more pronounced for overlap angles greater than 30° .

2. Voltage Distortion Factor

The effect of the commutating reactance on the voltage distortion factor at the point of common coupling P_{cc} is shown in Fig. 2.17. The figure shows that the voltage distortion factor is almost independent of K for firing angles of 30° and 60° .

3. System Waveforms

Figures 2.18 and 2.19 show the output voltage waveforms for delay angles of 30° and 101° . The plots are normalized with respect to E_m . As expected the waveforms show the six-pulse operation of the converter. The accuracy of the waveforms depend on the number of harmonics calculated.

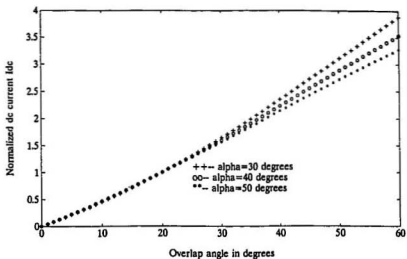


Figure 2.15: DC Current in the Three Phase Converter-Converter Operation

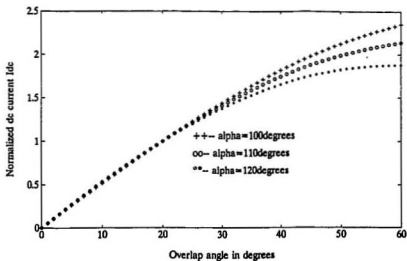


Figure 2.16: DC Current in the Three Phase Converter-Inverter Operation

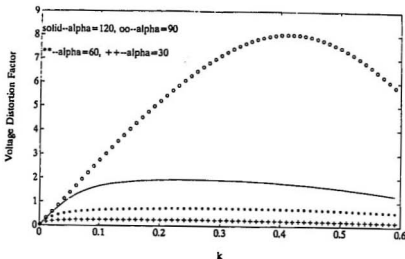


Figure 2.17: Voltage Distortion Factor in Three Phase Converter

Figures 2.20 and 2.21 show the normalized voltage at P_{cc} for delay angles 30° and 101° . The waveforms clearly show the commutation notches.

Figures 2.22 and 2.23 show the normalized line current waveforms for delay angles 30° and 101° . The plots are normalized with respect to the dc current. The waveforms are as expected.

2.3 Summary

The classical method of harmonic analysis presented in the chapter illustrates the limitations of the method. The accuracy of the results depends not only on the number of harmonic terms used in the calculation, but on the simplifying assumptions inherent in the prediction. For instance, the computation of voltage harmonic components at the point of common coupling, P_{cc} requires prior knowledge of the line current harmonics. However, the line current harmonics were obtained by neglecting the cross coupling between the ac-side and dc-side harmonics. A major limitation of the method is the inability to predict harmonic instabilities in the operation of the converters. In particular, for the single-phase converter, the classical

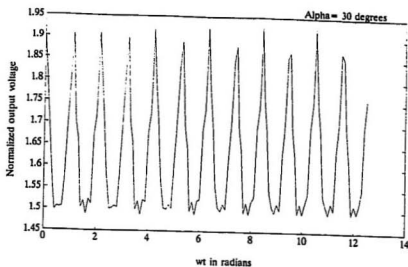


Figure 2.18: Output Voltage of the Three Phase Converter-Rectifier Operation

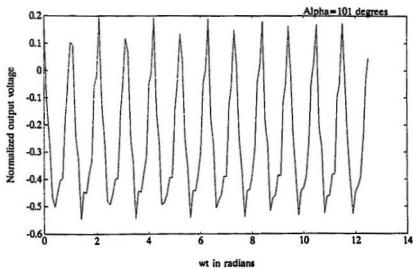


Figure 2.19: Output Voltage of the Three Phase Converter-Inverter Operation

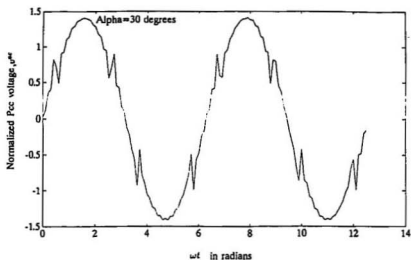


Figure 2.20: Voltage at P_{cc} of the Three Phase Converter-Rectifier Operation

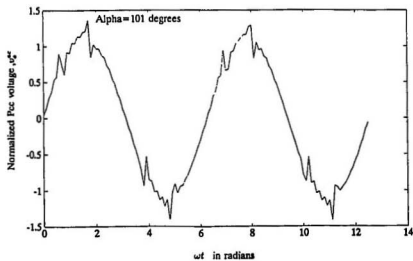


Figure 2.21: Voltage at P_{cc} of the Three Phase Converter-Inverter Operation

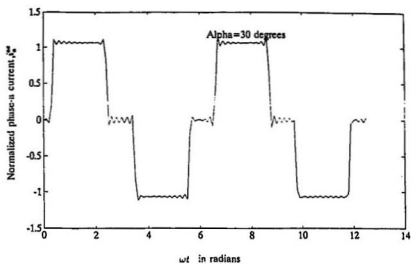


Figure 2.22: Line Current in the Three Phase Converter-Rectifier Operation

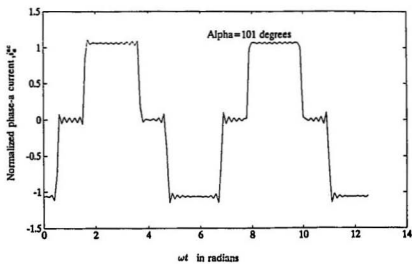


Figure 2.23: Line Current in the Three Phase Converter-Inverter Operation

method predicts stable operation for a wide range of firing angles and commutating overlap angles. In the next chapter it is shown that harmonic instabilities exist in the single-phase converter for a range of values of commutation overlap angles and firing angles.

Chapter 3

Harmonic Admittance Model for the Single Phase Converter

The objective of this chapter is to implement and verify the harmonic admittance method proposed by Jalali and Lasseter for the single phase converter [10]. Unlike the other methods, this method does not simplify the model of the power system and switching circuits. It provides both qualitative and quantitative information about the harmonic interactions between the ac system and the converter switching circuits. In this chapter, a harmonic admittance model is developed for a single phase ac/dc converter connected to the power system. The model is used to determine the harmonics at various nodes in the system, and the results thus obtained are verified using EMTP simulation.

3.1 The Single Phase Converter Connected to the AC System

In order to demonstrate the analysis procedure for determining the harmonic interaction of the single-phase converter with the ac systems, the single-phase line commutated bridge converter configuration shown in Fig. 3.1 is considered. The circuit has a thyristor bridge with a dc load consisting of a reactor and resistor in series with the dc source. The dc side inductance L_{dc} is sufficiently large to maintain a continuous dc current i_{dc} . The ohmic losses in the thyristors 1 through

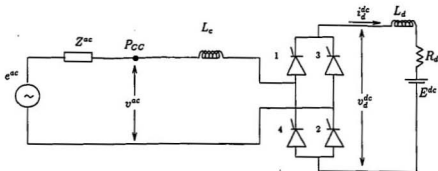


Figure 3.1: Single Phase Converter System

4 are neglected. The dc source voltage is assumed to be constant. The ac system impedance is represented by Z^{ac} . AC filters are located at the point of common coupling, P_{cc} . Any ac system network along with the filters and line impedance can be reduced to Z^{ac} (which is the Thevenin equivalent impedance of the network as seen from the P_{cc}) in series with the ac source, e^{ac} .

3.2 Harmonic Admittance Matrix for the Single Phase Converter

The single-phase converter and the commutating inductance may be modeled as a two-port network at the point of common coupling. The input variables of the two-port network are v^{ac} and i^{ac} and the output variables are i^{dc} and v^{dc} . Choosing v^{ac} and i^{dc} as the independent variables, the two-port network can be represented by the A, B, C, D parameters as

$$\begin{bmatrix} \mathbf{I}^{ac} \\ \mathbf{V}^{dc} \end{bmatrix} = \begin{bmatrix} \mathbf{A} & \mathbf{B} \\ \mathbf{C} & \mathbf{D} \end{bmatrix} \begin{bmatrix} \mathbf{V}^{ac} \\ \mathbf{I}^{dc} \end{bmatrix} \quad (3.1)$$

\mathbf{V}^{ac} is a matrix of Fourier series representation of the ac voltage at the point of common coupling (P_{cc}). \mathbf{I}^{ac} , \mathbf{V}^{dc} and \mathbf{I}^{dc} are the Fourier matrix representation of the ac current, i^{ac} , the dc voltage, v^{dc} and the dc current, i^{dc} respectively. The

matrices **A**, **B**, **C** and **D** are infinite dimensional and are dependent upon switching functions which determine the converter states and the commutating inductor L_c . All the elements in the input/output parameter matrix in equation (3.1) contain infinite dimensional Fourier series representations. Equation (3.1) is therefore referred to as the harmonic admittance matrix. It provides a relationship between the harmonics of the ac current, ac voltage, dc current and dc voltage.

3.3 Elements of the Harmonic Admittance Matrix

In this section, the Fourier series representation of the elements in the harmonic admittance matrix (equation 3.1) are derived. Since the harmonics in the converter are a result of the switching action of the thyristors, the switching states are defined by switching functions which carry on/off information of the thyristors in the converter. The switching functions consist of the following:

1. Switching functions that define the conduction of the two thyristor pairs, namely the positive pair (1, 2) and the negative pair (3, 4).
2. Switching functions that define the commutation overlap interval.

Figure 3.2 shows the ideal switching functions for the single-phase bridge converter. The switching function H^1 has a value of one when the thyristor pair (1, 2) is conducting and zero when it is off. The application of a firing pulse starts the commutation process which continues for a duration equal to the overlap angle, μ . The switching function H^{13} defines the commutation of thyristor 1 or thyristor 2. H^{13} has a value of one from the instant of firing of thyristors 1 and 2 till the lapse of the overlap interval. The switching functions H^3 and H^{31} respectively define the conduction of the thyristor pair (3, 4) and the commutation of thyristor 3 or thyristor 4.

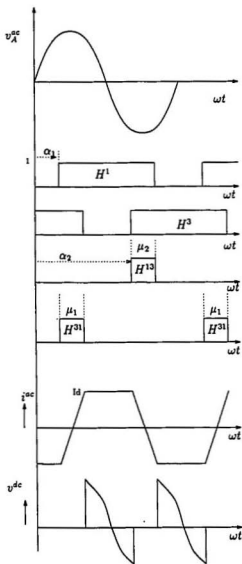


Figure 3.2: Switching Functions

3.3.1 Harmonic Representation of the Switching Functions

Any switching function can be mathematically represented by

$$H(\omega t) = \sum_{n=-\infty}^{n=\infty} h_n e^{-jn\omega t} \quad (3.2)$$

h_n is the n th harmonic component of the Fourier series representation of $H(\omega t)$, and is defined as

$$h_n = \frac{1}{2\pi} \int_{\omega t_1}^{\omega(t_1+T)} H(\omega t) e^{-jn\omega t} d(\omega t) \quad (3.3)$$

where t_1 is the beginning of the switching interval and T is the duration of the switching interval. $H(\omega t)$ has a value of unity during the interval t_1 to $t_1 + T$. If α_1 and α_2 are the firing angles and μ_1 and μ_2 are the overlap angles for each pair of thyristors respectively, the n th harmonic components of the switching functions can be derived using equations(3.2) and (3.3) as follows:

$$h_{n=0}^{31} = \frac{\mu_1}{2\pi} \quad (3.4)$$

$$h_{n \neq 0}^{31} = \frac{j}{2n\pi} e^{-jn\alpha_1} [e^{-jn\mu_1} - 1] \quad (3.5)$$

$$h_{n=0}^{13} = \frac{\mu_2}{2\pi} \quad (3.6)$$

$$h_{n \neq 0}^{13} = \frac{j}{2n\pi} [e^{-jn\alpha_2} (e^{-jn\mu_1} - 1)] \quad (3.7)$$

$$h_{n=0}^1 = \frac{\alpha_2 - \alpha_1 + \mu_2}{2\pi} \quad (3.8)$$

$$h_{n \neq 0}^1 = \frac{j}{2n\pi} [e^{-jn\alpha_1} (e^{-jn(\alpha_1 + \mu_1)} - 1)] \quad (3.9)$$

$$h_{n=0}^3 = \frac{2\pi - \alpha_2 + \alpha_1 + \mu_1}{2\pi} \quad (3.10)$$

$$h_{n \neq 0}^3 = \frac{j}{2n\pi} [e^{-jn(\alpha_1 + \mu_1)} - e^{-jn\alpha_2}] \quad (3.11)$$

3.3.2 Harmonic Representation of the AC Current

The ac current is obtained as a linear combination of the switching functions, the current during the commutation overlap and the dc current. The Fourier matrix

representation of the ac current can therefore be obtained as the sum of the Fourier matrix representation of the regions defined below:

1. Current in the regions where the thyristors are in inter-commutation mode. (i.e when only one thyristor pair is conducting)
2. Current during the commutation overlap interval. (i.e when both thyristor pairs are conducting).

When the converter is operating in the continuous mode, $i^{ac}(\omega t)$ is the sum of the current vectors corresponding to the four switching functions.

$$i^{ac}(\omega t) = I^1(\omega t) + I^2(\omega t) + I^{13}(\omega t) + I^{31}(\omega t) \quad (3.12)$$

The quantities in equation (3.12) are defined below.

1. Current during the inter commutation period

The quantities $I^1(\omega t)$ and $I^2(\omega t)$ are the components of currents when the positive pair of thyristors (1, 2) and the negative pair of thyristors (3, 4) conduct respectively. As the magnitude of the ac current during these periods is equal to the steady state dc current i^{dc} , the current are expressed in terms of the switching functions and the dc current.

The ac current when the positive pair (1, 2) is conducting is defined as

$$I^1(\omega t) = [H^1(\omega t) - H^{13}(\omega t) - H^{31}(\omega t)]i^{dc}(\omega t) \quad (3.13)$$

The ac current is equal to $-I^{dc}$ when the negative pair (2, 4) is conducting. The current during this period is given by

$$I^2(\omega t) = -[H^2(\omega t) - H^{23}(\omega t) - H^{32}(\omega t)]i^{dc}(\omega t) \quad (3.14)$$

The Fourier matrix representation of the ac current during these intervals can be obtained from equations (3.13) and (3.14) as

$$I^1 = [H^1 - H^{13} - H^{31}]I^{dc} \quad (3.15)$$

and

$$\mathbf{I}^3 = -[\mathbf{H}^3 - \mathbf{H}^{13} - \mathbf{H}^{31}]\mathbf{I}^{\text{dc}} \quad (3.16)$$

The matrices \mathbf{H}^1 , \mathbf{H}^3 , \mathbf{H}^{13} and \mathbf{H}^{31} are similar in structure. \mathbf{H}^{31} is defined as

$$\mathbf{H}^{31} = \begin{bmatrix} \cdot & \cdot \\ \cdot & \cdot \\ \cdot & \cdot & h_0^{31} & h_{-1}^{31} & h_{-2}^{31} & \cdot & \cdot & \cdot \\ \cdot & \cdot & h_1^{31} & h_0^{31} & h_{-1}^{31} & \cdot & \cdot & \cdot \\ \cdot & \cdot & h_2^{31} & h_1^{31} & h_0^{31} & \cdot & \cdot & \cdot \\ \cdot & \cdot \\ \cdot & \cdot \end{bmatrix} \quad (3.17)$$

From equations (3.15) and (3.16)

$$\mathbf{I}^1 + \mathbf{I}^3 = [\mathbf{H}^1 - \mathbf{H}^3]\mathbf{I}^{\text{dc}} \quad (3.18)$$

2. Current during the commutation interval

The quantities $I^{31}(\omega t)$ and $I^{13}(\omega t)$ are the components of currents during the commutation of thyristor 3 and thyristor 1 respectively. In terms of the switching functions, these currents are defined as

$$I^{31}(\omega t) = H^{31}(\omega t)I(\omega t) \quad (3.19)$$

and

$$I^{13}(\omega t) = H^{13}(\omega t)I(\omega t) \quad (3.20)$$

where $I(\omega t)$ is the current during the corresponding commutation interval.

During the commutation process all the thyristors (1, 2, 3 and 4) are conducting. The equivalent circuit during this interval consists of the inductor, L_c across the ac voltage at P_{cc} , v^{ac} . The current during the commutation interval, $I(\omega t)$ can be expressed as

$$I(\omega t) = \int_{\omega t_1}^{\omega t} \frac{v^{ac}}{L_c} d\omega t + i^{ac}(\omega t = \omega t_1) \quad (3.21)$$

where t_1 is the time instant at which the firing pulse is applied and $i^{ac}(\omega t = \omega t_1)$ is the current in the circuit at the start of commutation.

a. Commutation from thyristor 3 to 1

The ac current during the commutation interval is obtained from equation (3.21) as

$$i^{ac}(\omega t) = I(\omega t) = \int_{\alpha_1}^{\omega t} \frac{v^{ac}}{\omega L_c} d\omega t - i^{dc}(\omega t = \alpha_1) \quad (3.22)$$

where α_1 is the beginning of the commutation from thyristor 3 to thyristor 1 and $i^{dc}(\omega t = \alpha_1)$ is the ac current at the start of commutation. In the steady state when $I(\omega t)$, $v^{ac}(\omega t)$ are periodic, equation (3.22) can be represented by a Fourier series. The Fourier coefficients of $I(\omega t)$ are defined as follows [10].

$$\sum_{n=-\infty}^{\infty} I_n e^{jn\omega t} = \sum_{\substack{n=-\infty \\ n \neq 0}}^{\infty} \frac{V_n^{ac}}{jn\omega L_c} e^{jn\omega t} - \sum_{\substack{n=-\infty \\ n \neq 0}}^{\infty} \frac{V_n^{ac}}{jn\omega L_c} e^{jn\alpha_1} - \sum_{n=-\infty}^{\infty} I_n^{dc} e^{jn\alpha_1} \quad (3.23)$$

V_n^{ac} is the nth harmonic component of the voltage at P_{cc} , I_n^{dc} is the nth harmonic component of the dc current. Multiplying both sides of equation (3.23) by the orthogonal function $e^{-jn\omega t}$ and integrating over a period gives

$$I_{n=0} = - \sum_{\substack{m=-\infty \\ m \neq 0}}^{\infty} \frac{V_m^{ac}}{jm\omega L_c} e^{jm\alpha_1} - \sum_{m=-\infty}^{\infty} I_m^{dc} e^{jm\alpha_1} \quad (3.24)$$

$$I_{n \neq 0} = \frac{V_n^{ac}}{jn\omega L_c} \quad (3.25)$$

where the suffix n and m denote the order of harmonic. The Fourier representation of the ac current during the commutation interval in equations (3.24) and (3.25) can be rewritten in the general form

$$\mathbf{I}_n = \mathbf{YV}^{ac} - \mathbf{G}(\alpha_1)[\mathbf{I}^{dc} + \mathbf{YV}^{ac}] \quad (3.26)$$

where

$$\mathbf{I}_n = \begin{bmatrix} \vdots \\ I_{-1} \\ I_0 \\ I_1 \\ \vdots \end{bmatrix} \quad (3.27)$$

\mathbf{Y} is the diagonal matrix with elements defined by

$$Y = \frac{1}{jn\omega L_c} \quad (3.28)$$

$\mathbf{G}(\alpha_1)$ defines $e^{jn\alpha_1}$ terms in the matrix

$$\mathbf{G}(\alpha_1) = \begin{bmatrix} \cdot & \cdot \\ \cdot & \cdot \\ \cdot & \cdot & 0 & 0 & 0 & \cdot & \cdot & \cdot \\ \cdot & \cdot & e^{-j\alpha_1} & 1 & e^{j\alpha_1} & \cdot & \cdot & \cdot \\ \cdot & \cdot & 0 & 0 & 0 & \cdot & \cdot & \cdot \\ \cdot & \cdot \\ \cdot & \cdot \end{bmatrix} \quad (3.29)$$

The current during the commutation interval is obtained from equation (3.19), which can be written in the Fourier matrix form as

$$\mathbf{I}^{31} = \mathbf{H}^{31} \mathbf{I}_n \quad (3.30)$$

From equation (3.26), the Fourier matrix representation of \mathbf{I}^{31} can be written as

$$\mathbf{I}^{31} = \mathbf{H}^{31} [\mathbf{YV}^{ac} - \mathbf{G}(\alpha_1)[\mathbf{YV}^{ac} + \mathbf{I}^{dc}]] \quad (3.31)$$

b. Commutation from thyristor 1 to 3

Using the procedure outlined above, the Fourier matrix representation of the current during commutation from thyristor 1 to thyristor 3 can be obtained from equation (3.31) in terms of \mathbf{H}^{13} , $\mathbf{G}(\alpha_2)$ and \mathbf{I}^{dc} as

$$\mathbf{I}^{13} = \mathbf{H}^{13} [\mathbf{YV}^{ac} - \mathbf{G}(\alpha_2)[\mathbf{YV}^{ac} - \mathbf{I}^{dc}]] \quad (3.32)$$

where $\mathbf{G}(\alpha_2)$ is structurally identical to $\mathbf{G}(\alpha_1)$.

Finally, substituting equations (3.18), (3.31) and (3.32) into equation (3.12) the Fourier matrix expression for the ac current, \mathbf{I}^{ac} is obtained as

$$\begin{aligned} \mathbf{I}^{ac} = & (\mathbf{H}^1 - \mathbf{H}^3) \mathbf{I}^{dc} + \\ & \mathbf{H}^{31} [\mathbf{YV}^{ac} - \mathbf{G}(\alpha_1)(\mathbf{YV}^{ac} + \mathbf{I}^{dc})] + \\ & \mathbf{H}^{13} [\mathbf{YV}^{ac} \mathbf{G}(\alpha_2)(\mathbf{YV}^{ac} - \mathbf{I}^{dc})] \end{aligned} \quad (3.33)$$

3.3.3 Harmonic Representation of the DC Voltage

From Fig. 3.2, the output voltage, v^{dc} can be derived from the voltage at the converter terminals, v_A^{ac} and the switching functions as

$$v^{dc}(\omega t) = [H^1(\omega t) - H^3(\omega t)] v_A^{ac}(\omega t) \quad (3.34)$$

The Fourier matrix expression for the dc voltage V^{dc} can be found in terms of V_A^{ac} , I^{ac} and the switching functions. In the frequency domain V_A^{ac} is obtained as (Fig. 3.1)

$$V_A^{ac} = V^{ac} - ZI^{ac} \quad (3.35)$$

where Z is the diagonal matrix with elements $j\omega L_c$. The resulting Fourier matrix representation for the dc voltage is obtained from equations (3.34) and (3.35) as

$$V^{dc} = (H^1 - H^3)(V^{ac} - ZI^{ac}) \quad (3.36)$$

3.3.4 A, B, C and D parameters of the Single Phase Converter

From equation (3.1) the expressions for I^{ac} and V^{dc} are obtained as

$$I^{ac} = AV^{ac} + BI^{dc} \quad (3.37)$$

and

$$V^{dc} = CV^{ac} + DI^{dc} \quad (3.38)$$

Isolating the coefficients from the expression for I^{ac} (equation (3.33)) and comparing with equation (3.37) the A and B parameters can be obtained as

$$A = [H^{31}(I^M - G(\alpha_1)) + H^{13}(I^M - G(\alpha_2))]Y \quad (3.39)$$

$$B = H^1 - H^3 - (H^{31}G(\alpha_1)) + (H^{13}G(\alpha_2)) \quad (3.40)$$

where I^M is an identity matrix. Substituting equation (3.37) into equation (3.36), the expression for V^{dc} can be rewritten as

$$V^{dc} = (H^1 - H^3)[V^{ac} - Z(AV^{ac} + BI^{dc})] \quad (3.41)$$

Isolating the coefficients from the expression for V^{dc} (equation 3.41) and comparing with equation (3.38), the C and D parameters are obtained as

$$C = (H^1 - H^3)(I^M - ZA) \quad (3.42)$$

$$D = (H^3 - H^1)ZB \quad (3.43)$$

The above equations illustrate the coupling between the harmonics in a single phase ac system. For example the ac current in equation (3.37) has the following matrix representation:

$$\begin{bmatrix} \cdot \\ \cdot \\ I_{-1}^{ac} \\ I_0^{ac} \\ I_1^{ac} \\ \cdot \\ \cdot \end{bmatrix} = \begin{bmatrix} \cdot & \cdot & \cdot & \cdot & \cdot & \cdot & \cdot \\ \cdot & \cdot & \cdot & \cdot & \cdot & \cdot & \cdot \\ \cdot & \cdot & a_0 & a_{-1} & a_{-2} & \cdot & \cdot \\ \cdot & \cdot & a_1 & a_0 & a_{-1} & \cdot & \cdot \\ \cdot & \cdot & a_2 & a_1 & a_0 & \cdot & \cdot \\ \cdot & \cdot & \cdot & \cdot & \cdot & \cdot & \cdot \\ \cdot & \cdot & \cdot & \cdot & \cdot & \cdot & \cdot \end{bmatrix} \begin{bmatrix} \cdot \\ \cdot \\ V_{-1}^{ac} \\ V_0^{ac} \\ V_1^{ac} \\ \cdot \\ \cdot \end{bmatrix} + \begin{bmatrix} \cdot & \cdot & \cdot & \cdot & \cdot & \cdot & \cdot \\ \cdot & \cdot & \cdot & \cdot & \cdot & \cdot & \cdot \\ \cdot & \cdot & b_0 & b_{-1} & b_{-2} & \cdot & \cdot \\ \cdot & \cdot & b_1 & b_0 & b_{-1} & \cdot & \cdot \\ \cdot & \cdot & b_2 & b_1 & b_0 & \cdot & \cdot \\ \cdot & \cdot & \cdot & \cdot & \cdot & \cdot & \cdot \\ \cdot & \cdot & \cdot & \cdot & \cdot & \cdot & \cdot \end{bmatrix} \begin{bmatrix} \cdot \\ \cdot \\ I_{-1}^{dc} \\ I_0^{dc} \\ I_1^{dc} \\ \cdot \\ \cdot \end{bmatrix} \quad (3.44)$$

A single frequency of the ac current is coupled to all the harmonics of the ac voltage and dc current through the matrices A and B.

Equation (3.1) can be used to solve for the ac current, ac voltage at P_{cc} and the dc voltage at the converter output terminals. However in a practical system only the source voltage E^{ac} and the dc voltage E^{dc} are known. From Fig. 3.1, the relationship between the voltages is given by

$$\begin{bmatrix} V^{ac} \\ V^{dc} \end{bmatrix} = \begin{bmatrix} -Z^{ac} & 0 \\ 0 & Z^{dc} \end{bmatrix} \begin{bmatrix} I^{ac} \\ I^{dc} \end{bmatrix} + \begin{bmatrix} E^{ac} \\ E^{dc} \end{bmatrix} \quad (3.45)$$

where Z^{ac} and Z^{dc} are the diagonal matrices of the ac and dc impedances respectively. Substituting I^{ac} and V^{dc} (from equations (3.37) and (3.38)) and rearranging

results in the following equation.

$$\begin{bmatrix} \mathbf{E}^{dc} \\ \mathbf{E}^{ac} \end{bmatrix} = \begin{bmatrix} \mathbf{C} & \mathbf{D} - \mathbf{Z}^{dc} \\ \mathbf{I} + \mathbf{Z}^{ac}\mathbf{A} & \mathbf{Z}^{ac}\mathbf{B} \end{bmatrix} \begin{bmatrix} \mathbf{V}^{ac} \\ \mathbf{I}^{dc} \end{bmatrix} \quad (3.46)$$

For given system parameters and defined ac and dc voltages the harmonic components of \mathbf{V}^{ac} and \mathbf{I}^{dc} can be determined from equation (3.46).

3.4 Solution of System Equations

Using the harmonic admittance matrix the harmonics in the single phase converter system can be studied. In this section the procedure for calculating the harmonics is outlined.

3.4.1 Constraint Equation

The harmonic admittance matrix given by equation (3.1) relates the ac current, ac voltage, dc current and the dc voltage through the matrices \mathbf{A} , \mathbf{B} , \mathbf{C} and \mathbf{D} . These parameter matrices are functions of the firing angles α_1 , α_2 and the overlap angles μ_1 , μ_2 . It can be assumed that the firing instants are symmetrical. (i.e. $\alpha_1 = \alpha$, $\alpha_2 = \pi + \alpha$). The overlap angles are assumed to be of the same width (i.e. $\mu_1 = \mu_2 = \mu$).

To be able to solve for the quantities given in equation (3.46), it is necessary to have one more equation relating α and μ . This equation can be obtained by equating the ac side current and the dc side current at the end of commutation. For example, at the end of the commutation from thyristor 3 to thyristor 1 the ac side current is equal to the dc current, and the following relationship can be defined:

$$I^{ac}(\omega t = \alpha + \mu) = I^{dc}(\omega t = \alpha + \mu) \quad (3.47)$$

Equation (3.47) can be expressed in the Fourier matrix form as

$$\sum_{\substack{n=-\infty \\ n \neq 0}}^{\infty} \frac{V_n^{ac}}{jn\omega L_c} e^{jn\alpha} [e^{jn\mu} - 1] = \sum_{n=-\infty}^{\infty} I_n^{dc} e^{jn\alpha} [1 + e^{jn\mu}] \quad (3.48)$$

Equation (3.48) is the constraint equation which ensures unique solution of the system equations.

3.4.2 Procedure for the Solution of System Equations

The system harmonics can be determined from equations (3.1),

(3.45) and (3.46) using the procedure outlined below.

1. Select a firing angle α .
2. Choose a reasonable value of the overlap angle μ .
3. Evaluate the parameter matrices **A**, **B**, **C**, **D** from equations (3.39), (3.40), (3.42) and (3.43).
4. Solve for \mathbf{V}^{ac} and \mathbf{I}^{dc} using equation (3.46).
5. Check whether equation (3.48) is satisfied.
6. While equation (3.48) is not satisfied repeat steps 3 and 4 by updating the value of μ . Iterate until equation (3.48) is satisfied.
7. Solve for \mathbf{V}^{dc} and \mathbf{I}^{ac} using equation (3.1).

Since the system equations are infinite matrices, the accuracy of the solution depends on the number of harmonic components considered in the solution. In the thesis, taking harmonic components up to the 20th was found to provide reasonably accurate results. The system equations were solved using FORTRAN [26] and MATLAB [27]. The number of iterations varied from 10 to 15 and typically took about 1.5 min of CPU time to obtain results for a given firing angle.

3.5 System Example

The system shown in Fig. 3.3 is used as an example to demonstrate the use of the harmonic admittance procedure outlined above to determine the harmonics in a

single-phase converter system. The third harmonic filter shown in the figure has an inductance of $2.9mH$ in series with a capacitor of value $269.6\mu F$.

With the converter open, the impedance of the ac system as a function of frequency was determined. Figure 3.4 shows the characteristic of the ac system impedance. The figure shows that the ac system with the converter open is resonant at 4.5 times the fundamental frequency. The system is likely to exhibit harmonic resonance problem since the resonant point of the ac system is close to an odd harmonic number.

3.5.1 Simulation using the Harmonic Admittance Algorithm

Figure 3.5 shows the dc component of the dc current for operation in the rectifier mode. The dc current is normalized to the value of dc current corresponding to an overlap angle of 58° . As can be seen the harmonic admittance program predicts discontinuous characteristics made up of three regions. In region-1 the dc current increases with the overlap angle. This region ends close to an overlap angle of 26 degrees. In the next region the method does not yield a stable solution up to an overlap angle of roughly 46 degrees. Another set of stable solutions is obtained in region-2. In this region also the dc current increases with an increase in overlap angle. The values plotted are the ones corresponding to the firing angle for which the program converged for a given overlap angle. Figure 3.6 shows the variation of the dc voltage with overlap angle.

Figure 3.7 shows the harmonic content of the converter ac current. The plot is normalized to $I_{n=1}^{ac}$ corresponding to an overlap angle of 58° . In region-1 all odd harmonics increase with increasing overlap angle, indicating an approaching resonance in the no solution region. In region-2 the fundamental component increases with increasing overlap angle whereas the 3rd and the 5th harmonics decrease.

The voltage harmonics at the point of common coupling are shown in Fig. 3.8.

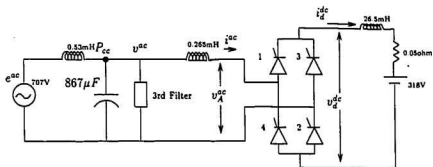


Figure 3.3: Single Phase Converter Example [10]

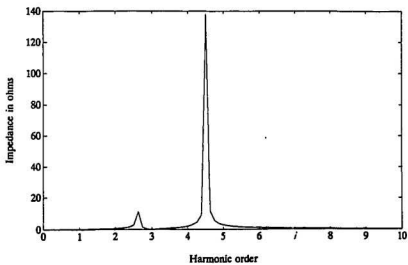


Figure 3.4: AC System Impedance

The plot is normalized to the no load ac voltage. The third harmonic is negligible due to the presence of the 3rd harmonic tuned filter. The 5th harmonic increases with increasing overlap angle indicating the existence of resonant condition close to the 5th harmonic component (Fig. 3.4).

Figures 3.9 and 3.10 show the converter output current and voltage harmonics. The plots are normalized to the dc component of the dc current and dc voltage corresponding to an overlap angle of 58° . The results predict that all harmonic components close to the system resonant points increase with increasing overlap angle.

Figure 3.11 shows the normalized frequency spectrum of the ac current. The figure shows that the harmonic admittance method clearly predicts the characteristic harmonics of the ac current. Figure 3.12 shows the frequency spectrum of the P_{ce} voltage. It is observed that the 5th harmonic component is significant. This is due to the resonance in the system impedance near the 5th harmonic order. Figure 3.13 shows the frequency spectrum of the output voltage. The 4th and 6th harmonics are significant because of the effect of resonant conditions near these harmonic components.

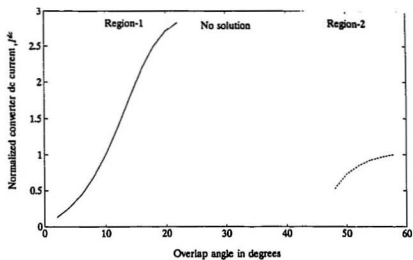


Figure 3.5: DC Component of the Converter Output Current

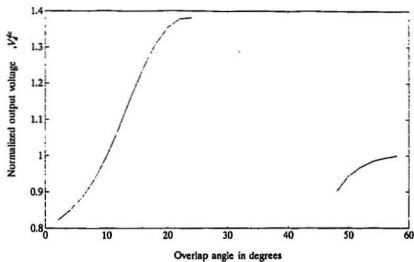


Figure 3.6: DC Component of the Converter Output Voltage

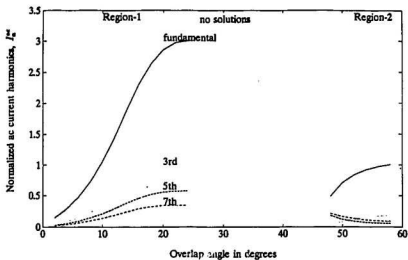


Figure 3.7: Harmonics in the AC Current

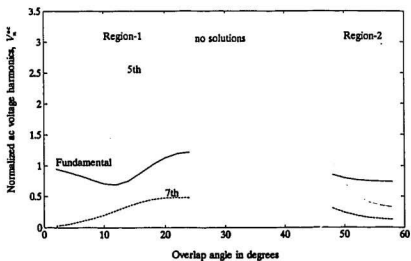


Figure 3.8: Harmonics in the Voltage at the Point of Common Coupling

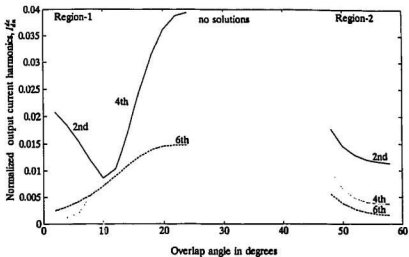


Figure 3.9: Harmonics in the Output Current

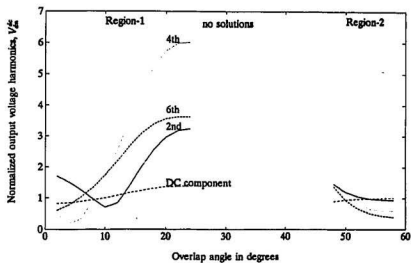


Figure 3.10: Harmonics in the Output Voltage

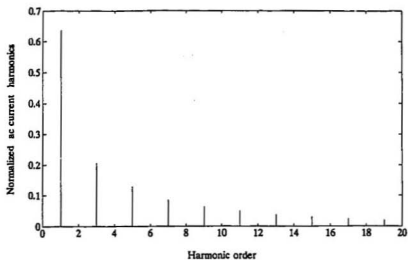


Figure 3.11: Frequency Spectrum of the AC Current for $\alpha = 45^\circ$

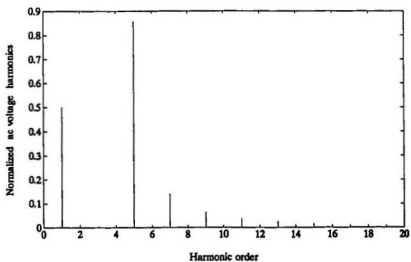


Figure 3.12: Frequency Spectrum of the AC Voltage at the Point of Common Coupling (P_{cc}) for $\alpha = 45^\circ$

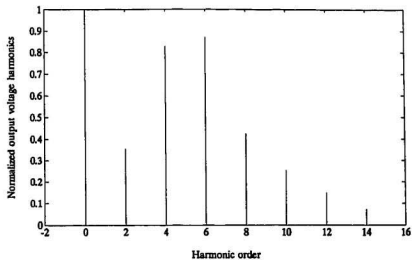


Figure 3.13: Frequency Spectrum of the Converter Output Voltage for $\alpha = 45^\circ$

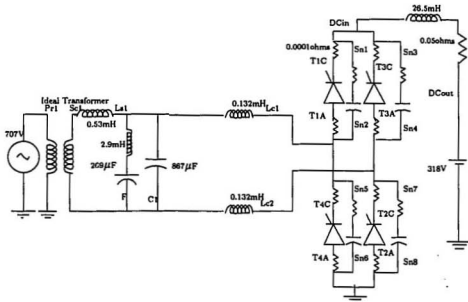


Figure 3.14: EMTP Model of the Single Phase Converter System

3.6 EMTP Simulation of the Single Phase Converter

The single phase converter system shown in Fig. 3.3 is simulated using the EMTP as the simulation tool to verify the harmonic admittance method. The node diagram of the EMTP model is shown in Fig. 3.14 which incorporates the following modifications to Fig. 3.3.

1. Since EMTP allows the ac source to be connected only between a node and ground, an ideal transformer was used on the ac side to provide isolation between the dc and ac grounds.
2. Type-11 switches were used to represent the thyristors in EMTP simulation. In order to avoid the type-11 switches forming a closed loop short circuit

during the commutation overlap interval, small resistances were introduced in series with the switches.

3. For better and smoother switching operations snubber circuits were placed in parallel with the thyristors. The snubbers used consist of series R-C circuit with a time constant 2.5 times the time step of $50 \mu s$ (i.e $R = 2k\Omega$, $C = 6nF$).
4. System independent voltage source was used for the generation of the triggering pulses. Details of the gate pulse generation are given in Appendix A.

3.6.1 System Waveforms

The results obtained using the harmonic admittance method were verified by EMTP simulation. The harmonics computed from the harmonic admittance method were recombined to obtain the steady-state voltage and current waveforms presented in this section. Harmonics up to the 20th order were used to obtain the waveforms.

Figure 3.15 and 3.16 show the ac voltage, v^{ac} , at the point of common coupling for two values of α as obtained by the harmonic admittance method and EMTP simulation. Both methods accurately predict the waveforms at P_{cc} . For $\alpha = 45^\circ$ the method predicts voltage instability in the system operation resulting in higher P_{cc} voltage.

Figures 3.17 and 3.18 show the voltage waveforms at the ac terminals of the converter for two values of α . The spikes on the EMTP waveform are produced by the switching action of the thyristors. It is also observed that the voltage instability at $\alpha = 45^\circ$ produces high frequency components in the voltage waveforms.

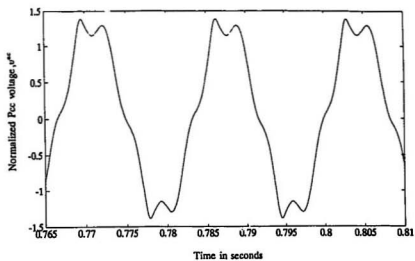
Figures 3.19 and 3.20 show the ac current waveforms for two values of α . It is observed that both methods accurately predict the overlap angle. This was verified using the *echo* feature in EMTP to observe the exact closing and opening instants of the thyristors. For $\alpha = 57^\circ$, an overlap angle $\mu = 3^\circ$ was obtained.

Figures 3.21 and 3.22 show the voltage waveforms at the dc terminals of the converter. The voltage instability at $\alpha = 45^\circ$ is reflected in the output voltage waveform.

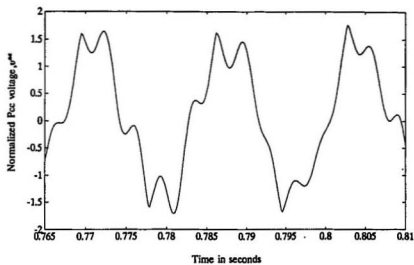
3.7 Summary

In this chapter, the harmonic admittance method was implemented to study the harmonic interactions in a single-phase converter connected to an ac network. The results give accurate information on the harmonic levels. In the example considered, the method predicted the existence of an unstable region of operation. The system waveforms indicate harmonic instability close to this region. The instability is caused by the resonance in the system impedance close to the fifth harmonic frequency.

The results of the harmonic admittance method were obtained using harmonic components up to the 20th. The results showed close agreement in system waveforms with the EMTF simulation. The harmonic admittance method was applied to a simple single-phase system. However, the method can be extended to a large system by representing the ac system with its Thevenin equivalent circuit.



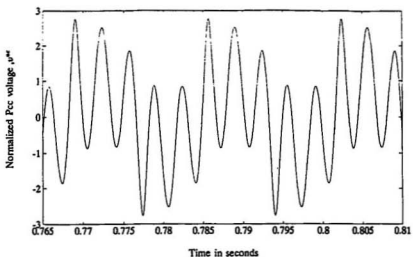
[a]



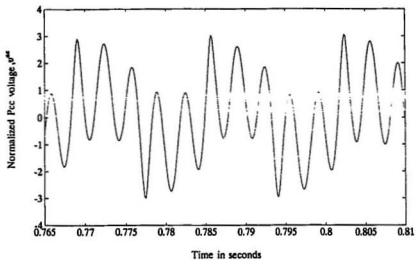
[b]

Figure 3.15: Voltage at the point of common coupling (P_{cc}), $\alpha = 57^\circ$

(a) Harmonic Admittance Method (b) EMTP Simulation



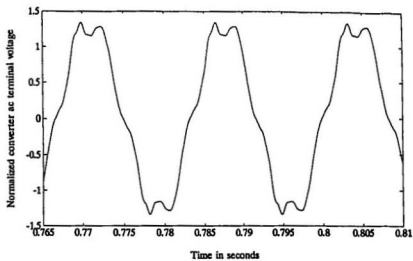
[a]



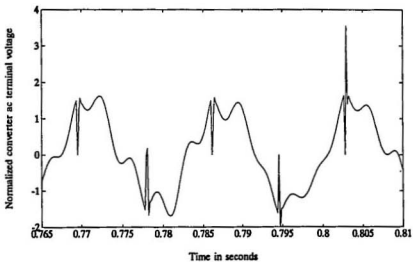
[b]

Figure 3.16: Voltage at the point of common coupling (P_{cc}), $\alpha = 45^\circ$

(a) Harmonic Admittance Method (b) EMTP Simulation



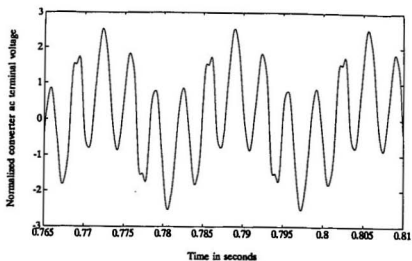
[a]



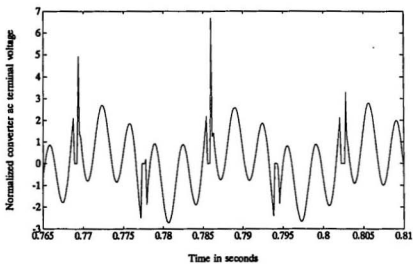
[b]

Figure 3.17: Voltage at the Converter AC Terminals, $\alpha = 57^\circ$

(a) Harmonic Admittance Method (b) EMTP Simulation



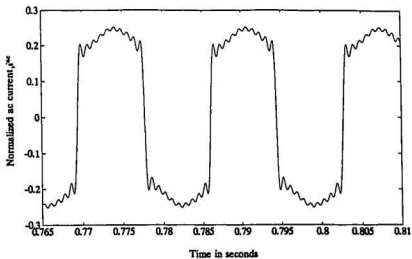
[a]



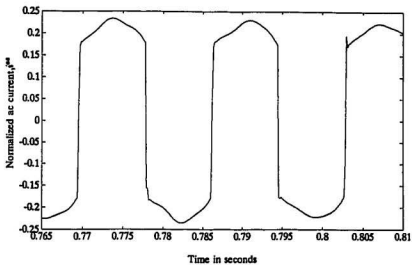
[b]

Figure 3.18: Voltage at the Converter AC Terminals, $\alpha = 45^\circ$

(a) Harmonic Admittance Method (b) EMTF Simulation



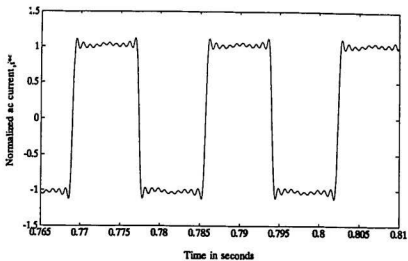
[a]



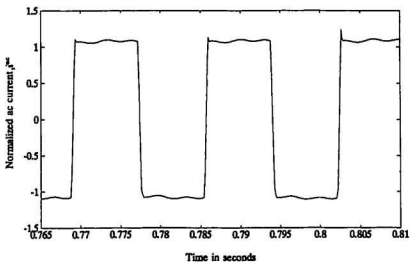
[b]

Figure 3.19: AC Current Waveform, $\alpha = 57^\circ$

(a) Harmonic Admittance Method (b) EMTP Simulation



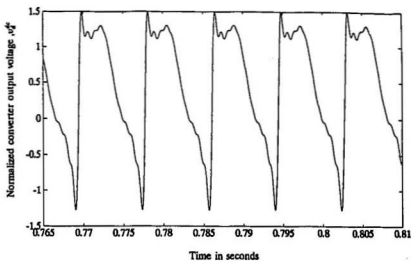
[a]



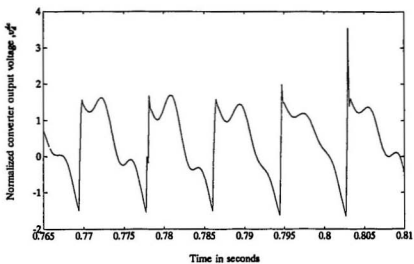
[b]

Figure 3.20: AC Current Waveform, $\alpha = 45^\circ$

(a) Harmonic Admittance Method (b) EMTF Simulation



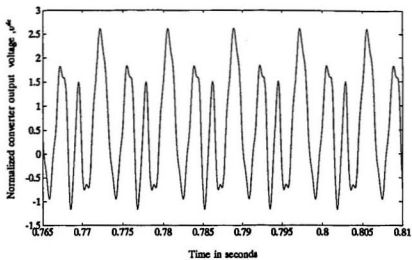
[a]



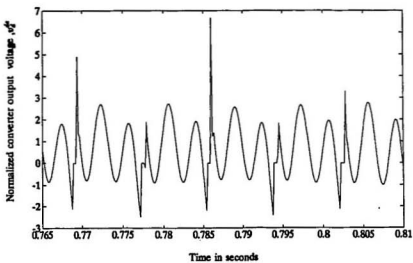
[b]

Figure 3.21: Voltage at the DC Terminals of the Converter, $\alpha = 57^\circ$

(a) Harmonic Admittance Method (b) EMTF Simulation



[a]



[b]

Figure 3.22: Voltage at the DC Terminals of the Converter, $\alpha = 45^\circ$

(a) Harmonic Admittance Method (b) EMTF Simulation

Chapter 4

Harmonic Admittance Model for the Three-Phase Converter

Based on the single phase model discussed in the last chapter a harmonic admittance model is developed for the three-phase ac/dc converter. As the three phase converter has three input ports and two output ports the standard m to n port network analysis procedure is employed to obtain a harmonic matrix which describes the harmonic interactions in the three-phase system. To the author's knowledge the harmonic admittance method has not been applied to the three-phase system.

4.1 The Three-Phase Converter System

Figure 4.1 shows the three-phase ac/dc converter. L_c represents the inductance of the converter transformer. For simplicity it is assumed that the source and transformer resistances are neglected and that the dc side inductance L_{dc} is sufficiently large to maintain continuous output current, i_d^{dc} . The ohmic losses in thyristors 1 through 6 are neglected. The dc link voltage, E^{dc} is assumed to be constant. In all the above quantities and those following, the suffixes a, b and c represent the corresponding phases.

In this chapter the harmonic admittance model for Fig. 4.1 is developed. In chapter 5 the three-phase converter connected to the ac input voltage via an ac network is studied using the model developed here.

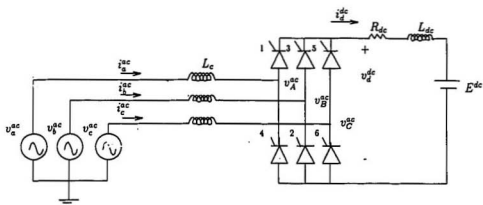


Figure 4.1: Three-Phase Converter Circuit

4.2 Harmonic Admittance Matrix for the Three-Phase Converter

The harmonic admittance matrix must provide a relationship between the currents in the three phases, voltages of the three phases, the dc current and the dc voltage. To ensure that the matrix couples all harmonics in the phase voltages, phase currents, the dc current and the dc voltage, the phase currents and the dc voltage are expressed as functions of the phase voltages and the dc current. The resulting structure of the harmonic admittance matrix relating the terminal variables is expressed as

$$\begin{bmatrix} I_a^{ac} \\ I_b^{ac} \\ I_c^{ac} \\ V_d^{dc} \end{bmatrix} = \begin{bmatrix} A_a & B_a & C_a & D_a \\ A_b & B_b & C_b & D_b \\ A_c & B_c & C_c & D_c \\ A_d & B_d & C_d & D_d \end{bmatrix} \begin{bmatrix} V_a^{ac} \\ V_b^{ac} \\ V_c^{ac} \\ I_d^{dc} \end{bmatrix} \quad (4.1)$$

V_a^{ac} , V_b^{ac} and V_c^{ac} are the Fourier matrix representation of the three-phase source voltages I_a^{ac} , I_b^{ac} and I_c^{ac} are the Fourier matrix representations of the currents in each of the three phases. V_d^{dc} and I_d^{dc} are the Fourier matrix representations of the dc voltage and dc current respectively. All the elements in the parameter matrix are infinite dimensional. The matrix $(A_a \dots D_d)$ representing the three-phase

converter is totally dependent upon the states of the converter and the commutating inductances.

4.3 Elements of the Harmonic Admittance Matrix

The Fourier series representation of the elements in the harmonic admittance matrix for the three-phase converter is derived in this section. As is the case in the single-phase converter, the voltage and current waveforms in the three-phase converter are determined by the switching action of the thyristors. However, in the three-phase converter, the changing states and modes of operation of the thyristors make it difficult to use one set of switching functions to generate both voltage and current waveforms. In order to simplify the analysis procedure, two switching functions are introduced, namely the current switching function and the voltage switching function. The voltage and current switching functions determine the states of the converter, and in steady-state, they define the voltage and current waveshapes respectively.

Figure 4.2 shows the ideal switching functions with respect to the source voltages v_a^{sc} , v_b^{sc} and v_c^{sc} , defined as

$$v_a^{sc} = V_m \sin \omega t \quad (4.2)$$

$$v_b^{sc} = V_m \sin \left(\omega t - \frac{2\pi}{3} \right) \quad (4.3)$$

$$v_c^{sc} = V_m \sin \left(\omega t - \frac{4\pi}{3} \right) \quad (4.4)$$

The resulting ideal current and voltage waveforms are shown in Fig. 4.3. For convenience the current waveforms are shown as trapezoidal waveforms. The reference point for the delay angle α is at $\omega t = \frac{\pi}{6}$.

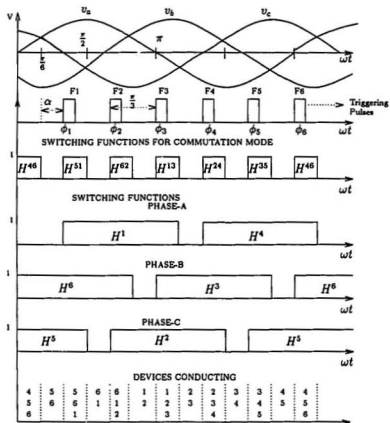


Figure 4.2: Switching Functions

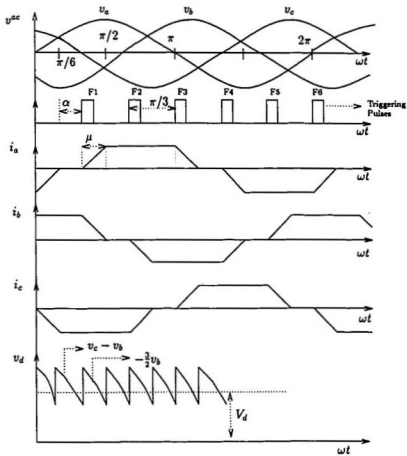


Figure 4.3: Phase Currents and Output Voltage

4.3.1 Harmonic Representation of the Current Switching Functions

The current switching functions define the relationships between the phase currents, the phase voltages and the dc current. These switching functions consist of the following:

- Switching functions that define currents through each of the six thyristors. These define the total period during which a thyristor is *on*. This includes the commutation as well as the inter commutation modes. For instance the switching function H^1 consists of intervals during which the following groups of thyristors conduct.
(5, 6, 1), (6, 1), (6, 1, 2), (1, 2) and (1, 2, 3).
- Switching functions in the commutation mode.

The elements in the converter transmission matrix are functions of both types of switching functions.

The switching functions H^1, H^2, H^3, H^4, H^5 and H^6 which determine the states of the thyristors are assumed to have a value of unity for the time intervals during which the thyristors 1, 2, 3, 4, 5 and 6 conduct. The switching functions $H^{46}, H^{51}, H^{62}, H^{13}, H^{24}$ and H^{35} are the switching functions which determine the commutation interval. These have a value of unity for the interval during which the transfer of current takes place between switch pairs (4, 6), (5, 1), (6, 2), (1, 3), (2, 4) and (3, 5). The current in each of the three phases is obtained by a linear combination of the switching functions $H^1 \dots H^6, H^{46} \dots H^{35}$, the current during the commutation overlap and the dc current. The time instants at which thyristors 1 through 6 are switched on are given by the angles ϕ_1 through ϕ_6 , defined as follows.

$$\phi_1 = \frac{\pi}{6} + \alpha \quad (4.5)$$

$$\phi_2 = \frac{\pi}{3} + \phi_1 \quad (4.6)$$

$$\phi_3 = \frac{\pi}{3} + \phi_2 \quad (4.7)$$

$$\phi_4 = \frac{\pi}{3} + \phi_3 \quad (4.8)$$

$$\phi_5 = \frac{\pi}{3} + \phi_4 \quad (4.9)$$

$$\phi_6 = \frac{\pi}{3} + \phi_5 \quad (4.10)$$

where α is the firing angle.

Assuming that in the steady-state the commutation angle μ is the same for each commutation interval, the Fourier coefficients for the switching functions are obtained as

$$h_{n \neq 0}^1 = \frac{1}{2\pi} \int_{\phi_1}^{\phi_3 + \mu} e^{-jn\omega t} d(\omega t) = \frac{j}{2\pi n} [e^{-jn(\phi_3 + \mu)} - e^{-jn\phi_1}] \quad (4.11)$$

$$h_{n=0}^1 = \frac{1}{2\pi} \left[\frac{2\pi}{3} + \mu \right] \quad (4.12)$$

$$h_{n \neq 0}^4 = \frac{1}{2\pi} \int_{\phi_4}^{\phi_6 + \mu} e^{-jn\omega t} d(\omega t) = \frac{j}{2\pi n} [e^{-jn(\phi_6 + \mu)} - e^{-jn\phi_4}] \quad (4.13)$$

$$h_{n=0}^4 = \frac{1}{2\pi} \left[\frac{2\pi}{3} + \mu \right] \quad (4.14)$$

$$h_{n \neq 0}^2 = \frac{1}{2\pi} \int_{\phi_2}^{\phi_4 + \mu} e^{-jn\omega t} d(\omega t) = \frac{j}{2\pi n} [e^{-jn(\phi_4 + \mu)} - e^{-jn\phi_2}] \quad (4.15)$$

$$h_{n=0}^2 = \frac{1}{2\pi} \left[\frac{2\pi}{3} + \mu \right] \quad (4.16)$$

$$h_{n \neq 0}^5 = \frac{1}{2\pi} \int_{\phi_5}^{\phi_6 + \frac{2\pi}{3} + \mu} e^{-jn\omega t} d(\omega t) = \frac{j}{2\pi n} [e^{-jn(\phi_6 + \frac{2\pi}{3} + \mu)} - e^{-jn\phi_5}] \quad (4.17)$$

$$h_{n=0}^5 = \frac{1}{2\pi} \left[\frac{2\pi}{3} + \mu \right] \quad (4.18)$$

$$h_{n \neq 0}^3 = \frac{1}{2\pi} \int_{\phi_3}^{\phi_5 + \mu} e^{-jn\omega t} d(\omega t) = \frac{j}{2\pi n} [e^{-jn(\phi_5 + \mu)} - e^{-jn\phi_3}] \quad (4.19)$$

$$h_{n=0}^3 = \frac{1}{2\pi} \left[\frac{2\pi}{3} + \mu \right] \quad (4.20)$$

$$h_{n \neq 0}^6 = \frac{1}{2\pi} \int_{\phi_6}^{\phi_6 + \frac{2\pi}{3} + \mu} e^{-jn\omega t} d(\omega t) = \frac{j}{2\pi n} [e^{-jn(\phi_6 + \frac{2\pi}{3} + \mu)} - e^{-jn\phi_6}] \quad (4.21)$$

$$h_{n=0}^6 = \frac{1}{2\pi} \left[\frac{2\pi}{3} + \mu \right] \quad (4.22)$$

By a similar procedure the Fourier coefficients of the switching functions for the commutation mode are obtained as

$$h_{n \neq 0}^{S1} = \frac{j}{2\pi n} [e^{-jn(\phi_1 + \mu)} - e^{-jn\phi_1}] \quad (4.23)$$

$$h_{n=0}^{51} = \frac{\mu}{2\pi} \quad (4.24)$$

$$h_{n \neq 0}^{62} = \frac{j}{2\pi n} [e^{-jn(\phi_2 + \mu)} - e^{-jn\phi_2}] \quad (4.25)$$

$$h_{n=0}^{62} = \frac{\mu}{2\pi} \quad (4.26)$$

$$h_{n \neq 0}^{13} = \frac{j}{2\pi n} [e^{-jn(\phi_3 + \mu)} - e^{-jn\phi_3}] \quad (4.27)$$

$$h_{n=0}^{13} = \frac{\mu}{2\pi} \quad (4.28)$$

$$h_{n \neq 0}^{24} = \frac{j}{2\pi n} [e^{-jn(\phi_4 + \mu)} - e^{-jn\phi_4}] \quad (4.29)$$

$$h_{n=0}^{24} = \frac{\mu}{2\pi} \quad (4.30)$$

$$h_{n \neq 0}^{35} = \frac{j}{2\pi n} [e^{-jn(\phi_5 + \mu)} - e^{-jn\phi_5}] \quad (4.31)$$

$$h_{n=0}^{35} = \frac{\mu}{2\pi} \quad (4.32)$$

$$h_{n \neq 0}^{46} = \frac{j}{2\pi n} [e^{-jn(\phi_6 + \mu)} - e^{-jn\phi_6}] \quad (4.33)$$

$$h_{n=0}^{46} = \frac{\mu}{2\pi} \quad (4.34)$$

4.3.2 Harmonic Representation of the Voltage Switching Functions

Voltage switching functions define the relationship between the phase voltages and the dc voltage. Similar to the current switching functions, the voltage switching functions have a value of unity in the regions where corresponding thyristors conduct. The voltage switching functions for the commutation overlap intervals when three thyristors conduct simultaneously are equivalent to the current switching functions for the commutation mode. Table 4.1 shows the voltage switching functions and their equivalents for the various intervals. Generally two of the three devices involved in the commutation process belong to the positive(negative) group while the other device belongs to the negative(positive) group. The harmonic components or the elements of the Fourier matrix for the voltage switching functions when three thyristors conduct simultaneously are defined by equations (4.23) to (4.34). The harmonic components of the rest of the voltage switching functions

Table 4.1: Voltage Switching Functions

Switching Function	Equivalent Switching Function	Switches Conducting	Start of Interval	End of Interval	Voltage Magnitude
H^{561}	H^{51}	5,6,1	ϕ_1	$\phi_1 + \mu$	$-\frac{3}{2}v_b^{ac}$
H^{16}		1,6	$\phi_1 + \mu$	ϕ_2	$v_a^{ac} - v_b^{ac}$
H^{162}	H^{62}	1,6,2	ϕ_2	$\phi_2 + \mu$	$\frac{3}{2}v_a^{ac}$
H^{12}		1,2	$\phi_2 + \mu$	ϕ_3	$v_a^{ac} - v_c^{ac}$
H^{123}	H^{13}	1,2,3	ϕ_3	$\phi_3 + \mu$	$-\frac{3}{2}v_c^{ac}$
H^{23}		2,3	$\phi_3 + \mu$	ϕ_4	$v_b^{ac} - v_c^{ac}$
H^{234}	H^{24}	2,3,4	ϕ_4	$\phi_4 + \mu$	$\frac{3}{2}v_b^{ac}$
H^{34}		3,4	$\phi_4 + \mu$	ϕ_5	$v_b^{ac} - v_a^{ac}$
H^{345}	H^{35}	3,4,5	ϕ_5	$\phi_5 + \mu$	$-\frac{3}{2}v_a^{ac}$
H^{45}		4,5	$\phi_5 + \mu$	ϕ_6	$v_c^{ac} - v_a^{ac}$
H^{456}	H^{46}	4,5,6	ϕ_6	$\phi_6 + \mu$	$\frac{3}{2}v_c^{ac}$
H^{56}		5,6	$\phi_6 + \mu$	$\phi_6 + \frac{\pi}{2}$	$v_c^{ac} - v_b^{ac}$

involving two devices can be obtained using the following generalized formula.

$$h = \frac{j}{2n\pi} [e^{-jn(\text{end of the function interval})} - e^{-jn(\text{start of the function interval})}] \quad (4.35)$$

For example, from Table 4.1, the harmonic components of the voltage switching function which describes the conduction of thyristors 1 and 2 are obtained as

$$h_{n \neq 0}^{12} = \frac{j}{2n\pi} [e^{-jn(\phi_2)} - e^{-jn(\phi_2 + \mu)}] \quad (4.36)$$

$$h_{n=0}^{12} = \frac{\mu}{2\pi} \quad (4.37)$$

4.3.3 Harmonic Representation of the Current in Phase-a

The Fourier matrix expression of the current in phase-a can be obtained as the sum of the Fourier matrix expressions for each of the regions defined below.

- Current in the regions where thyristors belonging to phase-a conduct, but are not involved in the commutation process.

- Current during the interval of commutation overlap where three thyristors conduct and one of the phase-a thyristors is involved in the commutation process.

The current in phase-a is due to the conduction of thyristors 1 and 4. From Figs. 4.2 and 4.3 the current in phase-a can be written as

$$i_a^{ac}(\omega t) = I^{16}(\omega t) + I^{12}(\omega t) + I^{126}(\omega t) + I^{43}(\omega t) + I^{45}(\omega t) + I^{345}(\omega t) \\ + I^{561}(\omega t) + I^{123}(\omega t) + I^{234}(\omega t) + I^{456}(\omega t) \quad (4.38)$$

The quantities in the equation (4.38) are defined below.

1. Currents when phase-a is not involved in the commutation process

The quantities $I^{16}(\omega t)$, $I^{12}(\omega t)$, $I^{126}(\omega t)$, $I^{43}(\omega t)$, $I^{45}(\omega t)$ and $I^{345}(\omega t)$ are the components of currents in phase-a when thyristors 1 and 4 conduct. During these conduction periods the thyristors belonging to phase-a are not involved in the commutation process. As the current during these periods is close to the steady-state dc current $I_d^{dc}(\omega t)$, these currents are expressed in terms of the switching functions and the dc current and are defined as follows (Fig. 4.2 and 4.3).

$$I^{16}(\omega t) + I^{12}(\omega t) + I^{126}(\omega t) = [H^1(\omega t) - H^{51}(\omega t) - H^{13}(\omega t)] I_d^{dc}(\omega t) \quad (4.39)$$

$$I^{43}(\omega t) + I^{45}(\omega t) + I^{345}(\omega t) = -[H^4(\omega t) - H^{24}(\omega t) - H^{46}(\omega t)] I_d^{dc}(\omega t) \quad (4.40)$$

The harmonic matrix representations of equations (4.39) and (4.40) are obtained by representing each component by its corresponding Fourier series. The resulting expressions are

$$I^{16} + I^{12} + I^{126} = [H^1 - H^{51} - H^{13}] I_d^{dc} \quad (4.41)$$

$$I^{43} + I^{45} + I^{345} = -[H^4 - H^{24} - H^{46}] I_d^{dc} \quad (4.42)$$

2. Currents when phase-a is involved in the commutation process

The quantities $I^{561}(\omega t)$, $I^{123}(\omega t)$, $I^{234}(\omega t)$ and $I^{456}(\omega t)$ represent the components of currents in phase-a during the commutation interval. In terms of the switching functions, these currents are defined as

$$I^{561}(\omega t) = [H^{51}(\omega t)]I(\omega t) \quad (4.43)$$

$$I^{123}(\omega t) = [H^{13}(\omega t)]I(\omega t) \quad (4.44)$$

$$I^{234}(\omega t) = [H^{24}(\omega t)]I(\omega t) \quad (4.45)$$

$$I^{456}(\omega t) = [H^{46}(\omega t)]I(\omega t) \quad (4.46)$$

where $I(\omega t)$ is the current during the corresponding commutation interval, defined by

$$I(\omega t) = \int_{t_s}^{\omega t} \frac{V^{ac}}{L} d(\omega t) + I_s \quad (4.47)$$

In equation (4.47), t_s is the time instant at which commutation starts and I_s is the current in the phase at the beginning of commutation.

In order to obtain the harmonic components of the current during the commutation period, the circuit equations during commutation are first derived. It is assumed that i_d^{dc} is constant during the commutation interval. Figure 4.4 shows the three-phase converter. At every instant the following equations can be derived.

$$i_1 + i_3 + i_5 = i_2 + i_4 + i_6 = i_d^{dc} = I_d = \text{constant} \quad (4.48)$$

$$i_a^{ac} = i_1 - i_4 \quad (4.49)$$

$$i_b^{ac} = i_3 - i_6 \quad (4.50)$$

$$i_c^{ac} = i_5 - i_2 \quad (4.51)$$

$$v_1 - v_3 = v_6 - v_4 \quad (4.52)$$

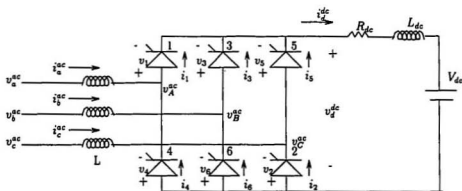


Figure 4.4: Three-Phase Line Commutated Converter

$$v_3 - v_5 = v_2 - v_6 \quad (4.53)$$

$$v_5 - v_1 = v_4 - v_2 \quad (4.54)$$

$$v_a^{ac} - v_b^{ac} = \omega L_c \frac{d(i_1 - i_4 - i_3 + i_6)}{d(\omega t)} + v_1 - v_3 \quad (4.55)$$

$$v_b^{ac} - v_c^{ac} = \omega L_c \frac{d(i_3 - i_6 - i_5 + i_2)}{d(\omega t)} + v_3 - v_5 \quad (4.56)$$

where ω is the angular frequency of the source.

a. Current during commutation from thyristor 1 to thyristor 3

During the commutation from thyristor 1 to thyristor 3, thyristors 1, 2 and 3 conduct. The following equations are obtained from Fig. 4.4.

$$i_4 = i_5 = i_6 = 0 \quad (4.57)$$

$$v_1 = v_2 = v_3 = 0 \quad (4.58)$$

and from equation (4.48)

$$i_1 + i_3 = i_2 = I_d = \text{constant} \quad (4.59)$$

Substituting equations (4.57) and (4.58) into equation (4.55) gives

$$v_a^{ac} - v_b^{ac} = \omega L_c \frac{d(i_1 - i_3)}{d(\omega t)} \quad (4.60)$$

and from equation (4.49)

$$\frac{di_a^{ac}}{d(\omega t)} = \frac{di_1}{d(\omega t)} \quad (4.61)$$

Equation (4.59) also gives

$$\frac{di_1}{d(\omega t)} = -\frac{di_3}{d(\omega t)} \quad (4.62)$$

Substituting equation (4.62) into (4.60) gives

$$v_a^{ac} - v_b^{ac} = 2\omega L_c \frac{di_a^{ac}}{d(\omega t)} \quad (4.63)$$

and

$$\frac{di_a^{ac}}{d(\omega t)} = \frac{v_a^{ac} - v_b^{ac}}{2\omega L_c} \quad (4.64)$$

The current in phase-a during the commutation interval is obtained from equations (4.64) and (4.47) as

$$i_a^{ac}(\omega t) = I(\omega t) = \int_{\phi_3}^{\omega t} \left(\frac{v_a^{ac} - v_b^{ac}}{2\omega L_c} \right) d(\omega t) + i_a^{dc}(\omega t = \phi_3) \quad (4.65)$$

where ϕ_3 is the beginning of the commutation from thyristor 1 to 3 and $i_a^{dc}(\omega t = \phi_3) = I_a^{dc}(\omega t)$ is the current in phase-a at the start of commutation. In the steady state when $I(\omega t)$ and v_a^{ac} , v_b^{ac} , $i_a^{ac}(\omega t)$ are periodic, the terms in equation (4.65) can be expressed as the Fourier series,

$$\begin{aligned} \sum_{n=-\infty}^{\infty} I_n e^{jn\omega t} &= \sum_{n=-\infty}^{\infty} \frac{(V_a^{ac} - V_b^{ac})_n}{2jn\omega L_c} e^{jn\omega t} \\ &\quad - \sum_{\substack{n=-\infty \\ n \neq 0}}^{\infty} \frac{(V_a^{ac} - V_b^{ac})_n}{2jn\omega L_c} e^{jn\omega\phi_3} + \sum_{n=-\infty}^{\infty} I_n^{dc} e^{jn\omega\phi_3} \end{aligned} \quad (4.66)$$

Multiplying both sides of equation (4.66) by the orthogonal function $e^{-jn\omega t}$ and integrating over a period gives

$$I_{n \neq 0} = \frac{(V_a^{ac} - V_b^{ac})_n}{2jn\omega L_c} \quad (4.67)$$

$$I_{nm0} = - \sum_{\substack{m=-\infty \\ m \neq 0}}^{\infty} \frac{(V_a^{ac} - V_b^{ac})_m}{jm\omega L_c} e^{jm\phi_3} + \sum_{m=-\infty}^{\infty} I_m^{dc} e^{jm\phi_3} \quad (4.68)$$

where the suffix n and m denote the order of the harmonic. The Fourier representation of phase-a current during the commutation overlap interval as defined by equations (4.67) and (4.68), can be written in the general form

$$I_n = Y_n(V_a^{ac} - V_b^{ac})[I^M - G(\phi_3)] + I_n^{dc}G(\phi_3) \quad (4.69)$$

where

$$I_n = \begin{bmatrix} \cdot \\ \cdot \\ \cdot \\ I_{-1} \\ I_0 \\ I_1 \\ \cdot \\ \cdot \\ \cdot \end{bmatrix} \quad (4.70)$$

Y_n is the diagonal matrix with elements defined by

$$Y_n = \frac{1}{2jn\omega L_c} \quad (4.71)$$

$G(\phi_3)$ defines $e^{jn\phi_3}$ terms in the matrix

$$G(\phi_3) = \begin{bmatrix} \cdot & \cdot \\ \cdot & \cdot \\ \cdot & \cdot & 0 & 0 & 0 & \cdot & \cdot & \cdot \\ \cdot & \cdot & e^{-j\phi_3} & 1 & e^{j\phi_3} & \cdot & \cdot & \cdot \\ \cdot & \cdot & 0 & 0 & 0 & \cdot & \cdot & \cdot \\ \cdot & \cdot \\ \cdot & \cdot \end{bmatrix} \quad (4.72)$$

and I^M is the identity matrix.

From equation (4.44) the current during the commutation interval is given by

$$I^{123}(\omega t) = I^{13}(\omega t) = H^{13}(\omega t)I_n(\omega t) \quad (4.73)$$

The Fourier series representation of equation (4.73) is given by

$$I^{13} = H^{13}I_n \quad (4.74)$$

which, from equation (4.69), can be expressed as

$$\mathbf{I}^{13} = \mathbf{H}^{13} \{ \mathbf{Y}_n(\mathbf{V}_a^{ac} - \mathbf{V}_b^{ac})[\mathbf{I}^M - \mathbf{G}(\phi_3)] + \mathbf{I}_d^{dc} \mathbf{G}(\phi_3) \} \quad (4.75)$$

\mathbf{H}^{13} is defined as

$$\begin{bmatrix} \cdot & \cdot \\ \cdot & \cdot \\ \cdot & \cdot & h_0^{13} & h_{-1}^{13} & h_{-2}^{13} & \cdot & \cdot & \cdot \\ \cdot & \cdot & h_1^{13} & h_0^{13} & h_{-1}^{13} & \cdot & \cdot & \cdot \\ \cdot & \cdot & h_2^{13} & h_1^{13} & h_0^{13} & \cdot & \cdot & \cdot \\ \cdot & \cdot \\ \cdot & \cdot \end{bmatrix} \quad (4.76)$$

and \mathbf{V}_a^{ac} , \mathbf{V}_b^{ac} and \mathbf{V}_c^{ac} are the harmonic matrix representations of voltages, $v_a^{ac}(\omega t)$, $v_b^{ac}(\omega t)$ and $v_c^{ac}(\omega t)$. \mathbf{I}_d^{dc} is the harmonic matrix representation of the dc current, $i_d^{dc}(\omega t)$.

b. Commutation current for other devices

Using the procedure outlined above the current during commutation for other thyristors can be obtained as follows.

For commutation from thyristor 5 to thyristor 1, the initial current $i_2^{dc}(\omega t = \phi_5) = 0$. Hence from equation (4.75),

$$\mathbf{I}^{51} = [\mathbf{H}^{51} \mathbf{Y}_n(\mathbf{V}_a^{ac} - \mathbf{V}_c^{ac})][\mathbf{I}^M - \mathbf{G}(\phi_1)] \quad (4.77)$$

Similarly, for commutation from thyristor 2 to thyristor 4,

$$\mathbf{I}^{24} = \mathbf{H}^{24} \mathbf{Y}_n(\mathbf{V}_a^{ac} - \mathbf{V}_c^{ac})[\mathbf{I}^M - \mathbf{G}(\phi_4)] \quad (4.78)$$

For commutation from thyristor 4 to thyristor 6,

$$\mathbf{I}^{46} = \mathbf{H}^{46} \{ \mathbf{Y}_n(\mathbf{V}_a^{ac} - \mathbf{V}_b^{ac}) - \mathbf{Y}_n(\mathbf{G}(\phi_6))(\mathbf{V}_a^{ac} - \mathbf{V}_b^{ac}) + (\mathbf{G}(\phi_6))\mathbf{I}_d^{dc} \} \quad (4.79)$$

Where $\mathbf{G}(\phi_1) \dots \mathbf{G}(\phi_6)$, $\mathbf{H}^{51} \dots \mathbf{H}^{46}$ are structurally identical to $\mathbf{G}(\phi_3)$ (equation 4.72) and \mathbf{H}^{13} (equation 4.76) respectively.

Substituting equations (4.41), (4.42), (4.75), (4.77), (4.78) and (4.79) into equation (4.38) the Fourier matrix representation of the phase-a current is obtained as

$$\begin{aligned}
\mathbf{I}_a^{ac} = & \left[\mathbf{H}^1 - \mathbf{H}^4 \right] \mathbf{I}_d^{dc} - \left[\mathbf{H}^{51} + \mathbf{H}^{13} - \mathbf{H}^{24} - \mathbf{H}^{26} \right] \mathbf{I}_d^{dc} \\
& + \mathbf{H}^{51} \left\{ \mathbf{Y}_n [\mathbf{V}_a^{ac} - \mathbf{V}_c^{ac}] [\mathbf{I}^M - \mathbf{G}(\phi_1)] \right\} \\
& + \mathbf{H}^{13} \left\{ \mathbf{Y}_n [\mathbf{V}_a^{ac} - \mathbf{V}_b^{ac}] - \mathbf{G}(\phi_3) \left[\mathbf{Y}_n (\mathbf{V}_a^{ac} - \mathbf{V}_b^{ac}) - \mathbf{I}_d^{dc} \right] \right\} \\
& + \mathbf{H}^{24} \left\{ \mathbf{Y}_n [\mathbf{V}_a^{ac} - \mathbf{V}_c^{ac}] [\mathbf{I}^M - \mathbf{G}(\phi_4)] \right\} \\
& + \mathbf{H}^{46} \left\{ \mathbf{Y}_n [\mathbf{V}_a^{ac} - \mathbf{V}_b^{ac}] - \mathbf{G}(\phi_6) \left[\mathbf{Y}_n (\mathbf{V}_a^{ac} - \mathbf{V}_b^{ac}) + \mathbf{I}_d^{dc} \right] \right\}
\end{aligned} \tag{4.80}$$

4.3.4 Harmonic Representation of the Currents in Phase-b and Phase-c

Following the procedure for obtaining phase-a current in the previous section, the currents in phase-b and phase-c can be determined. The final equations are given as follows:

For phase-b,

$$\begin{aligned}
\mathbf{I}_b^{ac} = & \left[\mathbf{H}^3 - \mathbf{H}^6 \right] \mathbf{I}_d^{dc} - \left[\mathbf{H}^{13} + \mathbf{H}^{35} - \mathbf{H}^{62} - \mathbf{H}^{46} \right] \mathbf{I}_d^{dc} \\
& + \mathbf{H}^{13} \left\{ \mathbf{Y}_n [\mathbf{V}_b^{ac} - \mathbf{V}_a^{ac}] [\mathbf{I}^M - \mathbf{G}(\phi_3)] \right\} \\
& + \mathbf{H}^{35} \left\{ \mathbf{Y}_n [\mathbf{V}_b^{ac} - \mathbf{V}_c^{ac}] - \mathbf{G}(\phi_5) \left[\mathbf{Y}_n (\mathbf{V}_b^{ac} - \mathbf{V}_c^{ac}) - \mathbf{I}_d^{dc} \right] \right\} \\
& + \mathbf{H}^{46} \left\{ \mathbf{Y}_n [\mathbf{V}_b^{ac} - \mathbf{V}_a^{ac}] [\mathbf{I}^M - \mathbf{G}(\phi_6)] \right\} \\
& + \mathbf{H}^{62} \left\{ \mathbf{Y}_n [\mathbf{V}_b^{ac} - \mathbf{V}_c^{ac}] - \mathbf{G}(\phi_2) \left[\mathbf{Y}_n (\mathbf{V}_b^{ac} - \mathbf{V}_c^{ac}) + \mathbf{I}_d^{dc} \right] \right\}
\end{aligned} \tag{4.81}$$

and for phase-c,

$$\begin{aligned}
\mathbf{I}_c^{ac} = & \left[\mathbf{H}^5 - \mathbf{H}^2 \right] \mathbf{I}_d^{dc} - \left[\mathbf{H}^{51} + \mathbf{H}^{35} - \mathbf{H}^{62} - \mathbf{H}^{24} \right] \mathbf{I}_d^{dc} \\
& + \mathbf{H}^{35} \left\{ \mathbf{Y}_n [\mathbf{V}_c^{ac} - \mathbf{V}_b^{ac}] [\mathbf{I}^M - \mathbf{G}(\phi_5)] \right\}
\end{aligned}$$

$$\begin{aligned}
& +H^{51} \{Y_n[V_c^{ac} - V_a^{ac}] - G(\phi_1) [Y_n(V_c^{ac} - V_a^{ac}) - I_d^{dc}]\} \\
& +H^{62} \{Y_n[V_c^{ac} - V_b^{ac}] [I^M - G(\phi_2)]\} \\
& +H^{24} \{Y_n[V_c^{ac} - V_a^{ac}] - G(\phi_4) [Y_n(V_c^{ac} - V_a^{ac}) + I_d^{dc}]\}
\end{aligned} \tag{4.82}$$

4.3.5 Harmonic Representation of the DC Voltage

Let v_A^{ac} , v_B^{ac} and v_C^{ac} represent the voltages at the ac terminals of the converter (i.e. at the ac nodes of the thyristors). The dc voltage $v_d^{dc}(\omega t)$ can be expressed in terms of the converter ac terminal voltages and the voltage switching functions. From Table 4.1, Figs. 4.2 and 4.3, the dc voltage can be expressed as

$$\begin{aligned}
v_d^{dc}(\omega t) = & H^{16}(\omega t) [v_A^{ac}(\omega t) - v_B^{ac}(\omega t)] + H^{12}(\omega t) [v_A^{ac}(\omega t) - v_C^{ac}(\omega t)] \\
& + H^{45}(\omega t) [v_C^{ac}(\omega t) - v_A^{ac}(\omega t)] + H^{23}(\omega t) [v_B^{ac}(\omega t) - v_C^{ac}(\omega t)] \\
& + H^{34}(\omega t) [v_B^{ac}(\omega t) - v_A^{ac}(\omega t)] + H^{56}(\omega t) [v_C^{ac}(\omega t) - v_B^{ac}(\omega t)] \\
& + \frac{3}{2} \{ (H^{162}(\omega t) - H^{345}(\omega t)) v_A^{ac}(\omega t) \} \\
& + \frac{3}{2} \{ (H^{234}(\omega t) - H^{561}(\omega t)) v_B^{ac}(\omega t) \} \\
& + \frac{3}{2} \{ (H^{456}(\omega t) - H^{123}(\omega t)) v_C^{ac}(\omega t) \}
\end{aligned} \tag{4.83}$$

Collecting the coefficients of $v_A^{ac}(\omega t)$, $v_B^{ac}(\omega t)$ and $v_C^{ac}(\omega t)$ together, equation (4.83) can be rewritten in the Fourier matrix form as

$$V_d^{dc} = H_a V_A^{ac} + H_b V_B^{ac} + H_c V_C^{ac} \tag{4.84}$$

where

$$H_a = H^{16} + H^{12} - H^{34} - H^{45} - \frac{3}{2} \{ H^{345} - H^{162} \} \tag{4.85}$$

$$H_b = -H^{23} + H^{34} - H^{16} - H^{56} - \frac{3}{2} \{ H^{561} - H^{234} \} \tag{4.86}$$

$$H_c = H^{45} + H^{56} - H^{12} - H^{23} - \frac{3}{2} \{ H^{123} - H^{456} \} \tag{4.87}$$

If Z is the diagonal matrix containing the harmonic components of the impedance between the converter and the source voltages v_a^{ac} , v_b^{ac} and v_c^{ac} , (i.e. $Z = jn\omega L_c$), then the Fourier matrix of the converter voltages V_A^{ac} , V_B^{ac} and V_C^{ac} are given by

$$V_A^{ac} = V_a^{ac} - ZI_a^{ac} \quad (4.88)$$

$$V_B^{ac} = V_b^{ac} - ZI_b^{ac} \quad (4.89)$$

$$V_C^{ac} = V_c^{ac} - ZI_c^{ac} \quad (4.90)$$

Substituting equations (4.88) through (4.90) into equation (4.84) gives

$$V_d^{dc} = H_a(V_a^{ac} - ZI_a^{ac}) + H_b(V_b^{ac} - ZI_b^{ac}) + H_c(V_c^{ac} - ZI_c^{ac}) \quad (4.91)$$

4.3.6 A, B, C and D Parameters of the Three-Phase Converter

The elements of the harmonic admittance matrix of the three-phase converter ($A_a \dots D_c$) can be obtained by extracting the coefficients of V_a^{ac} , V_b^{ac} , V_c^{ac} and I_d^{dc} for each phase, from equations (4.80) to (4.82).

From equation (4.1) the expression for I_a^{ac} is given by

$$I_a^{ac} = A_a V_a^{ac} + B_a V_b^{ac} + C_a V_c^{ac} + D_a V_d^{dc} \quad (4.92)$$

Comparing equation (4.92) and equation (4.80), the parameters A_a , B_a , C_a and D_a for phase-a are obtained as

$$A_a = H^{51} [I^M - G(\phi_1)] Y_n + H^{13} [I^M - G(\phi_3)] Y_n \\ + H^{24} [I^M - G(\phi_4)] Y_n + H^{46} [I^M - G(\phi_6)] Y_n \quad (4.93)$$

$$B_a = Y_n \{ -H^{13} [I^M - G(\phi_3)] - H^{46} [I^M - G(\phi_6)] \} \quad (4.94)$$

$$C_a = Y_n \{ -H^{51} [I^M - G(\phi_1)] - H^{24} [I^M - G(\phi_4)] \} \quad (4.95)$$

$$D_a = (H^1 - H^{51} - H^{13} - H^4 - H^{24} - H^{46}) + H^{13} G(\phi_3) - H^{46} G(\phi_6) \quad (4.96)$$

Similarly the expression for I_b^{ac} is obtained from equation (4.1) as

$$I_b^{ac} = A_b V_a^{ac} + B_b V_b^{ac} + C_b V_c^{ac} + D_b I_d^{dc} \quad (4.97)$$

and the parameters A_b , B_b , C_b and D_b for phase-b are obtained from equation (4.81) as

$$A_b = Y_n \{ -H^{13} [I^M - G(\phi_3)] - H^{46} [I^M - G(\phi_6)] \} \quad (4.98)$$

$$B_b = H^{13} [I^M - G(\phi_3)] Y_n + H^{35} [I^M - G(\phi_5)] Y_n \\ + H^{62} [I^M - G(\phi_2)] Y_n + H^{46} [I^M - G(\phi_6)] Y_n \quad (4.99)$$

$$C_b = Y_n \{ -H^{62} [I^M - G(\phi_2)] - H^{35} [I^M - G(\phi_5)] \} \quad (4.100)$$

$$D_b = (H^3 - H^{13} - H^{35} - H^6 - H^{62} - H^{46}) + H^{35} G(\phi_5) - H^{62} G(\phi_6) \quad (4.101)$$

Phase-c current I_c^{ac} is obtained from equation (4.1) as

$$I_c^{ac} = A_c V_a^{ac} + B_c V_b^{ac} + C_c V_c^{ac} + D_c I_d^{dc} \quad (4.102)$$

The parameters A_c , B_c , C_c and D_c for phase-c are obtained from equation (4.82) as

$$A_c = Y_n \{ -H^{51} [I^M - G(\phi_1)] - H^{24} [I^M - G(\phi_4)] \} \quad (4.103)$$

$$B_c = Y_n \{ -H^{35} [I^M - G(\phi_5)] - H^{62} [I^M - G(\phi_2)] \} \quad (4.104)$$

$$C_c = H^{24} [I^M - G(\phi_4)] Y_n + H^{35} [I^M - G(\phi_5)] Y_n \\ + H^{62} [I^M - G(\phi_2)] Y_n + H^{51} [I^M - G(\phi_1)] Y_n \quad (4.105)$$

$$D_c = (H^5 - H^{51} - H^{35} - H^2 - H^{62} - H^{24}) + H^{51} G(\phi_1) - H^{24} G(\phi_4) \quad (4.106)$$

From equation (4.1) the expression for V_d^{dc} is given by

$$V_d^{dc} = A_d V_a^{ac} + B_d V_b^{ac} + C_d V_c^{ac} + D_d I_d^{dc} \quad (4.107)$$

Substituting for I_a^{ac} , I_b^{ac} and I_c^{ac} from equation (4.1) into equation (4.91) gives

$$\begin{aligned} V_d^{dc} = & \{H_a - Z[A_a H_a + A_b H_b + A_c H_c]\} V_a^{ac} \\ & + \{H_b - Z[B_a H_a + B_b H_b + B_c H_c]\} V_b^{ac} \\ & + \{H_c - Z[C_a H_a + C_b H_b + C_c H_c]\} V_c^{ac} \\ & - Z[D_a H_a + D_b H_b + D_c H_c] I_d^{dc} \end{aligned} \quad (4.108)$$

Comparing equations (4.107) and (4.108) the parameters A_d , B_d , C_d and D_d parameters are obtained as

$$A_d = H_a - Z[A_a H_a + A_b H_b + A_c H_c] \quad (4.109)$$

$$B_d = H_b - Z[B_a H_a + B_b H_b + B_c H_c] \quad (4.110)$$

$$C_d = H_c - Z[C_a H_a + C_b H_b + C_c H_c] \quad (4.111)$$

$$D_d = -Z[D_a H_a + D_b H_b + D_c H_c] \quad (4.112)$$

Equation (4.1) can be used to solve for the current in the three phases if the Fourier components of the voltages v_a^{ac} , v_b^{ac} , v_c^{ac} and the output voltage v_d^{dc} are known. In a practical system only the ac source voltages v_a^{ac} , v_b^{ac} , v_c^{ac} and the dc terminal voltage E^{dc} are known. The relationships between the terminal variables are expressed as

$$\begin{bmatrix} V_a^{ac} \\ V_b^{ac} \\ V_c^{ac} \\ V_d^{dc} \end{bmatrix} = \begin{bmatrix} 0 & 0 & 0 & 0 \\ 0 & 0 & 0 & 0 \\ 0 & 0 & 0 & 0 \\ 0 & 0 & 0 & Z^{dc} \end{bmatrix} \begin{bmatrix} I_a^{ac} \\ I_b^{ac} \\ I_c^{ac} \\ I_d^{dc} \end{bmatrix} + \begin{bmatrix} V_a^{ac} \\ V_b^{ac} \\ V_c^{ac} \\ E^{dc} \end{bmatrix} \quad (4.113)$$

Substituting equation (4.113) into equation (4.1) gives the following relationship:

$$\begin{bmatrix} V_a^{ac} \\ V_b^{ac} \\ V_c^{ac} \\ E^{dc} \end{bmatrix} = \begin{bmatrix} I^M & 0 & 0 & 0 \\ 0 & I^M & 0 & 0 \\ 0 & 0 & I^M & 0 \\ A_d & B_d & C_d & D_d - Z^{dc} \end{bmatrix} \begin{bmatrix} V_a^{ac} \\ V_b^{ac} \\ V_c^{ac} \\ I_d^{dc} \end{bmatrix} \quad (4.114)$$

Equation (4.114) can be used to compute the harmonic components of I_d^{dc} for given ac source voltages and converter parameters.

The above equations illustrate the coupling between the harmonics in a three-phase ac-system. For example the current in phase-a (equation 4.92) has the following matrix representation:

$$\begin{bmatrix} \cdot \\ \cdot \\ I_{-1a} \\ I_{0a} \\ I_{1a} \\ \cdot \\ \cdot \end{bmatrix} = \begin{bmatrix} \cdot & \cdot & \cdot & \cdot & \cdot & \cdot & \cdot \\ \cdot & \cdot & \cdot & \cdot & \cdot & \cdot & \cdot \\ \cdot & \cdot & a_0 & a_{-1} & a_{-2} & \cdot & \cdot \\ \cdot & \cdot & \cdot & a_1 & a_0 & a_{-1} & \cdot \\ \cdot & \cdot & \cdot & \cdot & a_2 & a_1 & a_0 \\ \cdot & \cdot & \cdot & \cdot & \cdot & \cdot & \cdot \\ \cdot & \cdot & \cdot & \cdot & \cdot & \cdot & \cdot \end{bmatrix} \begin{bmatrix} \cdot \\ \cdot \\ V_{-1a}^{ac} \\ V_{0a}^{ac} \\ V_{1a}^{ac} \\ \cdot \\ \cdot \end{bmatrix} \\
 + \begin{bmatrix} \cdot & \cdot & \cdot & \cdot & \cdot & \cdot & \cdot \\ \cdot & \cdot & \cdot & \cdot & \cdot & \cdot & \cdot \\ \cdot & \cdot & b_0 & b_{-1} & b_{-2} & \cdot & \cdot \\ \cdot & \cdot & \cdot & b_1 & b_0 & b_{-1} & \cdot \\ \cdot & \cdot & \cdot & b_2 & b_1 & b_0 & \cdot \\ \cdot & \cdot & \cdot & \cdot & \cdot & \cdot & \cdot \\ \cdot & \cdot & \cdot & \cdot & \cdot & \cdot & \cdot \end{bmatrix} \begin{bmatrix} \cdot \\ \cdot \\ V_{-1b}^{ac} \\ V_{0b}^{ac} \\ V_{1b}^{ac} \\ \cdot \\ \cdot \end{bmatrix} \\
 + \begin{bmatrix} \cdot & \cdot & \cdot & \cdot & \cdot & \cdot & \cdot \\ \cdot & \cdot & \cdot & \cdot & \cdot & \cdot & \cdot \\ \cdot & \cdot & c_0 & c_{-1} & c_{-2} & \cdot & \cdot \\ \cdot & \cdot & \cdot & c_1 & c_0 & c_{-1} & \cdot \\ \cdot & \cdot & \cdot & c_2 & c_1 & c_0 & \cdot \\ \cdot & \cdot & \cdot & \cdot & \cdot & \cdot & \cdot \\ \cdot & \cdot & \cdot & \cdot & \cdot & \cdot & \cdot \end{bmatrix} \begin{bmatrix} \cdot \\ \cdot \\ V_{-1c}^{ac} \\ V_{0c}^{ac} \\ V_{1c}^{ac} \\ \cdot \\ \cdot \end{bmatrix} \\
 + \begin{bmatrix} \cdot & \cdot & \cdot & \cdot & \cdot & \cdot & \cdot \\ \cdot & \cdot & \cdot & \cdot & \cdot & \cdot & \cdot \\ \cdot & \cdot & d_0 & d_{-1} & d_{-2} & \cdot & \cdot \\ \cdot & \cdot & \cdot & d_1 & d_0 & d_{-1} & \cdot \\ \cdot & \cdot & \cdot & d_2 & d_1 & d_0 & \cdot \\ \cdot & \cdot & \cdot & \cdot & \cdot & \cdot & \cdot \\ \cdot & \cdot & \cdot & \cdot & \cdot & \cdot & \cdot \end{bmatrix} \begin{bmatrix} \cdot \\ \cdot \\ I_{-1d}^{dc} \\ I_{0d}^{dc} \\ I_{1d}^{dc} \\ \cdot \\ \cdot \end{bmatrix} \quad (4.115)$$

A single frequency of phase-a current is coupled to all the harmonics of the phase voltages and dc current through the matrices A_a , B_a , C_a and D_a .

4.4 Solution of System Equations

The harmonic admittance matrix is a function of the firing angles ϕ_1, \dots, ϕ_6 , the overlap angle μ and the inductance L_c . The harmonics generated by the converter can be studied by solving the system equations developed in the last section.

4.4.1 Constraint Equations

The harmonic admittance matrix given by equation (4.1) relates the ac side and dc side quantities through the matrices \mathbf{A}_a through \mathbf{D}_d . These sixteen matrices are functions of the firing angle, α and the overlap angle, μ . In order to solve the set of equations, it is necessary to obtain a relationship between α and μ . The equation for the three-phase model can be obtained by considering the commutation overlap interval, exemplified by the transfer of current from thyristor 5 to thyristor 1. After the lapse of this interval the current in phase-a is equal to the steady state dc current I_d^{dc} as shown in Fig. 4.2. Similar equations can be formed for the other two phases. However in the example studied it was verified that testing the equation for one phase was sufficient. This is because it is assumed that the three-phase system is balanced and symmetrical, and the overlap intervals are the same for all commutations in the three phases. The equation for the commutation overlap interval between thyristors 1 and 5 can be written as (equation 3.48)

$$\sum_{\substack{n=-\infty \\ n \neq 0}}^{\infty} \frac{V_{an}^{ac} - V_{bn}^{ac}}{2jn\omega L} \{e^{jn\phi_1} [e^{jn\mu} - 1]\} = \sum_{m=-\infty}^{\infty} I_{dm}^{dc} [e^{jm(\phi_1+\mu)}] \quad (4.116)$$

V_{an} and V_{bn} denote the nth harmonic component of v_a^{ac} and v_b^{ac} respectively.

4.4.2 Procedure for the Solution of Equations

1. Select a firing angle α .
2. Make a reasonable guess for overlap angle μ .
3. Evaluate parameter matrices \mathbf{A}_a through \mathbf{D}_d using equations (4.93) through (4.112).
4. Solve equation (4.114) to determine the components of \mathbf{V}_a^{ac} , \mathbf{V}_b^{ac} , \mathbf{V}_c^{ac} and \mathbf{I}_d^{dc} .
5. Check whether equation (4.116) is satisfied.

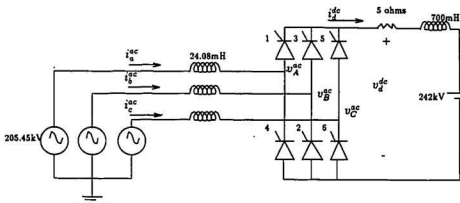


Figure 4.5: Example HVDC System [20]

6. While equation (4.116) is not satisfied repeat steps 3 and 4 by updating the value of the overlap angle, until equation (4.116) is satisfied.
7. Solve for V^{dc} , I_a^{ac} , I_b^{ac} and I_c^{ac} using equation (4.1).

4.5 System Example

The simplified HVDC system, shown in Fig. 4.5 is used as an example to demonstrate the use of the harmonic admittance method to determine the harmonics by the three-phase converter. The results obtained by the harmonic admittance method are verified using EMTP simulation.

4.5.1 Simulation Using the Harmonic Admittance Algorithm

The procedure outlined in section 4.4.2 is used to compute the harmonics in the input currents, the output dc voltage and the dc current in the three-phase converter. The results presented in this section are normalized with respect to voltage and current values corresponding to normal operating condition of $\alpha = 18^\circ$ and

$$\mu = 13.45^\circ [20].$$

Figures 4.6 and 4.7 show the plots of the dc component of the converter output current and dc voltage for different overlap angles. For comparison purposes the results of the classical method are also shown. It is observed that the classical method overestimates the output current as it neglects the cross-coupling between the harmonics.

Figures 4.8 and 4.9 show the frequency spectrum of the ac current and output voltage harmonics respectively. The current harmonics are normalized with respect to the magnitude of the dc current and the dc voltage harmonics are normalized with respect to the average dc voltage. The harmonic admittance method correctly predicts the characteristic harmonics generated by the converter.

Figure 4.10 shows the converter harmonics as a function of the overlap angle. As expected the fundamental component increases with increasing overlap angle because the firing angle decreases with increasing overlap angle. Comparison with the classical method shows that the classical method overestimates the fundamental component for higher overlap angles.

Figure 4.11 shows the dominant harmonic component of the the output voltage (i.e. the 6th harmonic) has a minimum value at an overlap angle of 16° .

4.6 Simulation Using EMTP

The example considered in the previous section was simulated using the EMTP as the simulation tool to verify the harmonic admittance method for the three-phase converter. Thyristor switches can be represented in EMTP by TACS-controlled type-11 switches. TACS was also used to generate the gate pulses using a control circuit simulation. The details of the gate pulse generator are given in Appendix A.

The node diagram of the EMTP model is shown in figure 4.12. For simulation

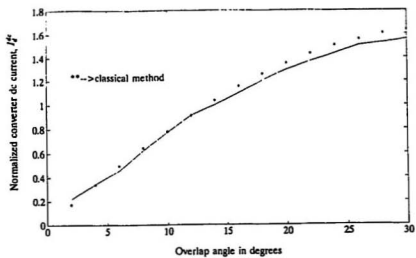


Figure 4.6: DC Component of the Converter Output Current

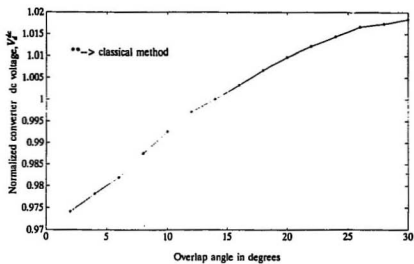


Figure 4.7: DC Component of the Converter Output Voltage

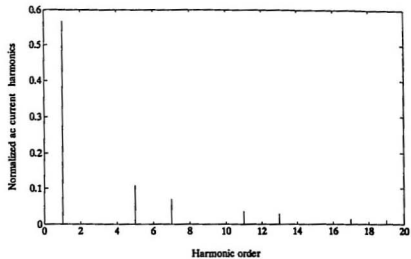


Figure 4.8: Frequency Spectrum of the AC Current

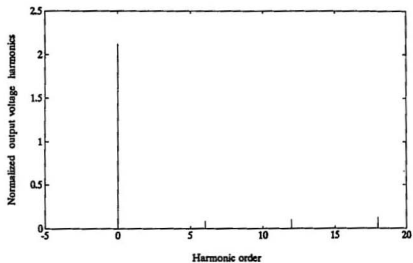


Figure 4.9: Frequency Spectrum of the Output Voltage

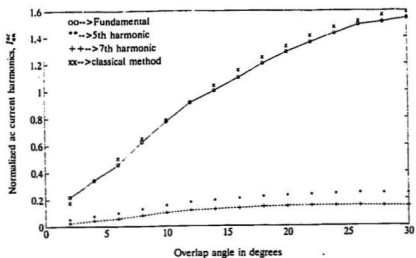


Figure 4.10: Harmonics in the AC Current

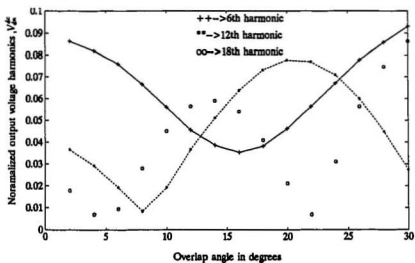


Figure 4.11: Harmonics in the Output Voltage

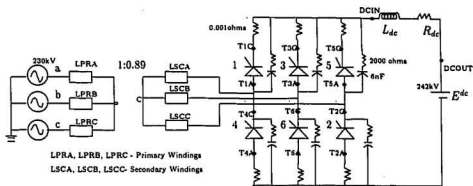


Figure 4.12: Node Details of EMTP Model

purposes, small series resistances and snubber circuits, shown in the figure were introduced.

The $Y - Y$ transformer shown in the circuit is replaced by three single phase transformers. The special request word *transformer* in the $R - L - C$ component cards is used to model each transformer [19]. The transformers have no magnetizing branches and saturation effects were not considered in the model.

The thyristors were modeled using type-11 TACS switches. The *echo* feature was activated to obtain the diagnostic output. This gives exact instants at which the thyristors open and close. This was useful in verifying the duration of the commutation overlap intervals.

4.7 System Waveforms

The system waveforms obtained using the harmonic admittance method were verified by EMTP simulation. The harmonics computed from the harmonic admittance method were recombined to obtain the steady-state voltage and current waveforms presented in this section. Harmonics up to the 20th order were used to obtain the waveforms. Voltage waveforms are normalized with respect to the rms value of the

source voltage and current waveforms are normalized with respect to the dc current at $\alpha = 18^\circ$.

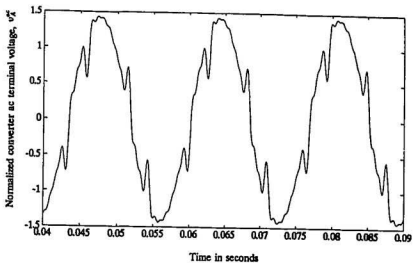
Figures 4.13 and 4.14 show the line-ground ac voltage, v_A^{ac} at the ac terminals of the converter for two values of α as obtained by the harmonic admittance method and the EMTF simulation. The waveforms clearly show the notches due to commutation. The EMTF simulated waveform shows the notches sharply even though there is some oscillation in the voltage waveform at the points where thyristors switch on and off. The values of the voltages in both the harmonic admittance method and the EMTF are in close agreement.

Figures 4.15 and 4.16 show the line current, i_a^{ac} for two values of firing angles as obtained by the harmonic admittance method and the EMTF simulation. The waveforms are as expected.

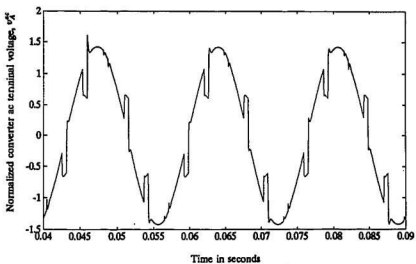
Figures 4.17 and 4.18 show the output voltage, v_d^{dc} for two values of α as obtained by the harmonic admittance method and the EMTF simulation. The values are about the same in both cases. The slight deviation in the waveshapes is due to the limited number of harmonic terms used in the harmonic admittance method.

4.8 Summary

A three-phase model of the converter system based on the harmonic admittance approach was developed. The parameter matrices \mathbf{A}_a through \mathbf{D}_d were derived in terms of the voltage and current switching functions. The system waveforms obtained were validated using EMTF and it was shown that the model predicts correct information on the harmonic levels.



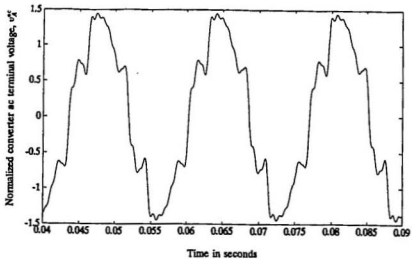
[a]



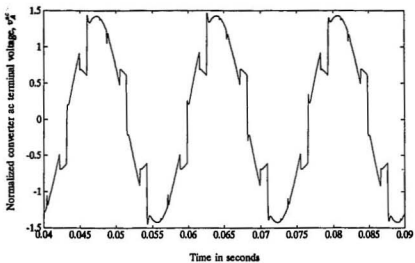
[b]

Figure 4.13: Voltage at the Converter AC Terminals v_A^c , $\alpha = 18^\circ$

(a) Harmonic Admittance Method (b) EMTF Simulation



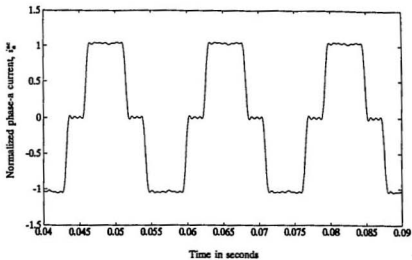
[a]



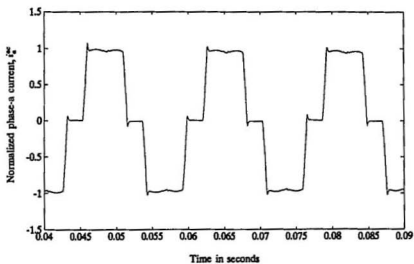
[b]

Figure 4.14: Voltage at the Converter AC Terminals v_{λ}^{ac} , $\alpha = 8^\circ$

(a) Harmonic Admittance Method (b) EMTP Simulation



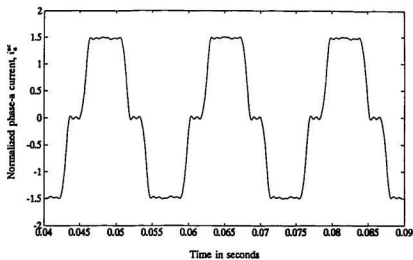
[a]



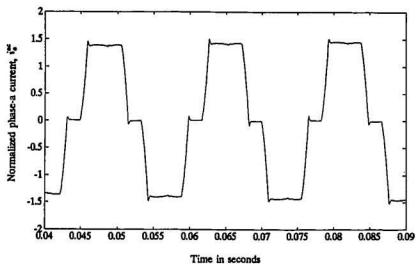
[b]

Figure 4.15: AC Current Waveform i_a^c , $\alpha = 18^\circ$

(a) Harmonic Admittance Method (b) EMTP Simulation



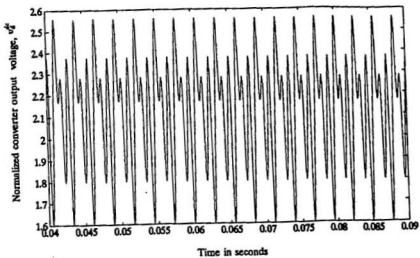
[a]



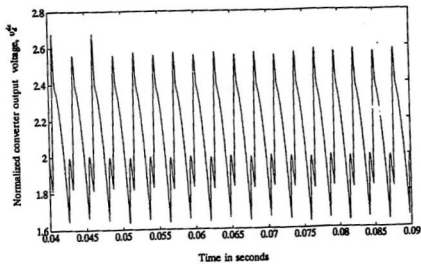
[b]

Figure 4.16: AC Current Waveform i_a^c , $\alpha = 8^\circ$

(a) Harmonic Admittance Method (b) EMTF Simulation

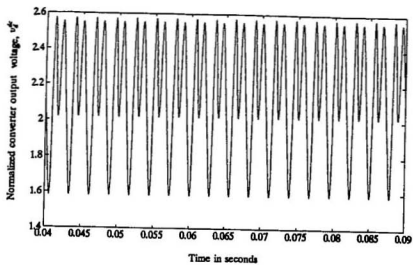


[a]

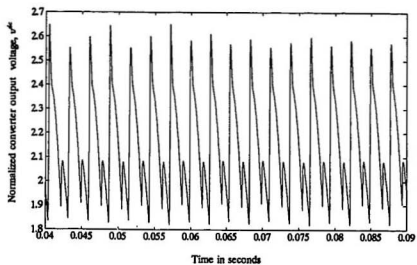


[b]

Figure 4.17: Voltage at the DC Terminals of the Converter v_d^{dc} , $\alpha = 18^\circ$
 (a) Harmonic Admittance Method (b) EMTF Simulation



[a]



[b]

Figure 4.18: Voltage at the DC Terminals of the Converter v_d^c , $\alpha = 8^\circ$

(a) Harmonic Admittance Method (b) EMTP Simulation

Chapter 5

Harmonic Analysis of an HVDC system

In the previous chapter, the basic three-phase converter without an ac source network was analyzed. In this chapter the harmonic admittance method is extended to study the harmonic interactions in a system with an ac network at the primary side of the converter transformer. In the later part of the chapter, input source containing harmonics and a converter system with unbalanced ac side impedances are considered.

5.1 The Three Phase Converter Connected to an AC Network

Figure 5.1 shows the three phase converter system connected to the source through an ac network. Z_a^{ac} , Z_b^{ac} and Z_c^{ac} represent the Thevenin equivalent impedance of the ac network. More complex circuits can be reduced to the circuit of figure 5.1 by representing the ac source and its complex network with its Thevenin equivalent circuit. For instance, the impedance of the ac system along with all the filters and line impedances can be reduced to Z_a^{ac} , Z_b^{ac} and Z_c^{ac} in series with the input voltages e_a^{ac} , e_b^{ac} and e_c^{ac} . L_c represents the inductance of the converter transformer. The dc side inductance L_{dc} is sufficiently large to maintain a continuous output current i_d^{dc} .

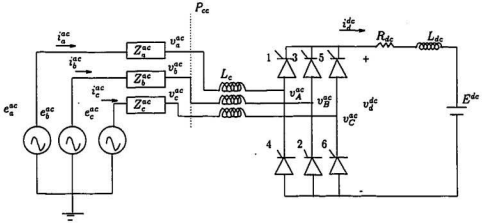


Figure 5.1: Three Phase Converter Connected to the AC Network

5.1.1 System Equations

Equation (4.1) can be used to solve for the current in each of the three phases if the Fourier matrix representation of the voltages at the point of common coupling, P_{cc} , V_a^{ac} , V_b^{ac} and V_c^{ac} and the output dc voltage, V_d^{dc} are known. In a practical system only the source voltages E_a^{ac} , E_b^{ac} , E_c^{ac} and the dc link voltage E_d^{dc} are known. These two sets of voltage quantities are related by the following equation.

$$\begin{bmatrix} V_a^{ac} \\ V_b^{ac} \\ V_c^{ac} \\ V_d^{dc} \end{bmatrix} = \begin{bmatrix} -Z_a^{ac} & 0 & 0 & 0 \\ 0 & -Z_b^{ac} & 0 & 0 \\ 0 & 0 & -Z_c^{ac} & 0 \\ 0 & 0 & 0 & Z^{dc} \end{bmatrix} \begin{bmatrix} I_a^{ac} \\ I_b^{ac} \\ I_c^{ac} \\ I_d^{dc} \end{bmatrix} + \begin{bmatrix} E_a^{ac} \\ E_b^{ac} \\ E_c^{ac} \\ E_d^{dc} \end{bmatrix} \quad (5.1)$$

where Z_a^{ac} , Z_b^{ac} , Z_c^{ac} represent the matrix representation of the network impedances.

Substituting equation (5.1) into equation (4.1) gives the following relationship.

$$\begin{bmatrix} E_a^{ac} \\ E_b^{ac} \\ E_c^{ac} \\ E_d^{dc} \end{bmatrix} = \begin{bmatrix} I^M + Z_a^{ac} A_a & Z_a^{ac} B_a & Z_a^{ac} C_a & Z_a^{ac} D_a \\ Z_b^{ac} A_b & I^M + Z_b^{ac} B_b & Z_b^{ac} C_b & Z_b^{ac} D_b \\ Z_c^{ac} A_c & Z_c^{ac} B_c & I^M + Z_c^{ac} C_c & Z_c^{ac} D_c \\ A_d & B_d & C_d & D_d - Z^{dc} \end{bmatrix} \begin{bmatrix} V_a^{ac} \\ V_b^{ac} \\ V_c^{ac} \\ I_d^{dc} \end{bmatrix} \quad (5.2)$$

The solution procedure described in section 4.4.2 is employed to determine V_a^{ac} , V_b^{ac} , V_c^{ac} and I_d^{dc} from equation (5.2) for specified source voltages and ac network

Table 5.1: Parameters of the Filters

Type	Tuned	Tuned	Damped
Order	5th	7th	11th
$C(\mu F)$	2.62	2.62	4.42
$L(mH)$	107.42	54.81	13.16
$R(\Omega)$	1.27	0.90	70.92

impedance.

5.1.2 System Example

The HVDC system used as an example is shown in Fig. 5.2. The system is reduced to the model shown in Fig. 5.1 by representing the inverter in the HVDC system with a dc source E^{dc} . The following are the system parameters [20].

- AC Source: 230kV L-L on the line side and 205.45kV on the converter side
- Transformer: $X_L = 10\%$ per phase and turns ratio is 1:0.89
- Inverter: $E^{dc} = 242\text{kV}$ DC, $L_d = 700\text{mH}$, $R_d = 5\Omega$
- Transmission lines: $R_s = 1.1572\Omega$, $L_s = 44.6\text{mH}$
- Shunt harmonic filters at the point of common coupling to provide a low impedance path to ground for the harmonic voltages generated. The values of the R, L and C components of the filters are as given in the Table 5.1.

For this example system the Thevenin equivalent impedance at the fundamental frequency is determined to be $Z^{ac} = 0.234 - j269.01$. The harmonic characteristic of the Thevenin impedance is shown in Fig 5.3. It can be seen that the filters have low impedance value at the 5th and 7th harmonic frequencies.

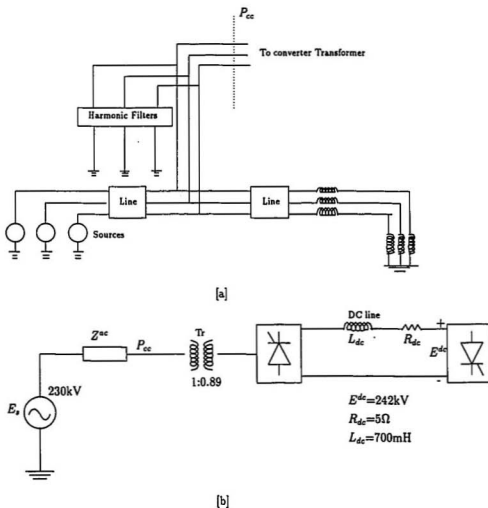


Figure 5.2: An HVDC System Example

(a) AC Network (b) Single line representation

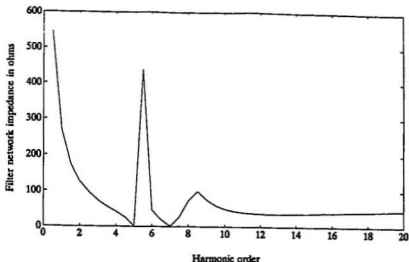


Figure 5.3: Harmonic Impedance of the Filter Network

5.1.3 Simulation Results

The impedance matrices Z_a^{ac} , Z_b^{ac} and Z_c^{ac} in equation (5.2) are obtained by forming a diagonal matrix containing the harmonic components of the impedance as the diagonal elements. The system is analyzed at the steady state operating conditions corresponding to $\alpha = 18^\circ$ and $\mu = 13^\circ$ using the harmonic admittance method.

Frequency spectrum of the ac current and output dc voltage are shown in Figs. 5.4 and 5.5 respectively. As expected the harmonic admittance algorithm predicts the characteristic harmonics of $6k \pm 1$ in the input current and $6k$ in the output voltage.

5.1.4 System Waveforms

System waveforms obtained using the harmonic admittance method were verified by EMTF simulation. The details of EMTF model are the same as in Fig. 4.12 with additional branch cards to represent the ac network. The reference voltage for the generation of triggering pulses are synchronized to the voltage at P_{ca} as detailed in Appendix B. A harmonic order of 20 was used to obtain the voltage

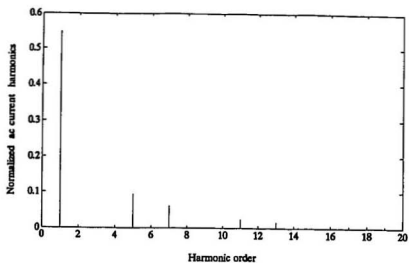


Figure 5.4: Frequency Spectrum of the AC Current

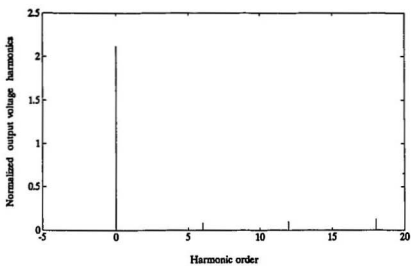


Figure 5.5: Frequency Spectrum of the Output Voltage

and current waveforms in the harmonic admittance method. Voltage waveforms are normalized with respect to the rms value of the source voltage and current waveforms are normalized with respect to the dc current at $\alpha = 18^\circ$.

Figure 5.6 shows the phase-a voltage at P_{ce} , v_a^{ac} as obtained by the harmonic admittance method and EMTP simulation. The values of the voltages in both harmonic admittance method and the EMTP are about the same.

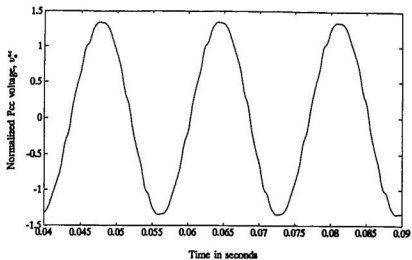
Figure 5.7 shows the phase-a ac terminal voltage v_A^{ac} for the two simulation methods. The waveforms show the commutation notches. The notches are not as sharp in the harmonic admittance method because of the number of harmonic components used to reconstruct the waveform. The values of the voltages in both harmonic admittance method and the EMTP are about the same.

Figure 5.8 shows the phase-a current as obtained by the harmonic admittance method and EMTP simulation. The shape and the values of the waveforms match well. Both methods predict an overlap angle of $\mu = 13^\circ$. This was further verified using the *echo* feature in EMTP to observe the instants of closing and opening of the thyristors.

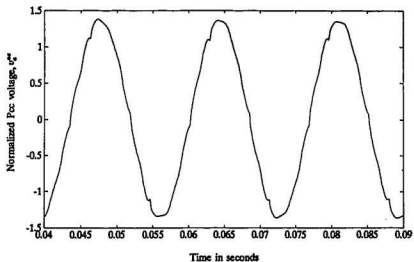
The output voltage waveforms as obtained by the harmonic admittance method and EMTP simulation are shown in Fig. 5.9. The values are about the same in both methods. The waveforms confirm the correctness of the harmonic admittance algorithm.

5.2 The Three-Phase Converter System with Source Harmonics

In the previous section the input source to the three-phase converter system was assumed to contain only the fundamental component. In this section the effect of source harmonics on the harmonic interactions in the system is considered. For simplicity, the source voltages are assumed to contain a 5th harmonic component.



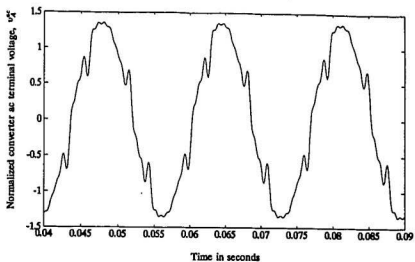
[a]



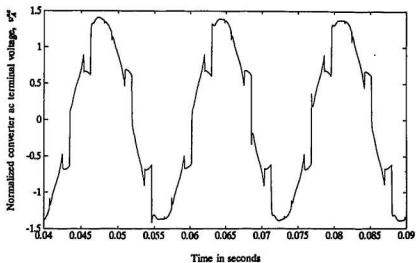
[b]

Figure 5.6: Voltage at the Point of Common Coupling, v_a^{pc} , $\alpha = 18^\circ$

(a) Harmonic Admittance Method (b) EMTP Simulation



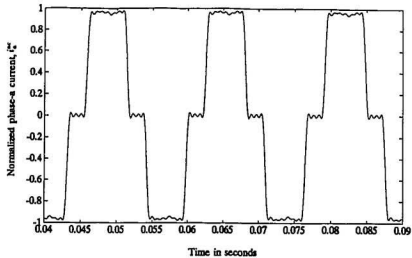
[a]



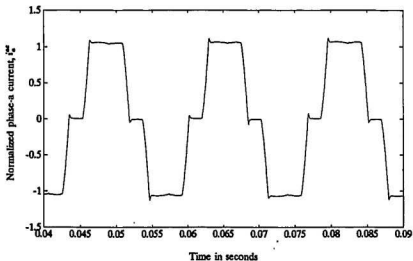
[b]

Figure 5.7: Voltage at the Converter AC Terminals, v_a^c , $\alpha = 18^\circ$

(a) Harmonic Admittance Method (b) EMTF Simulation



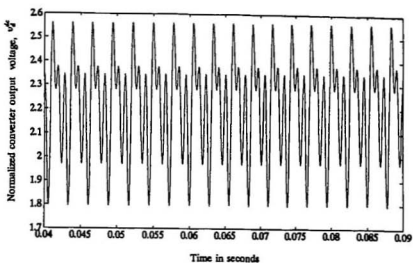
[a]



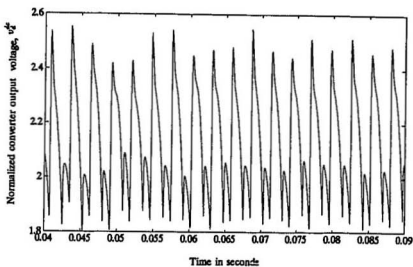
[b]

Figure 5.8: AC Current Waveform, i_a^{ac} , $\alpha = 18^\circ$

(a) Harmonic Admittance Method (b) EMTF Simulation



[a]



[b]

Figure 5.9: Voltage at the DC Terminals of the Converter, v_d^c , $\alpha = 18^\circ$

(a) Harmonic Admittance Method (b) EMTP Simulation

In order to characterize the effect of the source harmonics, the filters at the input are neglected and the line impedances, Z_a^{ac} , Z_b^{ac} and Z_c^{ac} are assumed to be balanced. The line resistance and inductance are $R_s = 1.157\Omega$ and $L_s = 44.58mH$.

5.2.1 Simulation using the Harmonic Admittance Algorithm

The matrices E_a^{ac} , E_b^{ac} and E_c^{ac} are initialized to contain a fifth harmonic Fourier component which is assumed to be 5% of the fundamental component. The rest of the solution procedure is the same as the previous case. Figure 5.10 shows the frequency spectrum of the input voltage. A significant 5th harmonic component can be observed. Figure 5.11 shows the frequency spectrum of the voltage at P_{cs} , which contain only the characteristic frequencies. Figure 5.12 shows the frequency spectrum of the phase-a current. It is observed that the 5th harmonic component in the ac source results in a slight increase in the 5th harmonic current. Figure 5.13 shows the frequency spectrum of the output voltage. It can be seen that the 5th harmonic component in the source produces a small 4th harmonic component on the dc side.

5.2.2 System Waveforms

Results obtained using the harmonic admittance method were verified by EMTP simulation. The details of the EMTP model are the same as the previous case with an additional 5th harmonic source voltage in parallel with the fundamental source voltage. Figures 5.14 to 5.17 show the waveforms in the system. The waveforms are as expected. The distortion in the waveforms, caused by the 5th harmonic component in the ac source, can be observed. The waveforms demonstrate that the harmonic admittance method accurately predicts the effect of source harmonics on the system voltages and currents.

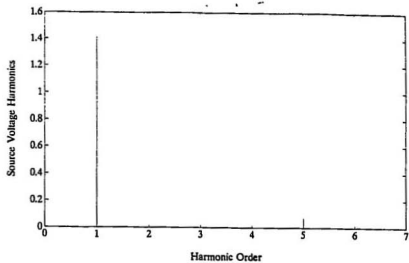
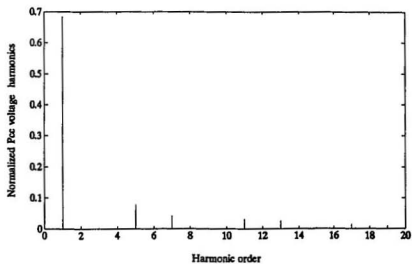


Figure 5.10: Source Voltage Spectrum

Figure 5.11: P_{cc} Voltage Spectrum

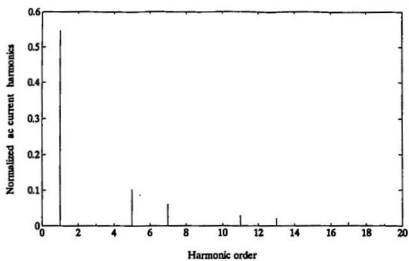


Figure 5.12: AC Current Spectrum

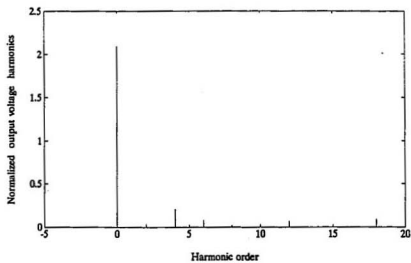
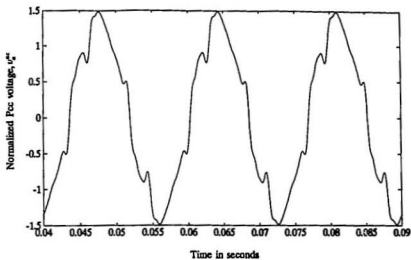
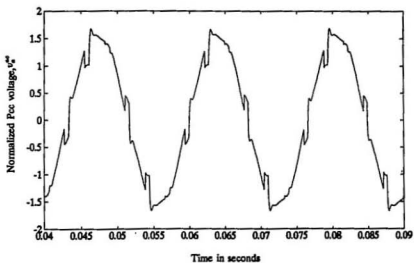


Figure 5.13: Output Voltage Spectrum



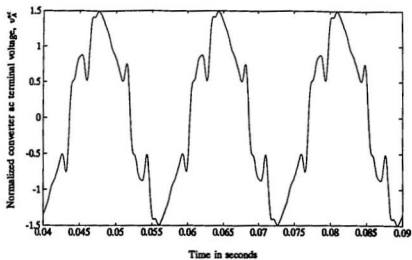
[a]



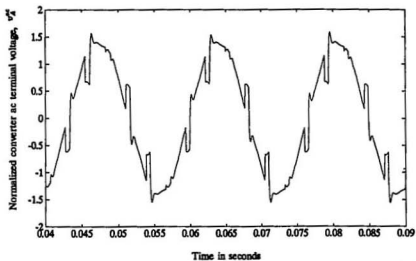
[b]

Figure 5.14: Voltage at the Point of Common Coupling, v_a^{pc} , $\alpha = 18^\circ$

(a) Harmonic Admittance Method (b) EMTP Simulation



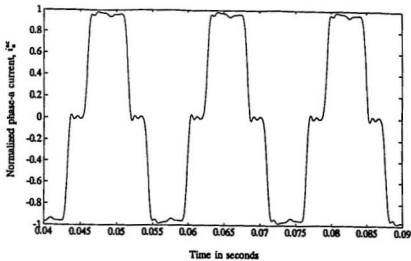
[a]



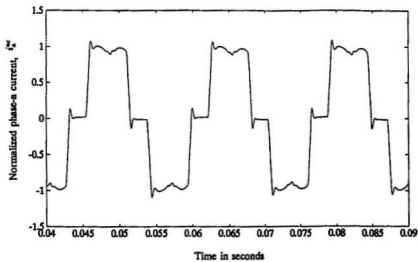
[b]

Figure 5.15: Voltage at the Converter AC Terminals, v_X^c , $\alpha = 18^\circ$

(a) Harmonic Admittance Method (b) EMTP Simulation



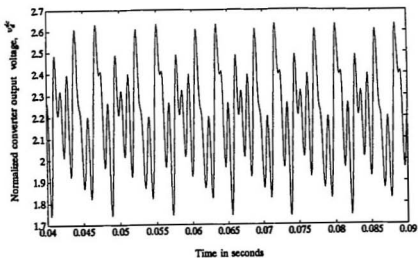
[a]



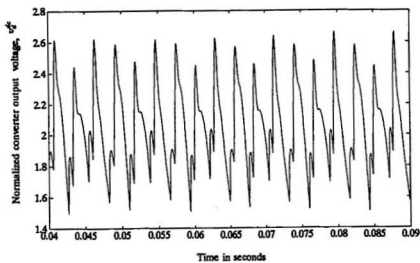
[b]

Figure 5.16: AC Current Waveform, i_a^{ac} , $\alpha = 18^\circ$

(a) Harmonic Admittance Method (b) EMTF Simulation



[a]



[b]

Figure 5.17: Voltage at the DC Terminals of the Converter, v_d^{dc} , $\alpha = 18^\circ$

(a) Harmonic Admittance Method (b) EMTP Simulation

5.3 The Three Phase Converter System with Unbalanced System Impedances

In the previous examples the impedances Z_a^{ac} , Z_b^{ac} and Z_c^{ac} were assumed to be balanced. In this section the harmonic admittance approach is extended to study the harmonic interactions of the three-phase converter system connected to unbalanced system impedances.

5.3.1 Simulation using the Harmonic Admittance Algorithm

The line resistance and inductance of the HVDC system in Fig 5.2 are $R_s = 1.157\Omega$, $L_s = 44.58mH$. Assuming $\pm P$ as the percentage imbalance in phase-b and phase-c, respectively the system impedances are represented by

$$Z_a^{ac} = 1.1572 + jn\omega 0.04458 \quad (5.3)$$

$$Z_b^{ac} = \left(1 + \frac{P}{100}\right) Z_a^{ac} \quad (5.4)$$

$$Z_c^{ac} = \left(1 - \frac{P}{100}\right) Z_a^{ac} \quad (5.5)$$

Unbalanced impedances lead to unequal overlap intervals. The harmonic admittance formulation presented in chapter 4 is still applicable. However, the switching functions are modified to account for the unequal overlap intervals. Tables 5.2 and 5.3 show the modified switching functions.

μ_1 through μ_6 represent the overlap angles for the corresponding commutation intervals. As there is no asymmetry in the firing angles, the following equations apply.

$$\mu_1 = \mu_4 \quad (5.6)$$

$$\mu_2 = \mu_5 \quad (5.7)$$

$$\mu_3 = \mu_6 \quad (5.8)$$

Table 5.2: Modified Voltage Switching Functions

Switching Function	Equivalent Switching Function	Switches Conducting	Start of Interval	End of Interval	Voltage Magnitude
H^{561}	H^{51}	5,6,1	ϕ_1	$\phi_1 + \mu_1$	$\frac{v_a^{sc} + v_c^{sc}}{2} - v_b^{sc}$
H^{16}		1,6	$\phi_1 + \mu_1$	ϕ_2	$v_a^{sc} - v_b^{sc}$
H^{162}	H^{62}	1,6,2	ϕ_2	$\phi_2 + \mu_2$	$v_a^{sc} - \frac{v_c^{sc} + v_b^{sc}}{2}$
H^{12}		1,2	$\phi_2 + \mu_2$	ϕ_3	$v_a^{sc} - v_c^{sc}$
H^{123}	H^{13}	1,2,3	ϕ_3	$\phi_3 + \mu_3$	$\frac{v_a^{sc} + v_b^{sc}}{2} - v_c^{sc}$
H^{23}		2,3	$\phi_3 + \mu_3$	ϕ_4	$v_b^{sc} - v_c^{sc}$
H^{234}	H^{24}	2,3,4	ϕ_4	$\phi_4 + \mu_4$	$v_b^{sc} - \frac{v_c^{sc} + v_a^{sc}}{2}$
H^{34}		3,4	$\phi_4 + \mu_4$	ϕ_5	$v_b^{sc} - v_a^{sc}$
H^{345}	H^{35}	3,4,5	ϕ_5	$\phi_5 + \mu_5$	$\frac{v_b^{sc} + v_c^{sc}}{2} - v_a^{sc}$
H^{45}		4,5	$\phi_5 + \mu_5$	ϕ_6	$v_c^{sc} - v_a^{sc}$
H^{456}	H^{46}	4,5,6	ϕ_6	$\phi_6 + \mu_6$	$v_c^{sc} - \frac{v_b^{sc} + v_a^{sc}}{2}$
H^{56}		5,6	$\phi_6 + \mu_6$	$\phi_6 + \frac{\pi}{3}$	$v_c^{sc} - v_b^{sc}$

Table 5.3: Modified Current Switching Functions

Switching Function	Start of interval	End of interval
H^1	ϕ_1	$\phi_3 + \mu_3$
H^2	ϕ_2	$\phi_4 + \mu_4$
H^3	ϕ_3	$\phi_5 + \mu_5$
H^4	ϕ_4	$\phi_6 + \mu_6$
H^5	ϕ_5	$\phi_5 + \frac{2\pi}{3} + \mu_1$
H^6	ϕ_6	$\phi_6 + \frac{2\pi}{3} + \mu_2$

The three different overlap angles involved require three constraint equations to obtain the solution of the system equations. The constraint equation for commutation from thyristor 1 to thyristor 5 is obtained from equation (4.116) as

$$\sum_{\substack{n=-\infty \\ n \neq 0}}^{\infty} \frac{V_{an}^{ac} - V_{bn}^{ac}}{2jn\omega L} \{e^{jn\phi_1} [e^{jn\mu_1} - 1]\} = \sum_{m=-\infty}^{\infty} I_{dm}^{dc} [e^{jm(\phi_1 + \mu_1)}] \quad (5.9)$$

Similarly, the constraint equation for commutation from thyristor 3 to thyristor 1, and thyristor 5 to thyristor 3 can be written respectively as

$$\sum_{\substack{n=-\infty \\ n \neq 0}}^{\infty} \frac{V_{bn}^{ac} - V_{an}^{ac}}{2jn\omega L} \{e^{jn\phi_2} [e^{jn\mu_2} - 1]\} = \sum_{m=-\infty}^{\infty} I_{dm}^{dc} [e^{jm(\phi_2 + \mu_2)}] \quad (5.10)$$

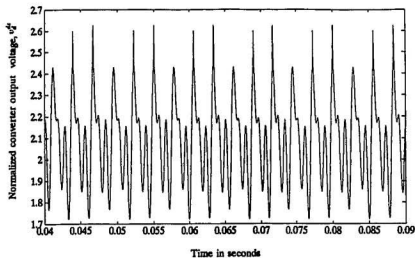
$$\sum_{\substack{n=-\infty \\ n \neq 0}}^{\infty} \frac{V_{cn}^{ac} - V_{bn}^{ac}}{2jn\omega L} \{e^{jn\phi_3} [e^{jn\mu_3} - 1]\} = \sum_{m=-\infty}^{\infty} I_{dm}^{dc} [e^{jm(\phi_3 + \mu_3)}] \quad (5.11)$$

5.3.2 Simulation Results

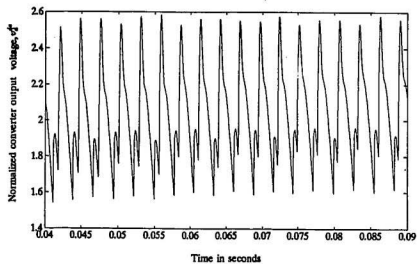
Figure 5.18 shows the output voltage as obtained by the harmonic admittance approach and EMTP simulation respectively for a percentage imbalance $P = 10\%$. The effect of unbalanced phase impedances can be observed as the peak voltages during the commutation intervals differ.

Unbalanced system impedance results in the generation of uncharacteristic harmonics in the ac-side and the dc-side [25]. Figure 5.19 shows the magnitude of the uncharacteristic harmonics in the voltage at the point of common coupling as the percentage imbalance is varied from 10 to 50%. It can be observed that the magnitude of the uncharacteristic harmonics (3rd, 9th and 15th) increase as the percentage imbalance increases.

Similarly the magnitude of the uncharacteristic output voltage harmonics (2nd, 4th and the 8th), shown in Fig 5.20 increase with increasing percentage imbalance. It is also observed that the magnitude of the uncharacteristic harmonics decrease considerably as the firing angle, α is increased.



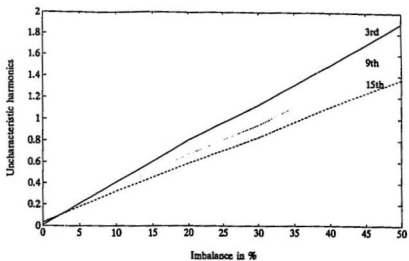
[a]



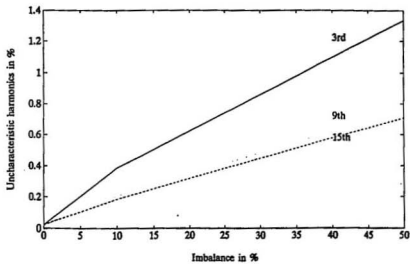
[b]

Figure 5.18: Voltage at the DC Terminals of the Converter v_d^c , $\alpha = 18^\circ$

(a) Harmonic Admittance Method (b) EMTP Simulation

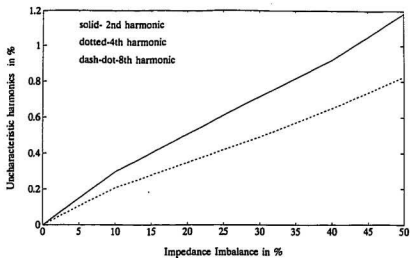


[a.]

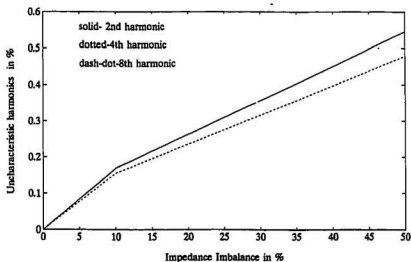


[b.]

Figure 5.19: Uncharacteristic Harmonics in the P_{cc} Voltage(a) $\alpha = 18^\circ$ (b) $\alpha = 26^\circ$



[a]



[b]

Figure 5.20: Uncharacteristic Harmonics in the Converter Output Voltage

(a) $\alpha = 18^\circ$ (b) $\alpha = 26^\circ$

5.4 Summary

The harmonic admittance model was extended to represent a three-phase converter system connected to an ac network which included harmonic filters and a transmission line. The method effectively represents the harmonic characteristic of the network impedance and accurately predicts the voltage harmonics at the point of common coupling. The effect of the source harmonics was studied. As a result of a fifth harmonic component in the ac source, the total harmonic distortion (THD) of the voltage at the point of common coupling and the output voltage increased. The effect of imbalance in source impedance was studied. As unbalanced source impedance results in unequal overlap intervals, three constraint equations were introduced in the solution procedure. It was observed that unbalanced ac system impedance results in the generation of uncharacteristic harmonics in the voltage at the point of common coupling and in the output voltage.

Chapter 6

Conclusions

In this thesis, an analysis of the phase-controlled ac/dc converter systems has been carried out using the harmonic admittance approach. The approach is found to be effective in studying the harmonic interaction in converter systems.

The harmonic admittance method was implemented to study the harmonic interactions in a single phase converter connected to the ac network. The results of the analysis showed that the approach gives accurate information on the harmonic levels. In addition, it has been shown that the harmonic admittance method predicts the existence of an unstable region of operation in the example single phase converter system considered. The system waveforms presented indicate harmonic instability in the operation close to this region.

A three-phase model of the converter system based on the harmonic admittance approach was developed. Transmission parameters (A, B, C, D parameters), defining the relationship between the ac currents, ac voltages, dc current and the dc voltage were formed in terms of the switching functions. The system waveforms obtained were verified with the results on the same system using EMTP.

The method was extended to represent a three-phase converter system connected to an ac network which included harmonic filters and a transmission line. It was shown that

- the method effectively represents the harmonic characteristic of the network

impedance.

- the method accounts for the cross-coupling between the harmonic components of the ac-side and the dc-side voltages and currents.
- voltage harmonics at the point of common coupling are available as part of the solution.
- the effect of harmonics in the source voltage can be studied using the method. The results obtained predict an increase in the total harmonic distortion (THD) at the point of common coupling due to the harmonics present in the source.
- the effect of unbalance in source impedance can be studied using the approach. The results presented indicate that the level of uncharacteristic harmonics in the dc-side and the ac-side increase with an increasing imbalance.

The method serves as an alternate tool for the harmonic evaluation in ac/dc converter systems. The major contributions of the thesis are the development of the three-phase model of the converter system based on the harmonic admittance technique and the study of simple HVDC systems using the harmonic admittance model. It is clear from the results presented in the thesis that most of the predicted results can be obtained using the EMTP package. However, the harmonic admittance method provides additional information on the voltage harmonics at the point of common coupling and gives the individual harmonic levels in the system. This data is required for the design of harmonic filters and also to predict the behaviour of the system.

6.1 Scope for Further Development

The harmonic admittance method developed in the thesis should be extended to investigate the following.

1. A complete model of the three-phase converter, covering the various modes of operation need to be developed. The procedure outlined in the thesis is applicable. However, appropriate switching functions which define the sequence of operation for the different modes need to be developed.
2. The HVDC systems studied were represented by a reduced model where the inverter was replaced by a dc voltage source. The harmonic admittance method can be extended to study a detailed model of the HVDC system by incorporating two sets of transmission parameters, the first set of parameters defining the ac to dc conversion and the second set defining the dc to ac conversion. As a further step, these two sets of parameters can be combined to form a set of parameters that will define the relationship between the sending end ac quantities and the receiving end ac quantities.
3. Systems with asymmetrical firing angles have been found to reduce the harmonic levels in the ac system. The harmonic admittance method can be used to investigate the effect of the control technique on uncharacteristic harmonics. This can be achieved by considering unequal overlap intervals and considering asymmetrical firing instants in the solution procedure.
4. The systems considered in the thesis were represented by single units. However in large power systems where several units are put in parallel, the mutual coupling between the units have to be considered in the model. A detailed model for such systems needs to be developed.

References

- [1] J. Reeve and T.S. Rao, *Dyanamic Analysis of Harmonic Interaction between AC and DC Systems*, IEEE Transactions on Power Apparatus and Systems, vol.PAS-93, no.2, pp.640-676, March/April, 1974.
- [2] R.H. Kitchin, *New Method for Digital Computer Evaluation of Converter Harmonics in Power Systems Using State Variable Analysis*, IEE Proceedings, vol.128, pt.C, pp.196-207, July, 1981.
- [3] A.G. Phadke and J.H. Harlow, *Generation of Abnormal Harmonics in High Voltage AC/DC Power Systems*, IEEE Transactions on Power Apparatus and Systems, vol.PAS-87, no.3, pp.873-882, March, 1968.
- [4] T.S. Rao and J. Reeve, *Harmonics caused by imbalanced transformer impedances and imperfect 12-pulse operation in HVDC conversion*, IEEE Transactions on Power Apparatus and Systems, vol.PAS-95, no.5, pp.1732-1737, September/October, 1976.
- [5] J. Reeve and P.C.S. Krishnayya, *Unusual Current Harmonics Arising from High-Voltage DC Transmission*, IEEE Transactions on Power Apparatus and Systems, vol.PAS-87, no.3, pp 883-889, March, 1968.
- [6] R.M. Mathur and A.M. Sharaf, *Harmonics on DC side in HVDC conversion*, IEEE Transactions on Power Apparatus and Systems, vol.PAS-96, pp.1631-1638, September/October, 1977.

- [7] J. Reeve and J.A. Baron, *Harmonic Interaction between HVDC converters and AC Power Systems*, IEEE Transactions on Power Apparatus and Systems, vol.PAS-90, no.6, pp.2785-2791, November/December, 1971.
- [8] G.P. Christoforidis and A.P. Sakis Melipoulos, *Effects of Modelling on the Accuracy of Harmonic Analysis*, IEEE Transactions on Power Delivery, vol.5, no.3, pp.1598-1607, July, 1990.
- [9] R. Yacamini and J.C. DC Oliveira, *Comprehensive Calculation of Converter Harmonics with System Impedances and Control Representation*, IEE Proceedings on Electric Power Applications, Vol.133, Part B, no.2, pp 95-102, March, 1986.
- [10] S.G. Jalali and R.H. Lasseter, *Harmonic Interactions of Power Systems with Static Switching Circuits*, IEEE Industry Applications Society, Annual Meeting, pp 330-337, 1991.
- [11] N.L. Shore, G. Anderson, A.P. Canelhas and G. Asplund, *A Three-Pulse Model of DC Side Harmonic Flow in HVDC Systems*, IEEE Transactions on Power Delivery, vol.4, no.3, pp.1945-54, July, 1989.
- [12] D.L. Dickmader and K.J. Peterson, *Analysis of DC Harmonics using the Three-Pulse Model for the Intermountain Power Project HVDC Transmission*, IEEE Transactions on Power Delivery, vol.4, no.2, pp.1195-204, April, 1989.
- [13] A.P.B. Joosten, J. Arillaga, C.P. Arnold and N.R. Watson, *Simulation of HVDC System Disturbances with Reference to the Magnetizing History of the Converter Transformers*, IEEE Transactions on Power Delivery, vol.5, no.1, pp.330-336, January, 1990.

- [14] E.V. Larsen, D.H. Baker and J.C. McIver, *Low-Order Harmonic Interactions on AC/DC Systems*, IEEE Transactions on Power Delivery, vol.4, no.1, pp.493-501, January, 1989.
- [15] A.K.S. Bhat and S.B. Dewan, *Input-Output Harmonics of Line-Current-Modulated High-Frequency Link DC to Utility Interface Power Converters*, IEEE Transactions on Power Electronics, vol.A, pp.253-264, 1989.
- [16] E.A. Taylor, S. Goldberg and M. Jackson, *An EMTP Simulation of the HVDC Power System of a Fusion Energy Machine*, Conference Record of the IEEE Industry Applications Society Annual Meeting(cat.no.89CH2792-0), vol.1, pp.1099-105, 1989.
- [17] W. Long, D. Cotcher, D. Ruiu, P.P. Adam, S. Lee and R. Adapa, *EMTP-A Powerful Tool for Analyzing Power System Transients*, IEEE Computer Applications in Power, vol.3, no.3, pp.36-41, July, 1990.
- [18] R.M. Mathur and X. Wang, *Real-Time Digital Simulator of the Electromagnetic Transients of Power Transmission Lines*, IEEE Transactions on Power Delivery, vol.4, no.2, pp.1275-80, April, 1989.
- [19] EPRI Report EL-4541, *Electromagnetic Transients Program Revised Rule Book*, version 2.0, vol.1 and 2., B.P.A, 1989.
- [20] R.H. Lasseter, *Electromagnetic Transients Program:TACS, Final Report* EPRI Report-EL-4651, vol.4, June, 1989.
- [21] S.B. Dewan and A. Straughen, *Power Semiconductor Circuits*, John Wiley and Sons, Toronto, 1975.

- [22] J.G. Kassakian, M.F. Schlecht and G.C. Verghese, *Principles of Power Electronics*, Addison-Wesley Publishing Co., New York, 1991.
- [23] E.W. Kimbark, *Direct Current Transmission*, vol.1, Wiley Interscience, New York, 1948.
- [24] Y. Baghzouz and S.M. Ertem, *A Direct Method to Compute Voltage Harmonic Distortion Caused by Static Power Converters*, Proceedings of the Third International Conference on Harmonics in Power Systems, Nashville, pp.46-50, September, 1988.
- [25] Y. Yao and A.M. Sharaf, *Uncharacteristic Harmonics Caused by AC System Imbalances and the Effects of Smoothing Reactor*, Proceedings of the Third International Conference on Harmonics in Power Systems, Nashville, pp.28-33, September, 1988.
- [26] *VAX FORTRAN User's Guide*, Version 4.0, Digital Equipment Corporation, Massachusetts, 1984.
- [27] *Matlab User's Guide*, Version 3.5g, The Mathworks, Inc., U.S.A., 1988.

Bibliography

Karni, Shlomo, *Intermediate Network Analysis*, Allyn and Bacon Inc., Boston, 1971.

M.A. Slonim, *Mathematical Analysis of Static Converter Systems*, Elsevier Publications, 1981.

J. Arillga, D.A. Bradley and P.S. Bodger, *Power System Harmonics*, John Wiley & Sons, 1985.

M.S. Garrido, *On Park's Model of a Three-Phase Diode Rectifier*, Electrical Machines and Converters - Modelling and Simulation, Elsevier Science Publishers B.V, North-Holland, pp.211-217, 1984.

R.P. Stratford, *Rectifier Harmonics in Power Systems*, IEEE Transactions on Industry Applications, vol.IA-16, no.2, pp. 271-276, March/April, 1980.

R. Yacmini, *Converter Harmonic Generation and Calculations*, Conference Record, International Conference on Harmonics in Power Systems, UMIST, Manchester, England, pp.15-36, 1981.

B.R. Pelly, *Thyristor Phase-controlled Converters and Cycloconverters*, Wiley Interscience, New York, 1971.

L.J. Bohman and R.H. Lasseter, *Harmonic Interactions in Thyristor Controlled Reactor Circuits*, IEEE Transactions on Power Delivery, vol.4, no.3, pp.1919-1925, July, 1989.

L.J. Bohmann and R.H. Lasseter, *Stability and Harmonics in Thyristor Controlled Reactors*, IEEE Transactions on Power Delivery, vol.5, no.2, pp.1175-1181, April, 1990.

Appendix A

Gate Pulse Generator

This appendix gives the details of the TACS cards used for the generation of gate pulses in the EMTP model of the three-phase converter system. The types of the cards used and the principles are the same for the single phase converter system. The gate pulse generator uses the value of firing angle α and generates a firing pulse exactly α degrees after the natural zero crossing of the particular commutating voltage. In the model used in this thesis, a gate pulse generator with TACS source type-14 representing the reference voltage is used. Figure A.1 shows the level trigger that forms a long pulse, H. This pulse is then delayed by a pulse width of 1ms to form the pulse D. By applying the following logical operations pulses P and N are produced.

$$P = (H.AND.(NOT.D)) \quad (A.1)$$

$$N = (D.AND.(NOT.P)) \quad (A.2)$$

These two pulses are delayed by α and passed on to the gates. Figure A.2 gives the details of the types of the EMTP cards used to build the gate pulse generator. The main details are as follows.

- Three type-14 sources are used to generate sinusoidal voltages which are in phase with the input line-line voltages.

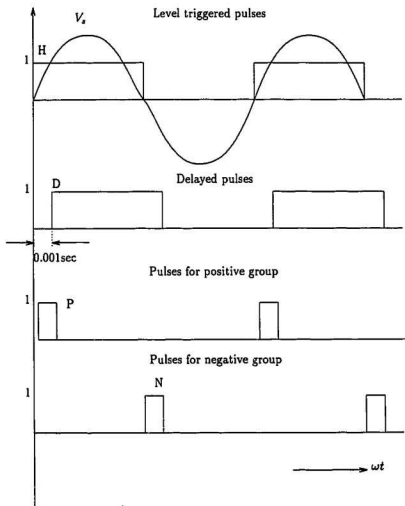


Figure A.1: Gate Pulse Generation Concept

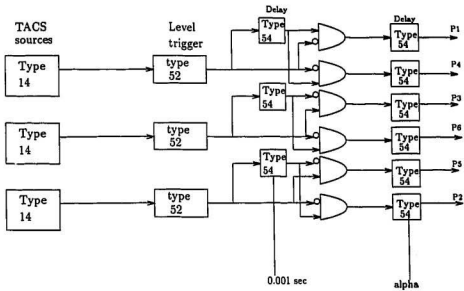


Figure A.2: Gate Pulse Generation Steps

- Type-52 level triggers are used to generate the long level- triggered pulses.
- Type-54 delay cards are used to delay the long pulses by the required duration of gate pulse (in this case 1ms).
- The AND and NOT gates in equations (A.1) and (A.2) are implemented using FORTRAN expression cards.
- The final pulses are delayed by α using type-54 pulses.
- The pulses ($P1$ through $P6$) are then forwarded to the Double Pulsing Block.

Double Pulsing

The double pulsing block is required to ensure the proper operation of the converter at start-up. During start-up two thyristors (in the positive and the negative group

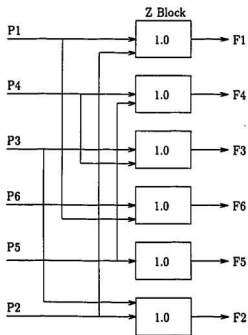


Figure A.3: Double Pulsing

respectively) need to be fired simultaneously to provide a path for the dc current. The arrangement shown in figure A.3 ensures that two thyristors are turned on simultaneously. For example at start-up when a pulse is applied to thyristor 1, thyristor 6 receives the same pulse, thus ensuring that 1 and 6 conduct simultaneously.

Appendix B

Synchronization of Triggering Pulses in an HVDC System [20]

The method used to synchronize the voltage at P_{CC} to the reference voltages used for the generation of the triggering pulses is detailed in this appendix. The AC voltages at the P_{CC} can be expressed as

$$\begin{aligned}v_a^{ac}(t) &= \sum_{n=1}^{\infty} V_{an} \cos(n\omega t + \theta_{an}) \\v_b^{ac}(t) &= \sum_{n=1}^{\infty} V_{bn} \cos(n\omega t + \theta_{bn}) \\v_c^{ac}(t) &= \sum_{n=1}^{\infty} V_{cn} \cos(n\omega t + \theta_{cn})\end{aligned}\tag{B.1}$$

where n refers to the harmonic order. The angles θ_{an} , θ_{bn} and θ_{cn} refer to the phase angle between the harmonic voltage and current. The fundamental components of the phase voltages in the Fourier form can be expressed as

$$\begin{aligned}v_{a1}^{ac}(t) &= a_a \cos(\omega t) + b_a \sin(\omega t) \\v_{b1}^{ac}(t) &= a_b \cos(\omega t) + b_b \sin(\omega t) \\v_{c1}^{ac}(t) &= a_c \cos(\omega t) + b_c \sin(\omega t)\end{aligned}\tag{B.2}$$

The Fourier components a and b in equation (B.2) can be obtained from TACS as shown in the block diagram of Fig. B.1.

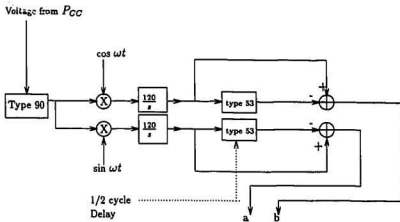


Figure B.1: TACS model for input voltage tracking

The Fourier components are obtained by integrating the sine and cosine terms over half a cycle. Type 90 source is used to continuously track the voltage at PCC . Type 53 delay is used to obtain the components over half a cycle. The positive sequence components of the tracked phase voltages can be expressed as

$$\begin{aligned}
 v_{a+}(t) &= \frac{1}{3} [V_a \cos(\omega t + \theta_a) + V_b \cos(\omega t + \theta_b + 120^\circ) + V_c \cos(\omega t + \theta_c - 120^\circ)] \\
 v_{b+}(t) &= \frac{1}{3} [V_a \cos(\omega t + \theta_a - 120^\circ) + V_b \cos(\omega t + \theta_b) + V_c \cos(\omega t + \theta_c + 120^\circ)] \\
 v_{c+}(t) &= \frac{1}{3} [V_a \cos(\omega t + \theta_a + 120^\circ) + V_b \cos(\omega t + \theta_b - 120^\circ) + V_c \cos(\omega t + \theta_c)]
 \end{aligned}
 \tag{B.3}$$

Using the Fourier coefficients obtained earlier and using the relationship between line voltage and phase voltage (line voltage lags the corresponding phase voltage by 30 degrees and differs in magnitude by a factor $\sqrt{3}$) the line-to-line voltages in terms of the Fourier coefficients can be expressed as

$$\begin{aligned}
 v_{ac}(t) &= \frac{1}{\sqrt{3}} [a_a \cos(\omega t - 30^\circ) + a_b \cos(\omega t + 90^\circ) + a_c \cos(\omega t - 150^\circ)] \\
 &\quad + \frac{1}{\sqrt{3}} [b_a \sin(\omega t - 30^\circ) + b_b \sin(\omega t + 90^\circ) + b_c \sin(\omega t - 150^\circ)]
 \end{aligned}
 \tag{B.4}$$

Similarly the other two line-to-line voltages are given by

$$\begin{aligned}
 v_{ba}(t) = & \frac{1}{\sqrt{3}} [a_a \cos(\omega t - 150^\circ) + a_b \cos(\omega t - 30^\circ) + a_c \cos(\omega t - 90^\circ)] \\
 & + \frac{1}{\sqrt{3}} [b_a \sin(\omega t - 150^\circ) + b_b \sin(\omega t - 30^\circ) + b_c \sin(\omega t + 90^\circ)]
 \end{aligned}
 \tag{B.5}$$

$$\begin{aligned}
 v_{ca}(t) = & \frac{1}{\sqrt{3}} [a_a \cos(\omega t + 90^\circ) + a_b \cos(\omega t - 150^\circ) + a_c \cos(\omega t - 30^\circ)] \\
 & + \frac{1}{\sqrt{3}} [b_a \sin(\omega t - 90^\circ) + b_b \sin(\omega t - 150^\circ) + b_c \sin(\omega t - 30^\circ)]
 \end{aligned}
 \tag{B.6}$$

The reference voltages as required for the triggering pulse generation are given by equations (B.4), (B.5) and (B.6).



